MARTIN MARIETTA ENERGY SYSTEMS LIBRARIES

3 4456 0378583 9

ornl

ORNL/TM-12418/V1

OAK RIDGE NATIONAL LABORATORY

MARTIN MARIETTA

Validation and Verification of RELAP5 for Advanced Neutron Source Accident Analysis: Part I, Comparisons to ANSDM and PRSDYN Codes

OAK RIDGE NATIONAL LABORATORY
CENTRAL RESEARCH LIBRARY
CIRCULATION SECTION
4500N ROOM 175
LIBRARY LOAN COPY
DO NOT TRANSFER TO ANOTHER PERSON
If you wish someone else to see this report, send in name with report and the library will arrange a loan.

Advanced Neutron Source

MANAGED BY
MARTIN MARIETTA ENERGY SYSTEMS, INC.
FOR THE UNITED STATES
DEPARTMENT OF ENERGY

This report has been reproduced directly from the best available copy.

Available to DOE and DOE contractors from the Office of Scientific and Technical Information, P.O. Box 62, Oak Ridge, TN 37831; prices available from (615) 576-8401, FTS 626-8401.

Available to the public from the National Technical Information Service, U.S. Department of Commerce, 5285 Port Royal Rd., Springfield, VA 22161.

This report was prepared as an account of work sponsored by an agency of the United States Government. Neither the United States Government nor any agency thereof, nor any of their employees, makes any warranty, express or implied, or assumes any legal liability or responsibility for the accuracy, completeness, or usefulness of any information, apparatus, product, or process disclosed, or represents that its use would not infringe privately owned rights. Reference herein to any specific commercial product, process, or service by trade name, trademark, manufacturer, or otherwise, does not necessarily constitute or imply its endorsement, recommendation, or favoring by the United States Government or any agency thereof. The views and opinions of authors expressed herein do not necessarily state or reflect those of the United States Government or any agency thereof.

ORNL/TM-12418/V1

VALIDATION AND VERIFICATION OF RELAP5 FOR ADVANCED NEUTRON SOURCE ACCIDENT ANALYSIS: PART 1, COMPARISONS TO ANSDM AND PRSDYN CODES

N. C. J. Chen
M. Ibn-Khayat
J. A. March-Leuba
M. W. Wendel

December 1993

Prepared by the
OAK RIDGE NATIONAL LABORATORY
Oak Ridge, Tennessee 37831-6285
managed by
MARTIN MARIETTA ENERGY SYSTEMS, INC.
for the
U.S. DEPARTMENT OF ENERGY
under contract DE-AC05-84OR21400

MARTIN MARIETTA ENERGY SYSTEMS LIBRARIES

3 4456 0378583 9

CONTENTS

Page

LIST OF FIGURES v

LIST OF TABLES vii

LIST OF ACRONYMS ix

ACKNOWLEDGMENTS xi

ABSTRACT xiii

1. INTRODUCTION 1

2. MODEL DESCRIPTIONS 3
   2.1 RELAP5 3
      2.1.1 RELAP5 Code Description 3
      2.1.2 RELAP5 Model Description 3
      2.1.3 RELAP5 Model Limitations 7
   2.2 ADVANCED NEUTRON SOURCE DYNAMIC MODEL 7
      2.2.1 Advanced Neutron Source Dynamic Model Code Description 7
      2.2.2 Advanced Neutron Source Dynamic Model Description 8
      2.2.3 Advanced Neutron Source Dynamic Model Correlations 12
      2.2.4 Advanced Neutron Source Dynamic Model Limitations 13
   2.3 PRSDYN 13
      2.3.1 PRSDYN Code Description 13
      2.3.2 PRSDYN Model Description 13
         2.3.2.1 Core Neutronics 14
         2.3.2.2 Channel Thermal Hydraulics 16
         2.3.2.3 Pipe Thermal Hydraulics 20
         2.3.2.4 Heat Exchangers 22
         2.3.2.5 Main Circulation Pumps 24
         2.3.2.6 Gas Accumulators 25
         2.3.2.7 Loss of Coolant Accident Modeling 26
      2.3.3 PRSDYN Model Limitations 26

3. COMPARISON OF RESULTS 29
   3.1 SMALL LOSS OF COOLANT ACCIDENT 29
      3.1.1 Steady-State 30
      3.1.2 Transient 32
      3.1.3 Discussion 43
   3.2 STATION BLACKOUT ACCIDENT 43
      3.2.1 Steady-State 43
      3.2.2 Transient 44
      3.2.3 Discussion 46

3.3 LARGE LOSS OF COOLANT ACCIDENT 57
3.3.1 Steady-State 57
3.3.2 Transient 57
3.3.3 Discussion 63
3.4 REACTIVITY INSERTION ACCIDENT 68
3.4.1 Steady-State 68
3.4.2 Transient 69
3.4.3 Discussion 69

4. CONCLUSIONS AND RECOMMENDATIONS 79
4.1 CONCLUSIONS 79
4.2 RECOMMENDATIONS 80

REFERENCES 83

LIST OF FIGURES

Figure		Page
1	RELAP5—Advanced Neutron Source reactor nodalization diagram	4
2	Advanced Neutron Source dynamic model nodalization diagram	9
3	Advanced Neutron Source reactor primary loop dynamic model block diagram	15
4	Comparison in fission, decay, and total power during the 51-mm-diam core pressure boundary tube break with 250-ms opening time	34
5	Break flow comparison during the 51-mm-diam core pressure boundary tube outlet break with 250-ms opening time	35
6	Mass flow comparison at locations upstream and downstream of the break during the 51-mm-diam core pressure boundary tube outlet break with 250-ms opening time	36
7	Comparison in pressure responses at the core pressure boundary tube (CPBT) inlet and outlet during the 51-mm-diam CPBT outlet break with 250-ms opening time	37
8	Heat flux comparison at the hot spot of the upper core showing Costa, Gambill/Weatherhead, and local surface heat fluxes during the 51-mm-diam core pressure boundary tube outlet break with 250-ms opening time	38
9	Heat flux comparison at the hot spot of the lower core showing Costa, Gambill/Weatherhead, and local surface heat fluxes during the 51-mm-diam core pressure boundary tube outlet break with 250-ms opening time	39
10	Comparison in bulk coolant temperature at the hot channel outlet for the lower and upper cores during the 51-mm-diam core pressure boundary tube outlet break with 250-ms opening time	40
11	Makeup and letdown flow comparison during the 51-mm-diam core pressure boundary tube outlet break with 250-ms opening time	41
12	Accumulator injection flow comparison during the 51-mm-diam core pressure boundary tube outlet break with 250-ms opening time	42
13	Total (fission plus decay heat) power generated in the two models during the station blackout accident	47
14	Comparison in coolant temperature at the lower-core hot-channel outlet during the station blackout accident	48
15	Coolant temperature at the lower-core hot-channel outlet during the station blackout accident	49
16	Main circulation pump coastdown speed during the station blackout accident	50
17	Core coolant velocity during the station blackout accident	51
18	Core coolant mass flow during the station blackout accident	52
19	Comparison in core outlet pressure during the station blackout accident	53
20	Comparison in core outlet pressure during the station blackout accident	54
21	RELAP5-calculated thermal limit ratios during the station blackout accident	55

22 Advanced Neutron Source reactor core region showing the primary supply vessel adapter weldment 58
23 Comparison in total core and break flows during the double-ended guillotine break at primary supply vessel adapter weldment with 1100-ms opening time 60
24 Comparison in pressures at the lower core inlet and outlet during the double-ended guillotine break with 1100-ms opening time 61
25 Costa limit and local surface heat fluxes at the lower core exit during the double-ended guillotine break with 1100-ms opening time 62
26 Good agreement in heat fluxes at the lower core exit during the double-ended guillotine break at primary supply vessel adapter weldment when three models used the same setpoint. 64
27 Pressure difference (change from steady state) at the hot leg riser outlet and accumulator inlet during the double-ended guillotine break with 1.1 s opening time 65
28 Advanced Neutron Source dynamic model-calculated heat fluxes showing the importance of pressure setpoints in terms of the nominal value during the double-ended guillotine break with 1100-ms opening time 66
29 RELAP5-calculated flows showing the total core flow, break flows upstream and downstream of the break, and individual accumulator flows during the double-ended guillotine break with 1100-ms opening time 67
30 Advanced Neutron Source dynamic model (ANSDM) vs RELAP5 comparison in total and fuel surface heat powers for the $0.80 reactivity step accident before correction of ANSDM fuel heat capacity 70
31 Advanced Neutron Source dynamic model (ANSDM) vs RELAP5 comparison in total and fuel surface heat powers for the $0.80 reactivity step accident after correction of ANSDM fuel heat capacity 71
32 Advanced Neutron Source dynamic model vs RELAP5 comparison in thermal limit ratios for the $0.80 reactivity step accident 72
33 Advanced Neutron Source dynamic model vs RELAP5 comparison in local surface heat flux at the lower core exit for the $0.80 reactivity step accident 73
34 Advanced Neutron Source dynamic model vs RELAP5 comparison in the local coolant velocity and saturation temperature at the lower core exit for the $0.80 reactivity step accident 74
35 Advanced Neutron Source dynamic model vs RELAP5 comparison in the local pressure and coolant temperature for the $0.80 reactivity step accident 75
36 RELAP5-calculated pressure changes with reference to the steady-state showing the acoustic propagation during the power burst along the loop for the $0.80 reactivity step accident 76

LIST OF TABLES

Table		Page
1	Distribution of fission and decay-heat powers used by RELAP5, Advanced Neutron Source dynamic model and PRSDYN at 100% power	5
2	Nominal operation conditions	29
3	Normalized power density of I3 fuel grading at the end-of-cycle	30
4	Core input parameters	31
5	Accumulator input parameters	31
6	Inertial flow diode input parameters	31
7	Core output parameters	32
8	Main circulation pump output parameters	33
9	Initial conditions for a station blackout comparison	44
10	Steady-state comparison for 200-MW nominal core	45
11	Sequence of events for station blackout benchmark	46
12	Post-scram decay heat regional distribution extrapolated from the Institut Laue-Langevin	56
13	Parameters for a large loss of coolant accident	57
14	Steady-state comparison for 330-MW nominal core	59
15	Improvement to the Advanced Neutron Source reactor thermal-hydraulic models based on comparison findings	80

LIST OF ACRONYMS

ACSL	Advanced Continuous Simulation Language
ANSDM	Advanced Neutron Source dynamic model
ANSI/ANS	American National Standards Institute/American Nuclear Society
ANS	Advanced Neutron Source
ANSR	Advanced Neutron Source reactor
BOC	beginning-of-cycle
CDR	conceptual design report
CHF	critical heat flux
CSAR	conceptual safety analysis report
CPBT	core pressure boundary tube
DEG	double-ended guillotine
EOC	end-of-cycle
FE	flow excursion
HFIR	High Flux Isotope Reactor
IB	incipient boiling
ILL	Institut Laue-Langevin
INEL	Idaho National Engineering Laboratory
LOCA	loss-of-coolant accident
LWR	light water reactor
NPSH	net positive suction head
ORNL	Oak Ridge National Laboratory
PSVAW	primary supply vessel adapter weldment
SDD	system design description
THTL	Thermal-Hydraulic Test Loop

ACKNOWLEDGMENTS

The authors would like to acknowledge the support of the ANS Project Office that made this work possible. The authors also thank R. M. Harrington for his enthusiastic encouragement and support, and C. D. Fletcher of INEL for his consultation on RELAP5 analyses and comments on the report.

ABSTRACT

As part of verification and validation, the Advanced Neutron Source reactor RELAP5 system model was benchmarked by the Advanced Neutron Source dynamic model (ANSDM) and PRSDYN models. RELAP5 is a one-dimensional, two-phase transient code, developed by the Idaho National Engineering Laboratory for reactor safety analysis. Both the ANSDM and PRSDYN models use a simplified single-phase equation set to predict transient thermal-hydraulic performance. Brief descriptions of each of the codes, models, and model limitations were included. Even though comparisons were limited to single-phase conditions, a broad spectrum of accidents was benchmarked: a small loss-of-coolant-accident (LOCA), a large LOCA, a station blackout, and a reactivity insertion accident. The overall conclusion is that the three models yield similar results if the input parameters are the same. However, ANSDM does not capture pressure wave propagation through the coolant system. This difference is significant in very rapid pipe break events. Recommendations are provided for further model improvements.

1. INTRODUCTION

This report documents a series of code-to-code comparisons that are part of the verification and validation of the RELAP5 Advanced Neutron Source reactor (ANSR) model that will be used for ANSR safety analyses. Two codes have been used for these comparisons: Advanced Neutron Source dynamic model (ANSDM), and PRSDYN. Both of these codes are in-house developed and both use models that have been developed independently of RELAP5.

These code-to-code comparisons are only a partial step in the verification of RELAP5 for this purpose. Other activities to reach the final goal include (1) comparison of RELAP5 predictions for pressure drop, flow excursion (FE), and critical heat flux (CHF) to experimental results from the ANSR thermal-hydraulic test loop (THTL) being operated at Oak Ridge National Laboratory (ORNL), (2) comparison of RELAP5 predictions of flow excursion to the data gathered by Costa[1] in support of Institut Laue-Langevin (ILL) design, (3) investigation of RELAP5 ability to predict correct void fractions under prototypic ANSR FE conditions, and (4) follow-on thermal-hydraulic experiments and activities that are still in the planning stage.

To accomplish these comparisons, a broad spectrum of accidents have been modeled. The particular conditions and transients benchmarked include: a series of steady states, a small loss-of-coolant accident (LOCA), a large LOCA, a station blackout, and a reactivity insertion accident. The LOCA calculations include a small core outlet break and a double-ended guillotine (DEG) core inlet break, both assuming a finite time break opening. The station blackout accident analysis is an unusual case that includes a simultaneous occurrence of a standard loss of off-site power, a loss of pony motors, and a small LOCA because of a stuck-open letdown valve. A reactivity step of $0.8 was chosen for reactivity insertion accident studies because it is the most limiting reactivity event considered in the *Conceptual Safety Analysis Report* (CSAR).[2]

This code comparison study is limited to single-phase and noninstantaneous break comparisons. The RELAP5[3] code is a one-dimensional, transient, and two-phase flow code developed at the Idaho National Engineering Laboratory (INEL). By contrast, ANSDM uses a simplified single-phase incompressible equation set to predict transient thermal-hydraulic performance. PRSDYN assumes single-phase conditions but takes into account the compressibility of heavy water (i.e., finite sound speed). The use of three different models is beneficial because it allows cross-checking of the results of independently developed models. Furthermore, the speed and ease of use of both ANSDM and PRSDYN allow many scoping calculations to be run to define trends more completely.

This study spans 1.5 years—from the preconceptual to the conceptual designs. Over this time, numerous changes in reactor operating conditions, fuel grading, and system designs took place. Because steady-state conditions varied, a reference steady state was established for each case studied, so that a consistent initial condition was ensured for transient comparisons. To reach a meaningful comparison in steady-state results requires a set of common input parameters: power, pressure, velocity, oxide growth, correlations, peaking factors, and probability levels. Moreover, to reach a meaningful comparison in transient results further requires another set of common input parameters: pump performance characteristics, break opening formation, reactivity profile after scram, engineered safety feature actuations, and a plant protection system.

The cross-checking among three models is a painstaking process, but rewarding. In general, for every comparison, a number of iterations is required before a satisfactory agreement can be obtained. The initial comparisons revealed good agreements in some parameters but disagreements in other parameters. Once these discrepancies were identified, possible causes were examined by performing additional parametric studies until the discrepancies were resolved within acceptable accuracy. Through

this repeated process, a better understanding in models is gained, so that a better improvement in models becomes possible. Discussions of results, comments for future updates, and reasons for discrepancies are provided whenever possible in the conclusions and recommendations.

2. MODEL DESCRIPTIONS

2.1 RELAP5

The RELAP5 code has been and is being used in several other research reactor safety analysis efforts. Other similar, highly subcooled, plate-type fuel systems being analyzed with RELAP5 include the High Flux Isotope Reactor (HFIR)[4] at ORNL, the High Flux Beam Reactor (HFBR)[5] at Brookhaven National Laboratory, the Advanced Test Reactor (ATR)[6] at INEL, the heavy water production reactors[7] at Savannah River Laboratory and the Heavy Water New Production Reactor design studies. Each of these efforts has expanded both the experience and confidence in using RELAP5 for highly subcooled reactor systems while concurrently identifying areas in the code that need improvement.

2.1.1 RELAP5 Code Description

RELAP5 is a one-dimensional systems analysis computer code based on nonhomogeneous, nonequilibrium, two-phase fluid models in a six-equation formulation for mass, momentum, and energy conservation. Through the companion studies, two versions of RELAP5 were used—RELAP5/MOD2/VERSION3t and RELAP5/MOD3/VERSION7AC.

The ANSR core geometry and conditions are significantly different from those found in the commercial nuclear power plants for which the RELAP5 code was developed and previously assessed. The ANSR features plate-type geometries with narrow coolant gaps and high coolant velocities, and LWR power plants use assemblies of pin-type fuel rods and have moderate normal coolant velocities. To account for these differences, RELAP5/MOD3/VERSION7AC was modified to better represent thermal-hydraulic phenomena in the ANSR geometry. The code modifications were based on ANSR steady-state design conditions and relevant experimental data.[8] Three code modifications were implemented for the core region of the model.

The first modification replaced the Dittus-Boelter[9] single-phase turbulent forced convection heat transfer correlation with the Petukhov[10] correlation. The Petukhov correlation has been shown to provide better predictive capability than the Dittus-Boelter correlation at the conditions of ANSR normal operation.

The second modification implemented the Gambill correlation[11] for subcooled CHF prediction, along with the Weatherhead[12] correlation for predicting the wall temperature. The Gambill correlation is used for mass fluxes >10,000 kg/m^2/s; the Groeneveld[13] lookup table is retained for mass fluxes <7,500 kg/m^2/s; and a linear interpolation is used between these limits.

The third modification altered the interfacial drag in the slug-flow regime with a disk-churn flow regime based on the drift-flux formulation developed by Griffith[14] to describe two-phase density in narrow channels. The modification lowers the interfacial drag, resulting in a lower void fraction for a given flow quality.

2.1.2 RELAP5 Model Description

The ANSR RELAP5 system model includes three major regions (see Fig. 1). The core model (region 1) consists of the two fuel elements (each constituting approximately half of the core), the core bypass channels, and the central control rod region. The core is surrounded by the core pressure boundary tube (CPBT), which separates the high-pressure primary system from the low-pressure reflector tank.

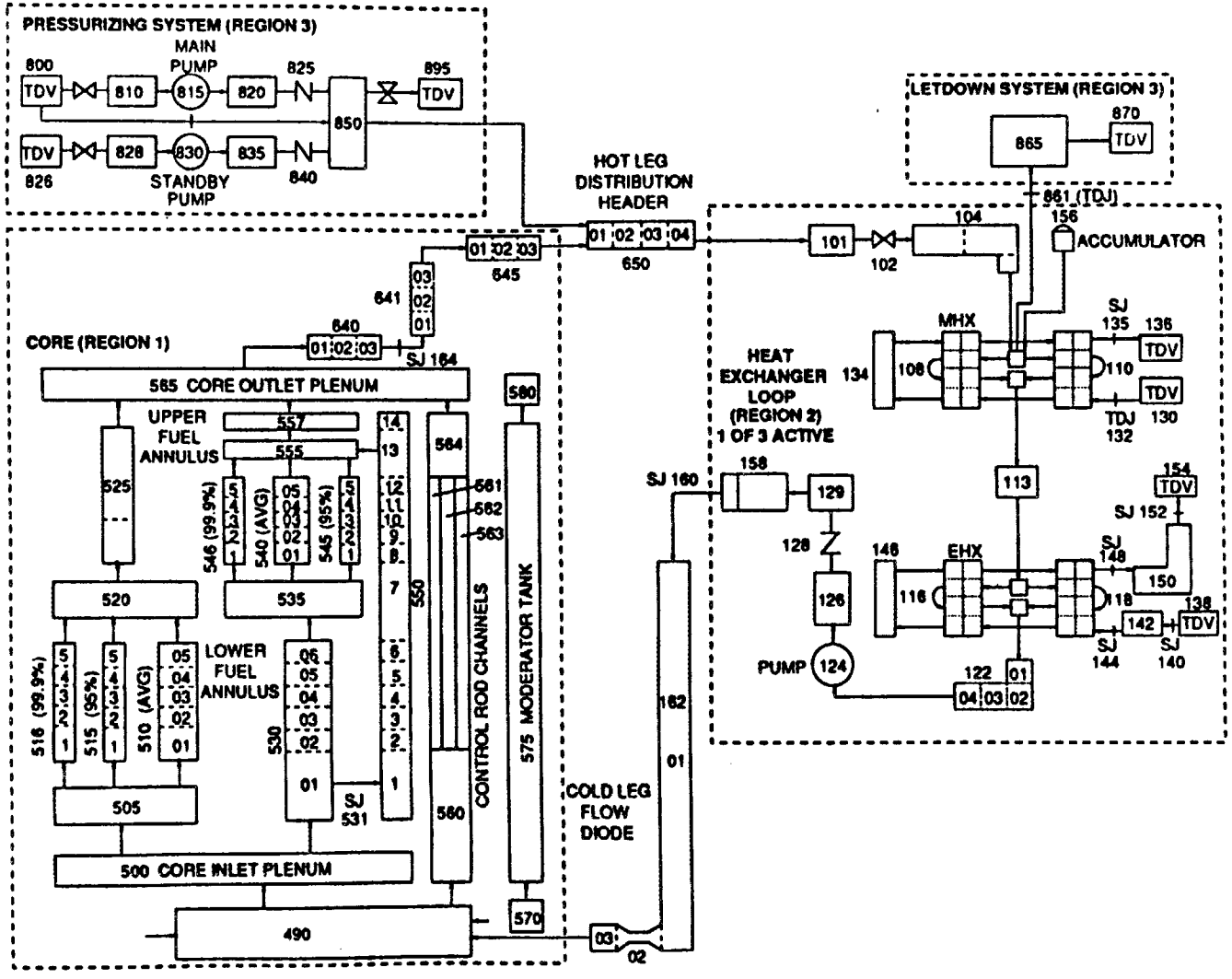

Fig. 1. RELAP5—Advanced Neutron Source reactor nodalization diagram.

Core power is calculated using a point kinetics model with reactivity feedback from coolant density change and reactivity input as a function of control rod movement. Power is distributed among the various metal and fluid regions according to independent, off-line, steady-state calculations that use the MCNP[15] computer code to calculate the transport of neutrons and gamma rays from the fuel to all parts of the reactor core and reflector. Table 1 summarizes the regional distribution for several key regions. In addition, the axial nodal power distribution input for each average and hot channel in the core is based on similar detailed, off-line nuclear calculations (BOLD-VENTURE)[16] that take into account the design distribution of fuel within the plates. The ANSR uses both axial and radial grading of fuel within each fuel plate to reduce power peaking and put the highest heat fluxes nearest the core inlet, to the extent possible, to increase the CHF ratios.

Table 1. Distribution of fission and decay-heat power used by RELAP5, Advanced Neutron Source dynamic model and PRSDYN at 100% power

Reactor component	Fraction of fission power	Fraction of decay heat power
Fuel elements	0.94050	0.6302
Reactor core coolant	0.01	0.01
Bypass components	0.02908	0.2106
Annulus components	0.01042	0.0700
Reactor components	0.010	0.0792

Each fuel element is modeled as an average channel (which incorporates all but two of the fuel plates) and two hot channels representing the most limiting axial relative power density profile in each core half. Manufacturing, design, correlation, and measurement uncertainties are combined in an appropriate manner, considering the frequency category of the event being analyzed. For each fuel element, the uncertainties affecting heat flux in one of the hot channels are combined at a 95% probability of nonexceedance for analysis of unlikely events (i.e., frequency <0.01/year but $>10^{-4}$/year), and the uncertainties in the other hot channel are combined at a 99.9% nonexceedance probability level for analysis of anticipated events (frequency >0.01/year). The purpose of the hot channels is to calculate the most severe axial bulk temperature profile within the core that is consistent with the two probability levels. This calculation is performed primarily for the prediction of FE, which is of concern because it could lead to CHF and probable fuel damage.

Each of the three channels (average, 95% hot, and 99.9% hot) is divided into five axial nodes, and results of off-line, steady-state BOLD-VENTURE neutronic calculations determine the input for the relative power level in the five nodes. The relative power density assigned to each axial segment of the average channel is determined by averaging the neutronically calculated relative power density of all radial regions in that axial segment. The relative power density for each of the five axial segments in the hot channel is determined from the most limiting radial region of the core (as determined from steady-state neutronic and thermal-hydraulic calculations). The hot spot factors for the "hot stripe" used to predict spot CHF are based on the neutronically determined maximum relative

power density within each segment. The hot spot heat flux is much greater because it includes the uncertainties on spot fuel distribution.

The loop model (region 2) contains four independent heat exchanger loops—three active and one standby. Each loop further consists of an isolation valve, a hot/cold leg, an accumulator, horizontal U-tube main and emergency heat exchangers, a centrifugal main circulating pump, and an inertial flow diode (a preferred directional flow device). The heavy water primary coolant is located on the shell side of both heat exchangers for easier maintenance. In the event of a loss of secondary cooling, the temperature rise in the primary system coolant and corresponding increase in temperature differential between the primary system and the pool light water initiates natural circulation of the pool water on the secondary side of the emergency heat exchanger. The heat transfer coefficients and pressure drop coefficients used in the main and emergency heat exchanger models are derived from design data. The single-phase homologous curve of the main circulation pumps was developed from three-quadrant Byron Jackson[17] design curves, and correlations used to describe pumping behavior in the event that two-phase flow should develop during a transient are based on Semiscale[18] data.

An open-loop representation of the letdown and pressurizing system (region 3) is included in the model. Letdown flow is extracted from the inlet plena of the three main heat exchangers, directed through letdown valves into the large (~50 m^3) letdown tank, and returned through high-head pressurizing pumps to the hot leg distribution header. The primary system core outlet pressure is controlled through modulation of the letdown valves. The input for initial valve opening allows the valve to pass the design nominal 15 kg/s letdown flow at normal operating pressure. A feedback loop based on deviation of core outlet pressure from nominal determines the valve modulation open or closed after time zero.

The pressurizing system contains two independent parallel operating pumps—main and standby. Injection flow is drawn from a constant temperature heavy-water source (e.g., the letdown tank) by the main pressurizing pump. The standby pump does not operate during normal operation but is started if the letdown valve closes on a low pressure signal. Following letdown isolation, flow through the pressurizing pump is assumed to continue until the integrated injected flow exhausts the letdown tank.

In the model, letdown flow is controlled via valves and isolated gradually, such as would occur with a motor operated valve. Primary coolant system pressure is controlled by adjusting the letdown flow area, which is represented as follows:

$$d = k\left(P - P_s\right)$$

and (1)

$$\dot{x} = \frac{d - x}{\tau} ,$$

where

d = demanded valve position (normalized),
k = the proportional-controller constant (Pa^{-1}),
P = the measured sensor pressure (Pa),
P_s = the setpoint pressure (Pa),

$\dot{x}$ = time derivative of normalized valve position (s^{-1}),
x = normalized valve position (-1 for fully closed, 1 for fully open, and 0 at normal position),
τ = the valve time constant (s).

2.1.3 RELAP5 Model Limitations

As do ANSDM and PRSDYN, RELAP5 uses a point kinetics space independent (zero-dimensional) formalism for the neutron dynamics in the core region. The power is distributed among different components (e.g., fuel elements, reflector, bypass region, etc.) based on steady-state power fraction distributions that have been estimated for the specific ANSR conditions. This estimation is not a bad approximation since most transients result in a reactor scram within the first few milliseconds, and then the power is determined by a decay heat calculation using the American National Standards Institute/American Nuclear Society (ANSI/ANS)[19] standard that is built into the RELAP5 code. INEL has developed a one-dimensional (axial) model to account for spatial variation in the core power response during control rod insertions. A full three-dimensional model is under development for beam tube flooding events.

The RELAP5 accumulator model is deficient for modeling the ANSR accumulator because it is incapable of representing flow into the tank and the honeycomb insert heat structure. INEL is developing a new model and assessing the validity of the model against the Savannah River Laboratory data. In the interim, a simple accumulator model without these limitations was used.

The RELAP5 pump model features the capability (with suitable test data to support the input) for modeling two-phase degradation effects resulting from the appearance of void in the pump suction but does not include the more limiting cavitation effects resulting from the appearance of void on the pump impeller. The easiest cavitation modeling is to degrade pump performance by reducing pump speed to effect the desired head degradation whenever indication of pump cavitation is sensed. This approach was incorporated in the HFIR upgraded safety analysis and implemented in the current ANSR RELAP5 system model.

2.2 ADVANCED NEUTRON SOURCE DYNAMIC MODEL

ANSDM has been programmed in the Advanced Continuous Simulation Language (ACSL),[20] which gives it fairly good flexibility of operation at run time. This model was originally designed to test and define control and plant protection system design requirements, but it has also been used to evaluate the reactivity events in the *Conceptual Safety Analysis Report* (CSAR).[2] ANSDM is composed of a collection of modules, most of which are reused throughout the model.

2.2.1 Advanced Neutron Source Dynamic Model Code Description

The "code" for ANSDM is ACSL, level 10R. ACSL automatically controls all numerical aspects of the equations used to model the physical behavior of the reactor (e.g., time-steps used, numerical convergence, etc.). This programming language contains only the numerical aspects and no physics. All aspects of fluid flow, heat transfer, neutronics, etc. are contained within the model described below. At run time, the user can select the integration algorithm and precision. As a default, ANSDM uses a Gears-stiff, fully implicit integration method; ACSL automatically adjusts

the time step size to maintain the estimated error within $<10^{-3}$ relative or 10^{-4} absolute for every integration interval.

2.2.2 Advanced Neutron Source Dynamic Model Description

A simplified nodalization diagram is shown in Fig. 2. The main characteristics of ANSDM can be described as follows.

- Core neutronics are modeled using the point kinetics approximation. The photodelayed neutrons are treated as an additional group of delayed neutrons. Decay heat is tabulated based on an ANS-specific correlation, which includes the distribution of decay heat among reactor internals. As a default, it is assumed that ~94% of the fission power remains inside the fuel plate and the rest is deposited by direct energy deposition in the reflector and vessel components. However, only ~65% of the decay heat is deposited in the fuel plate (see Table 1). The difference is caused by the fact that decay heat generates mostly gamma rays, which deposit their energy outside the core. The 65% is based on ILL extrapolations; new INEL calculations appear to indicate that the fraction of decay heat deposited in the fuel should be on the order of 72%.

- The fuel and coolant dynamics are modeled on an average channel basis. The average channel determines the core outlet conditions as well as the neutronic and thermohydraulic feedback that couples the core to the rest of the cooling system. A single axial node is used for this calculation. As a default, a constant 25-μm oxide layer is assumed to estimate fuel temperatures, and oxide growth is not modeled.

- The hot channels' fuel and coolant dynamics are simulated to represent the dynamic behavior of the hot streak of the upper and lower element. The lower element is typically limited at beginning-of-cycle (BOC) and the upper element at end-of-cycle (EOC). Thus, in this model, the BOC axial power shape and hot streak factors for the lower element hot channel and the EOC conditions for the upper element are used. The hot channels are divided into as many as 50 axial nodes (typically 27) where local temperatures, pressures, and heat fluxes are estimated to determine their margin to incipient boiling (IB), CHF, and FE instability. Hot channels do not contribute any feedback to the neutronics or thermohydraulic calculations of the rest of the cooling system.

- A bypass region models the flow of heavy water that bypasses the fuel elements inside the CPBT. This coolant is typically colder than the core outlet coolant so that when it mixes, the vessel outlet temperature (which is computed dynamically) is lower than the core outlet temperature.

- A reflector region is modeled with a very simplified one node approach. The reflector provides some (but not much) reactivity feedback to the core as a result of direct neutron and gamma heating.

- Cooling system pipes that release heat to the appropriate surrounding light water pools are modeled.

- In-containment light water pools are modeled including the main reactor pipe chase and heat exchanger pools. These pools remove heat from the reactor piping according to relative temperature and natural convection heat transfer coefficients. The heat exchanger pool also cools the emergency heat exchanger secondary side by natural circulation.

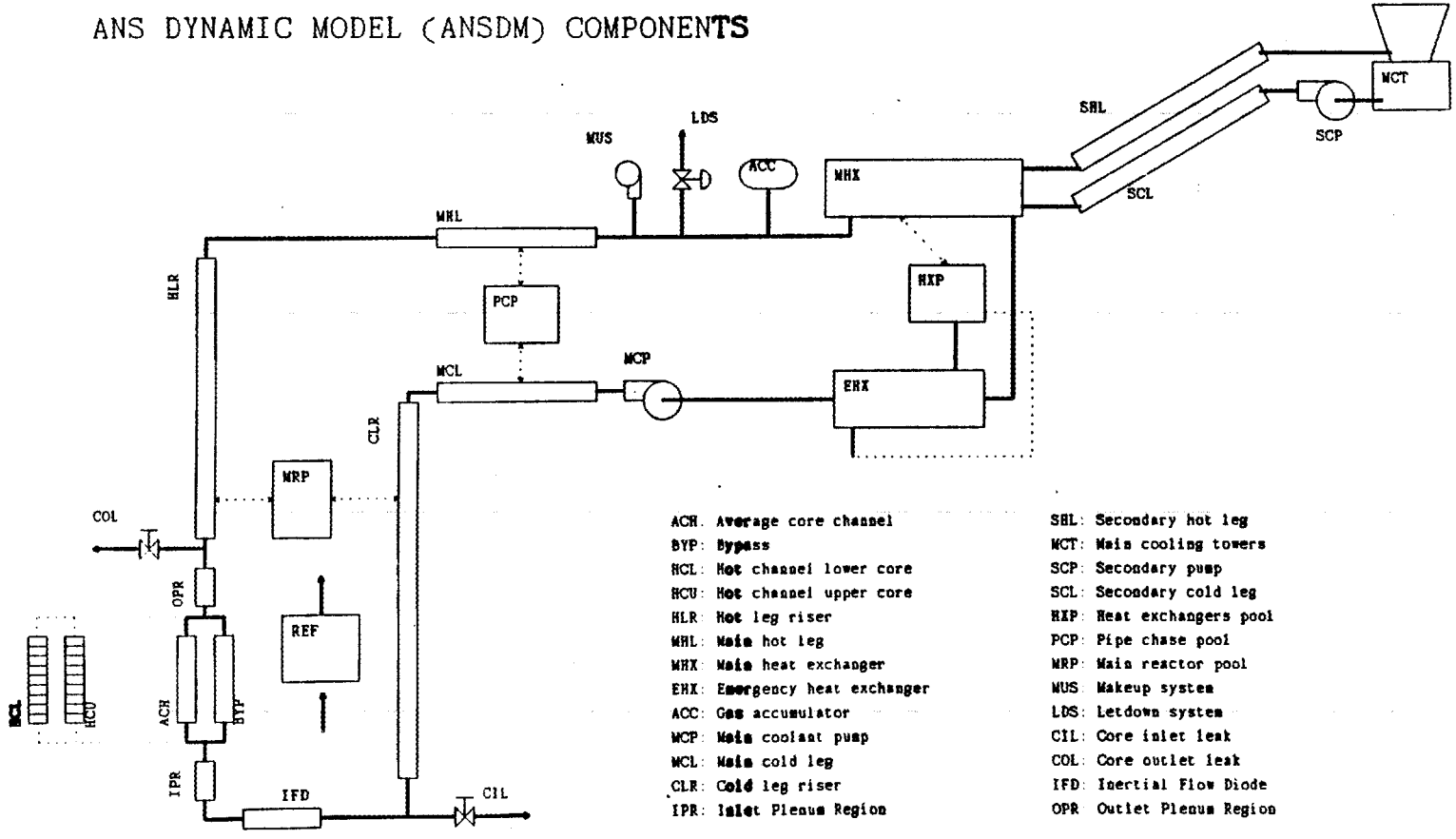

Fig. 2. Advanced Neutron Source dynamic model nodalization diagram.

- The main heat exchanger is modeled with the primary flow in the shell side and the secondary flow in the tube side. Heat transfer characteristics are adjustable; typically used values include a fouling heat transfer resistance factor. The heat exchanger model uses a single node with the logarithmic mean-temperature approximation.

- The emergency heat exchanger is modeled in series with the main heat exchanger. Primary flow is in the shell side and secondary flow is on the tube side. The shell side (primary) assumes that the flow is never laminar, regardless of Reynolds number. The diameter of the tubes is designed to be on the order of 0.05 m (2 in.) so that the Reynolds number will be large enough to ensure turbulent flow even at the low natural circulation flow rates. The secondary side of the emergency heat exchanger is connected to the heat exchangers pool; cooling flow occurs by natural circulation.

- Main circulation pumps are modeled according to the head-flow characteristic curve. The characteristic curve scales the flow directly proportional to the pump rotational speed; the pump head is proportional to the square of the pump speed; and the power required is proportional to the third power of the speed. Pump coastdown is modeled based on a conservation of angular momentum and assuming no friction. The resulting differential equation that is solved by the model is:

$$\frac{dn}{dt} = \frac{(n^2 - n_0^2)}{\tau} , \tag{2}$$

where

n = the pump rotational speed (s^{-1}),
n_0 = the desired equilibrium speed (e.g., n_0 = 10% if a reduction to pony flow is desired),
τ = the pump half speed time constant (nominally 2 s in ANSR).

The coastdown flow and pump head are computed by scaling the characteristic pump curve using the calculated speed, n. To simulate the effects of friction, a negative equilibrium speed (n_0) may be input to force the speed (n) to drop to zero in a finite time. By adjusting n_0 and τ, practically any pump coastdown may be achieved. During normal operation, the pump speed is assumed to remain constant (i.e., synchronous ac motors) regardless of the coolant conditions.

- The gas accumulator is assumed to follow the ideal gas law, so that the accumulator gas pressure is estimated from the following equations:

$$P = P_0 \left[\frac{V_0}{V}\right]^{\gamma} \tag{3}$$

and

$$\frac{dV}{dt} = \frac{\omega}{\rho} \tag{4}$$

where

P = pressure (Pa),
P_0 = initial pressure (Pa),
V_0 = initial volume (m^3),
V = volume (m^3),
γ = expansion coefficient,
ω = the mass flow rate of liquid leaving the accumulator (kg/s),
ρ = the density (kg/m^3).

It is assumed that the accumulators expand isothermally (i.e., $\gamma = 1.0$) as a default, but the parameter γ can be changed to 1.4 on demand to simulate an adiabatic expansion. The initial gas to liquid ratio is such that the liquid level will not reach the bottom of the accumulator after the gas has expanded to the depressurized condition. In the ANS baseline conceptual design, each accumulator has 0.52 and 7 m^3 of gas and liquid, respectively. Because ANSDM is a single-loop model, the single accumulator in ANSDM has three times those volumes.

- Primary coolant is maintained at pressure by the makeup flow. The model simulates this flow with a pump module (the pressurizer pump) that takes suction on a constant pressure tank (the letdown tank). The makeup pump speed is maintained constant unless a coastdown (i.e., loss of off-site power) is required. The pump speed can be altered on demand to simulate the initiation of the standby makeup pump. Pressure regulation is accomplished by modulating the flow through the letdown valves. The letdown valves are modeled as a pressure drop with variable coefficient (according to valve opening); the letdown flow is collected in the letdown tank. The model does not simulate the low pressure cleanup system; the letdown tank is assumed to have an infinite supply of D_2O so that makeup can always be maintained. Makeup supply problems can be simulated at any time by tripping the makeup pump. The makeup pump is assumed to have a perfect (i.e, no reverse flow) check valve.

- The secondary side of the ANS cooling system is represented by: (1) the secondary side of the main heat exchanger in the tube side, (2) the secondary hot leg, (3) the main cooling towers and cooling towers basin, (4) the secondary circulation pump, and (5) the secondary cold leg. All of these components use approximations similar to those in the primary system.

- A preliminary control system is simulated in the model. The control system includes: (1) control rod position based on the measured power-to-flow ratio, (2) pressure control that actuates the letdown valve based on hot leg pressure measurements, and (3) core inlet temperature control that actuates on the secondary flow based on the temperature measured at heat exchangers outlet.

- Sensor dynamics are modeled as first-order lag systems. The required time constants have been determined through simulation of control and plant protection system challenges. The time constants currently in the model are those required to satisfy most design basis events

requirements. The neutron flux sensors have a conservative 25-ms delay to simulate the "neutron-wave" time delay introduced by the large heavy water reflector.

- Breaks are simulated as a flow through an orifice (of the break effective diameter) from the inside of the main piping system to the light water pools. The leak flow, W_{lk}, is estimated from the orifice relation as:

$$W_{lk} = \frac{C_v}{\sqrt{1-\left(\frac{D_b}{D}\right)^4}} \frac{\pi D^2}{4} \sqrt{2\rho(P-P_{lk})} \quad , \tag{5}$$

where

C_v = the orifice coefficient (taken as 0.6 for sharp orifice),
D_b = the break effective diameter (m),
D = the pipe diameter (m),
P = the system pressure (Pa),
P_{lk} = the pool pressure (Pa).

2.2.3 Advanced Neutron Source Dynamic Model Correlations

ANSDM uses the standard set of correlations developed by the ANS Project. These correlations are fully documented in Sect. 4.4.2.7 of the CSAR[2] and can be summarized as follows.

- Filonenko correlation for friction coefficient in the core region. A multiplier can be input to ANSDM to adjust the pressure drop calculated using Filonenko. In this way, agreement may be forced between different codes. As an example, for the benchmarks in this report, a multiplier of 113% was added to match ANSDM pressure drops with those of RELAP5. This large multiplier was required because ANSDM computes coolant parameters (especially viscosity) using the core outlet temperature (i.e., hot conditions), and RELAP5 was adjusted to agree with the ANSR steady-state model that uses local conditions.

- Colebrook and White correlation for friction in the piping system. Note that Filonenko is only valid for the smooth surfaces in the core, the piping surfaces require a surface roughness of 45.7 μm.

- Petukhov heat transfer coefficient in the core region.

- Gambill-Weatherhead correlation for CHF in subcooled flow. ANSDM computes the ratio of actual flux to CHF at each of the (typically 27) axial nodes for the hot channels in the upper and lower core using the local pressure and temperature conditions. ANSDM typically prints the minimum of these ratios and their respective axial locations to the screen.

- Costa correlation for FE. Although the Costa correlation was developed based on outlet conditions only, ANSDM computes the FE limiting heat flux ratio at every axial location and prints out the minimum ratio and its axial location.

- Standard coolant properties correlations developed by the ANS Project for D_2O properties.

- Gibson correlation (shell side) and the Churchill correlation (tube side) for heat transfer characteristics in the heat exchangers.

2.2.4 Advanced Neutron Source Dynamic Model Limitations

The most important limitations of the ANSDM are described below.

- **Point kinetics for the neutron dynamics in the core region.** The power is distributed among different components (e.g., upper and lower elements, reflector, bypass region, etc.) based on steady-state power fraction distributions that have been estimated for the specific ANSR conditions. This method of approximation is not particularly bad since most transients result in a reactor scram within the first few milliseconds, and then the power is determined by a decay heat correlation.

- **Incompressible flow.** The model is limited to liquid and incompressible phase state. This assumption results in an infinite speed of sound and yields significant errors when acoustic-wave propagation is a relevant phenomenon (for instance, during fast-opening large break LOCAs). This approximation, however, is fairly accurate for other scenarios that do not involve fast pressure transients.

- **Single phase flow.** The model is limited to the liquid phase state; whenever a transient results in saturated boiling, the simulation fails. Note that the core typically is damaged (resulting from either CHF or FE instabilities) well before saturated boiling can be established, and, thus, this approximation is fairly accurate for most scenarios.

- **Single loop flow dynamics.** All three loops are simulated by one effective loop. Because of this approximation, the model is not able to simulate imbalances between loops; for instance, the shutdown of one pump cannot be modeled while the other two pumps are operating.

- **Poor reverse flow model.** The model fails to compute enthalpies properly if reverse flow is established. Note, however, that reverse flow occurs only during large break LOCAs in the hot leg, and the hot leg enthalpy is fairly irrelevant during these transients.

2.3 PRSDYN

2.3.1 PRSDYN Code Description

PRSDYN is similar to ANSDM in that ACSL is used to take care of all numerical details, and the PRSDYN model contains all of the physics necessary to describe the transient behavior of the reactor.

2.3.2 PRSDYN Model Description

This section deals with the description of a dynamic model (PRSDYN) for ANSR that is capable of simulating possible accident and operation scenarios of the plant, including events with

very rapid pressure dynamics. The model is written in modular form as shown in the block diagram in Fig. 3 and is programmed in ACSL. The model includes the following modules: core neutronics, channel and pipe thermal hydraulics, vessel bypass and annulus, heat exchangers, main circulation pumps, gas accumulators, makeup and control systems, and sensor and break modules.

2.3.2.1 Core Neutronics

The ANSR neutronics are described by a point kinetics model that includes both delayed neutrons and photo-neutrons. Equations 6 and 7 show the mathematical formulation for the neutron flux and the precursor concentrations normalized to the nominal reactor power.

$$\dot{\Phi} = \frac{(\rho_{tot}-1)\beta}{\Lambda}\Phi + \Sigma\lambda_i C_i \quad , \tag{6}$$

where

$\dot{\Phi}$ =rate of change of normalized flux, (s^{-1})
ρ_{tot} =total reactivity ($),
β =total delayed neutron fraction,
Λ =effective neutron lifetime (s),
Φ =normalized flux (fraction of full power value),
λ_i =decay constant of the ith group of delayed neutrons (s^{-1}),
C_i =normalized i^{th} precursor concentration (fraction of full power value).

$$\dot{C}_i = \Phi\frac{\beta_i}{\Lambda} - \lambda_i C_i \quad , \tag{7}$$

where

$\dot{C}$ =rate of change of normalized i^{th} precursor concentration (s^{-1}),
β_i =delayed fraction for the ith delay group,
Λ =effective neutron lifetime (s).

The reactivity feedback, ρ_{fb}, is computed as follows:

$$\rho_{fb} = \alpha_c\frac{\varrho_c}{\varrho_{c0}} + \alpha_b\frac{\varrho_b}{\varrho_{b0}} + \alpha_r\frac{\varrho_r}{\varrho_{r0}} + \alpha_f(T_f - T_{f0}) \quad , \tag{8}$$

where

α_c =core coolant density reactivity coefficient ($),
ϱ_c =core coolant density (kg/m^3),
ϱ_{c0} =initial core coolant density (kg/m^3),
α_b =bypass coolant density reactivity coefficient ($),
ϱ_b =bypass coolant density (kg/m^3),
ϱ_{b0} =initial bypass coolant density (kg/m^3),

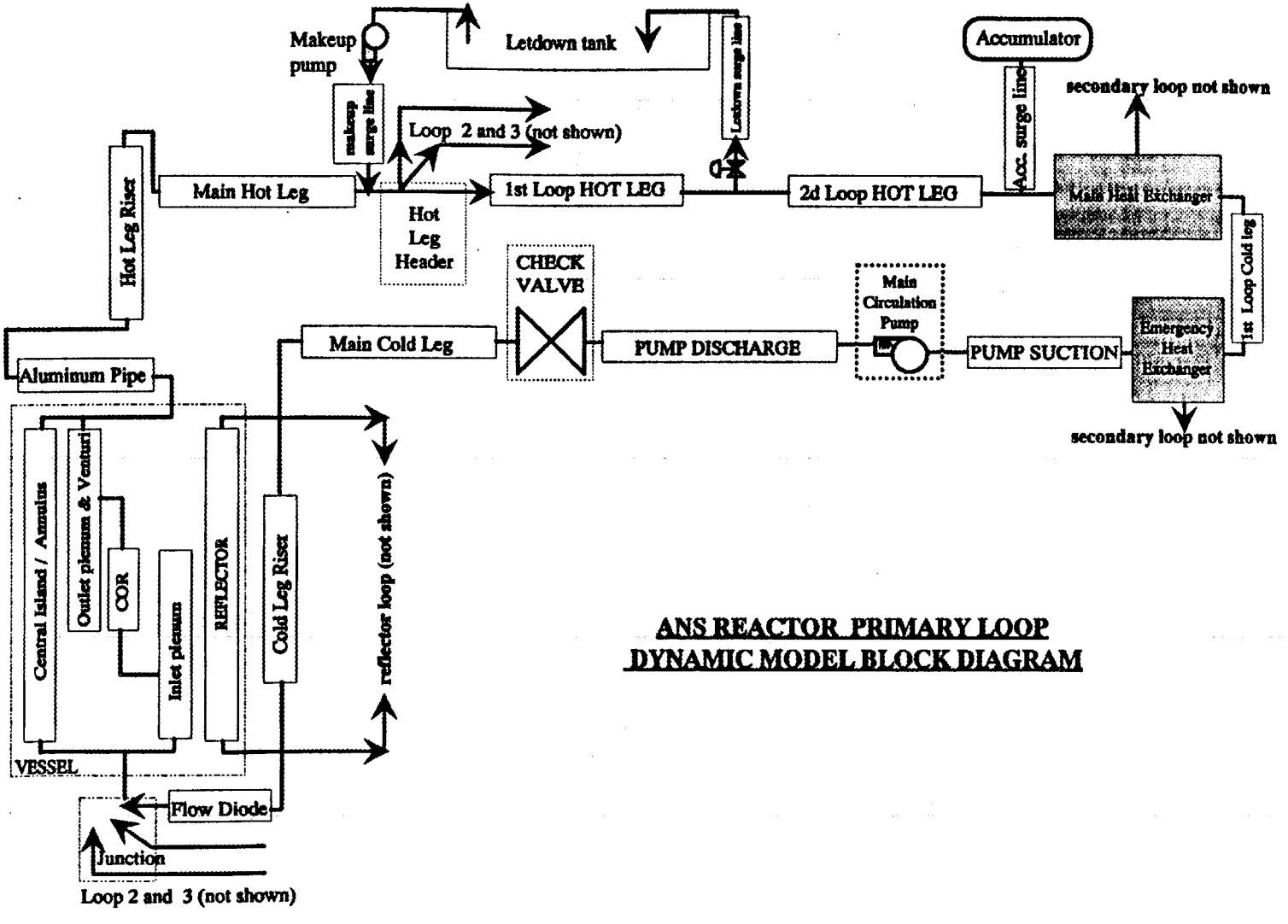

Fig. 3. Advanced Neutron Source reactor primary loop dynamic model block diagram.

α_r = reflector coolant density reactivity coefficient ($),
ρ_r = reflector coolant density (kg/m^3),
ρ_{r0} = reflector coolant density at time 0 (kg/m^3),
α_f = fuel temperature reactivity coefficient ($/°C),
T_f = fuel temperature (°C),
T_{f0} = initial fuel temperature (°C).

The total reactivity is

$$\rho_{tot} = \rho_{fb} + \rho_{sd} + \rho_{cont} \quad , \tag{9}$$

where

ρ_{fb} = reactivity feedback ($),
ρ_{sd} = shutdown system reactivity ($),
ρ_{cont} = control system reactivity ($).

The total power, P_{tot}, is the sum of the fission power, P_n, and decay-heat power, P_g. The distribution of fission power and decay-heat power among reactor components is shown in Table 1.

2.3.2.2 Channel Thermal Hydraulics

This subsection deals with thermal-hydraulics of the average channel, which is modeled in a single-node approximation. PRSDYN describes the coolant enthalpy and the oxide surface cladding, and fuel surface temperatures.

The channel exit enthalpy, h_{out}, is determined from an energy balance that results in the following differential equation:

$$h_{out} = \frac{q_{cool} - \Delta(\omega h)}{m_{cool}} \quad , \tag{10}$$

where

q_{cool} = power transferred to coolant (W),
ω = coolant flow rate (kg/s),
h = enthalpy (J/kg),
m_{cool} = node coolant mass (kg).

An equation for determination of the wall temperature, T_{wall}, is obtained from:

$$\frac{d(M_{wall} C_{p_{wall}} T_{wall})}{dt} = q_{clad} - H_{film} A_{wall} (T_{wall} - T_{D_2O}) \quad , \tag{11}$$

where

M_{wall} = mass of the wall [oxide (kg)],
$C_{P_{wall}}$ = wall heat capacity (J/kg/°C),
T_{wall} = wall (oxide) temperature (°C),
q_{clad} = power inside the wall (W),
H_{film} = film heat transfer (W/°C/m²),
A_{wall} = wall heat transfer area (m²),
T_{D_2O} = average coolant temperature (°C);

and

$$T_{wall} = \frac{q_{wall} - H_{film} A_{wall} (T_{wall} - T_{D_2O})}{M_{wall} C_{P_{wall}}} , \tag{12}$$

where

q_{wall} = power transferred from the cladding to the wall (oxide) as defined in Eq. 13 (W),
H_{film} = film heat transfer (W/°C/m²),
A_{wall} = wall heat transfer area (m²),
T_{wall} = wall (oxide) temperature (°C),
T_{D_2O} = average coolant temperature (°C),
M_{wall} = mass of the wall [oxide (kg)],
$C_{P_{wall}}$ = wall heat capacity (J/kg/°C).

The power transferred from the cladding to the wall (oxide), q_{wall}, is given by:

$$q_{wall} = \frac{2\pi r_{wall} l_{wall} \kappa_{wall}}{(\Delta x)_{wall}} (T^s_{clad} - T_{wall}) , \tag{13}$$

where

r_{wall} =average wall radius (m),
l_{wall} =wall length (m),
κ_{wall} =wall thermal conductivity (W/m/°C),
$(\Delta x)_{wall}$ =wall thickness (m),
T^s_{clad} =cladding surface temperature (°C),
T_{wall} =wall (oxide) temperature (°C).

The cladding outer surface temperature, T^s_{clad}, is given by:

$$T^s_{clad} = \frac{q_{clad} - q_{wall}}{M_{clad} C_{P_{clad}}} , \tag{14}$$

where

q_{clad} =power inside the wall (W),
q_{wall} =power transferred from the cladding to the wall (oxide) as defined in Eq. 13 (W),
M_{clad} =mass of the clad [oxide (kg)],
T_{clad} =cladding temperature (°C),
$C_{P_{clad}}$ =cladding heat capacity (J/kg/°C).

The power transferred from the fuel to the cladding, q_{clad}, is determined by:

$$q_{clad} = \frac{2\pi r_{clad} l_{clad} \kappa_{clad}}{(\Delta x)_{clad}} (T^s_{fuel} - T^s_{clad}) \quad , \tag{15}$$

where

r_{clad} =average cladding radius (m),
l_{clad} =cladding length (m),
κ_{clad} =cladding thermal conductivity (W/m/°C),
$(\Delta x)_{clad}$ =cladding thickness (m),
T^s_{fuel} =fuel surface temperature (°C),
T^s_{clad} =cladding surface temperature (°C).

The fuel surface temperature, T^s_{fuel} is given by:

$$T^s_{fuel} = \frac{q_{fuel} - q_{clad}}{M_{fuel}\, C_{P_{fuel}}} \quad , \tag{16}$$

where

q_{fuel} =power inside the cladding (W),
q_{clad} =power inside the wall (W),
M_{fuel} =mass of the fuel (kg),
$C_{P_{fuel}}$ =fuel heat capacity (J/kg/°C),
T_{fuel} =fuel temperature (°C).

The localized film heat transfer H_{film} is given by:

$$H_{film} = \frac{\mathrm{N}_b}{\kappa_{D_2O}\, D_e} \quad , \tag{17}$$

where

N_b =Nusselt number,
κ_{D_2O} =coolant thermal conductivity (W/m/°C),
D_e =equivalent diameter (m).

For the steady-state regime, the Nusselt number, N_b^s, is computed using the Petukhov correlation at the bulk coolant speed and temperature.

$$N_b^s = \frac{\left[\frac{f}{8}\right] Re_b Pr_b \left[1 + 0.334 \left[\frac{D_e}{L}\right]^{\frac{2}{3}}\right] \left[\frac{\mu_b^{D_2O}}{\mu_s^{D_2O}}\right]^{0.11}}{(1 + 3.4f) + \left[11.7 + \frac{1.8}{Pr_b^{\frac{1}{3}}}\right] \left[\frac{f}{8}\right]^{0.5} \left[Pr_b^{\frac{2}{3}} - 1\right]}, \tag{18}$$

where

f = friction factor,
Re_b = bulk coolant Reynolds number,
Pr_b = bulk coolant Prandtl number,
D_e = equivalent diameter (m),
L = length of the heated area (m),
$\mu_b^{D_2O}$ = bulk coolant viscosity (Pa·s),
$\mu_s^{D_2O}$ = surface viscosity (Pa·s).

The friction factor f, used for the Petukhov correlation, is given by the Filonenko correlation:

$$f = a_f \, [1.82\log(Re_b) - 1.64]^{-2} \quad , \tag{19}$$

where

f = friction factor,
a_f = correction factor,
Re_b = bulk coolant Reynolds number.

Solution of the Petukhov correlation requires an iterative process. To avoid this iteration during transient scenarios, the Nusselt number, N_b, is approximated by:

$$N_b = N_b^s \left[\frac{\omega}{\omega_0}\right]^{0.8} \quad , \tag{20}$$

where

N_b = Nusselt number,
N_b^s = Nusselt number at steady state,
ω = actual flow rate (kg/s),
ω_0 = initial flow rate (kg/s).

Thermal properties, such as D_2O density, heat capacity, conductivity, surface tension, latent heat, and viscosity, which are used in the heat transfer calculations, are computed from tables based on experimental results.

2.3.2.3 Pipe Thermal Hydraulics

This subsection presents the dynamics modeling of the ANS flow rate and pressure state variables. The relationship between flow speed (u) and the pressure in each node is expressed by the relation:

$$P_{out} = P_{inlet} - \Delta p - L\rho\dot{u} \quad , \tag{21}$$

where

P_{out} =pressure at the outlet of the node (Pa),
P_{inlet} =pressure at the inlet of the node (Pa),
Δp =total pressure drop (Pa),
L =length of the node (m),
ρ =heavy water density (kg/m^3),
$\dot{u}$ =flow acceleration (m/s^2).

Rewriting the above equation in terms of flow rate ($\dot{\omega}$) and eliminating small-contribution terms, the following expression is obtained:

$$\dot{\omega} = \frac{P_{inlet} - P_{out} - \Delta P}{\frac{L}{A}} \quad , \tag{22}$$

where

$\dot{\omega}$ =rate of change of flow (kg/s^2),
P_{inlet} =inlet node pressure (Pa),
P_{out} =outlet node pressure (Pa),
ΔP =total pressure loss or drop (Pa),
L =length of the node/pipe (m),
A =flow area (m^2).

The total pressure drop, ΔP, is given by:

$$\Delta P = \frac{\left[\frac{fL}{D_e} + K_f\right] \omega^2}{2\,\rho\,A^2} + \rho g z \tag{23}$$

where

ΔP =total pressure drop (Pa),
f =friction factor,
L =length of the node [pipe (m)],
D_e =equivalent diameter (m),
K_f =total pipe average-velocity heads lost,
ω =flow rate (kg/s),
ρ =coolant density (kg/m^3),
A =flow area (m^2),
g =gravitational acceleration (m/s^2),
z =height of the node (m).

To calculate the node-outlet pressure, P_{out}, it is necessary to start from the time derivative of the equation of state:

$$\dot{P}_{out} = \frac{\partial P}{\partial m}\Big|_T \dot{m}_{cool} + \frac{\partial P}{\partial h}\Big|_v \dot{h} \quad , \tag{24}$$

where

$\dot{P}$ =rate of change of pressure (Pa/s),
$\frac{\partial P}{\partial m}$ =pressure change with respect to mass at constant temperature (m^{-1} s^{-2}),
$\frac{\partial P}{\partial h}$ =pressure change with respect to enthalpy at constant volume (kg/m^3),
$\dot{m}_{cool}$ =rate of change of mass (kg/s),
$\dot{h}$ =rate of change of enthalpy (J/kg/s).

The mass variation, m_{cool}, is given by:

$$\dot{m}_{cool} = \frac{dm}{dt} = \frac{\partial m}{\partial t} + \left[\frac{\partial m}{\partial h}\right]_P \dot{h} \quad , \tag{25}$$

where

$\dot{m}_{cool}$ =rate of change of mass (kg/s),
$\left[\frac{\partial m}{\partial h}\right]_P$ =mass changes with respect to enthalpy at constant pressure (kg·s^2/m^2),
$\dot{h}$ =rate of change of enthalpy (J/kg/s).

In terms of mass flow rate and density, the mass variation may be rewritten as follows:

$$\dot{m}_{cool} = \omega_{inlet} - \omega_{outlet} + V \left[\frac{\partial \rho}{\partial h}\right]_P \dot{h} \quad , \tag{26}$$

where

ω_{inlet} =flow rate at the inlet of the node (kg/s),
ω_{outlet} =node flow rate (kg/s),
V =volume of the node (m^3),
$\left[\frac{\partial \rho}{\partial h}\right]_P$ =density changes with respect to enthalpy at constant pressure ($kg \cdot s^2/m^5$),
$\dot{h}$ =rate of change of enthalpy (J/kg/ s).

After eliminating the irrelevant terms, the following equation for the node-outlet pressure is obtained:

$$\dot{P}_{out} = \frac{1}{V} \left[\frac{\partial P}{\partial \rho}\right]_T (\omega_{inlet} - \omega_{outlet}) \quad , \tag{27}$$

where

$\dot{P}_{out}$ =rate of change of outlet node pressure (Pa/s),
$\left[\frac{\partial P}{\partial \rho}\right]_T$ =liquid compressibility at constant temperature (m^2/s^2),
ω_{inlet} =flow rate at inlet of node (kg/s),
ω_{outlet} =outlet node flow rate (kg/s).

The heavy water compressibility factors $\partial P/\partial \rho$ and $\partial P/\partial h$ are either determined from their dependence on the speed of sound and from the Joule-Thompson coefficient for D_2O or read from a table of experimental values. Both methods yield a consistent value of 2.043×10^6 m^2/s^2 for $\partial P/\partial \rho$ and 5 Pa/J for $\partial P/\partial h$.

2.3.2.4 Heat Exchangers

PRSDYN uses the logarithmic-mean-temperature approximation to model the heat transferred through the heat exchanger, q.

$$q = U_{all} A_{all} \left[\frac{\Delta T_{outlet} - \Delta T_{inlet}}{\ln\left[\frac{\Delta T_{outlet}}{\Delta T_{inlet}}\right]}\right] \quad , \tag{28}$$

where

q =heat exchange [rejected (W)],
U_{all} =overall heat transfer coefficient (W/m²/°C),
A_{all} =overall heat transfer area (m²),
ΔT_{outlet} =temperature difference between the outlet of tube and shell side (°C),
ΔT_{inlet} =temperature difference between the inlet of tube and shell side (°C).

The heat transfer coefficient used for the shell side, H_{shell}, is given by Gibbon's correlation:[21]

$$H_{shell} = \frac{0.3\ \rho_{D_2O}\ \nu_{D_2O}\ C_{p_{D_2O}}}{R_e^{0.2}\ P_r^{\frac{2}{3}}}\ , \tag{29}$$

where

H_{shell} =film heat transfer shell side (W/m²/°C),
ρ_{D_2O} =liquid density for heavy water (kg/m³),
C_{PD_2O} =liquid heat capacity for heavy water (J/kg/°C),
R_e =Reynolds number,
P_r =Prandtl number,
ν_{D_2O} =liquid surface tension for heavy water (kg/s²).

The heat transfer resistance coefficient (fouling), F_{res}, is given by:

$$F_{res} = \frac{2}{\left\{\frac{1}{\sqrt{\left[\left(\frac{8}{R_e}\right)^{10} + \left(\frac{R_e}{36500}\right)^{20}\right]}} + 2.21 \log\left(\frac{R_e}{7}\right)^{10}\right\}^{0.2}}\ . \tag{30}$$

The tube side heat transfer coefficient, H_{tube}, is based on Churchill's correlation:[22]

$$\theta_1 = \frac{6.3 + 0.079 \sqrt{\frac{F_{rus}}{2}}\, R_e\, P_r}{\left(1 + P_r^{0.8}\right)^{\frac{5}{8}}} \quad , \tag{31}$$

$$\theta_2 = \left\{ 4.364^{10} + \left[\frac{e^{\frac{(2200 - R_e)}{365}}}{19.0445} + \theta_1^{-2} \right]^{-5} \right\}^{0.1} \quad , \tag{32}$$

and

$$H_{tube} = \frac{\mu_{D_2O}\,(\theta_1 + \theta_2)}{\kappa_{D_2O}} \quad , \tag{33}$$

where

H_{tube} =film heat transfer tube side (W/m²/°C),
μ_{D_2O} =coolant dynamic viscosity (Pa·s),
κ_{D_2O} =liquid thermal conductivity (W/m/°C).

The overall heat transfer coefficient, U_{all}, is given by:

$$U_{all} = \left[\frac{1}{H_{shell}} + \frac{1}{H_{tube}} + \frac{1}{H_{ext}} \right]^{-1} A_{all} \quad , \tag{34}$$

2.3.2.5 Main Circulation Pumps

The main circulation pumps coastdown is modeled on a conservation of angular momentum, which yields the relation:

$$\frac{dn}{dt} = \frac{(n^2 - n_0^2)}{\tau_{pump}} \quad , \tag{35}$$

where

n =normalized pump speed (fraction of reference value),
t =time (s),

n_0 =nominal normalized pump speed (fraction of reference value),
τ_{pump} =pump time constant (s).

The coastdown flow and pump head are computed by scaling the characteristic pump curve using the calculated normalized speed, n.

2.3.2.6 Gas Accumulators

The gas accumulator is a tank filled with heavy water with a high pressure gas bubble at the top designed to discharge its liquid quickly in the event of a reactor cooling failure. The gas accumulators are modeled assuming the validity of the ideal gas law given by:

$$P_{gas} = \frac{P^0_{gas}\, V^0_{gas}}{V_{gas}} \quad , \tag{36}$$

where

P_{gas} =pressure of gas (Pa),
P^0_{gas} =nominal gas pressure (Pa),
V^0_{gas} =nominal gas volume (m^3),
V_{gas} =gas volume (m^3).

The initial gas-to-liquid ratio is such that the liquid level will not reach the bottom of the accumulator after the gas has expanded to the depressurized condition. The flow of liquid to and from the accumulator is given by:

$$\dot{\omega}_{acc} = \frac{(P_{acc} - P_{system} - \Delta P_{acc})}{\frac{L}{A}} \quad , \tag{37}$$

where

$\dot{\omega}_{acc}$ =mass flow rate acceleration (kg/s^2),
P_{acc} =pressure at the accumulation surge line (Pa),
P_{system} =main hot leg pressure (Pa),
ΔP_{acc} =total pressure drop at the surge line (Pa),
L =surge line length (m),
A =surge line flow area (m^2).

The gas volume inside the accumulator is given by:

$$V_{gas} = V^o_{gas} + \int_o^{\tau} \frac{\omega_{acc}}{\rho_{acc}}\, dt \quad , \tag{38}$$

where

ω_{acc} = flow rate out from the accumulator (kg/s),
ρ_{acc} = liquid density (kg/m^3).

2.3.2.7 Loss of Coolant Accident Modeling

Breaks are simulated from any reactor component to the pool or from the annulus to the reflector as a flow through an orifice. The leak flow is computed and the orifice coefficient is given by the following equation:

$$W_{lk} = C_v \frac{\pi D_{break}^2}{4} \sqrt{2\rho(P_{system} - P_{pool})} \quad , \tag{39}$$

where

W_{lk} = leak flow (kg/s),
C_v = break loss coefficient,
D_{break} = break diameter (m),
P_{system} = pressure at the leak location (Pa),
P_{pool} = pool pressure (Pa).

C_v is determined by:

$$C_v = C_{v0} \frac{\pi\sqrt{\rho}}{4} \quad , \tag{40}$$

where

ρ = coolant density (kg/m^3).

The break diameter (D_{break}) is represented by the following formulation:

$$D_{break}(t) = \min\left[D_{break}^{max} \times (2^{\frac{t}{\tau}} - 1) \ , \ D^{max}\right] \tag{41}$$

and

$$D^{max} = \max(2 \times D_{pipe}) \quad .$$

2.3.3 PRSDYN Model Limitations

The most important limitations of this model are described below.

- Point kinetics is used for the neutron dynamics in the core region.

- The model is limited to liquid phase state (incompressible flow). Whenever a transient results in saturated boiling for a long time, the simulation fails. Note, however, that for most events initiated from full power, subcooled boiling would result in CHF or FE well before the establishment of saturated boiling.

3. COMPARISON OF RESULTS

Results of two LOCAs, one station blackout, and one reactivity insertion accident are presented below. Steady-state results are compared first, followed by transient results. Following these comparisons, the findings are discussed, and the basis for the recommendations is explained.

ANSDM cannot model instantaneous pipe breaks because of its incompressible flow model. To allow for these comparisons, breaks were opened in all three models exponentially over a finite period of time, τ, according to the following expressions.

$$D(t) = D_b(2^{\frac{t}{\tau}} - 1) \quad if\ 0 \le t \le \tau$$

and (42)

$$D(t) = D_b \quad if\ t > \tau \quad ,$$

where $D(t)$ is the break effective diameter (m), D_b is the final break size (m), and τ is the break time constant (typically 250 ms).

3.1 SMALL LOSS OF COOLANT ACCIDENT

This comparison between RELAP5 (MOD2/VERSION3t) and ANSDM was based on the reactor system responses for a 51-mm-diam break opened in 250 ms. Some of the operational and design parameters used for this simulation are different than those selected for the final conceptual designs. For example, for this transient, the main coolant pumps are not tripped when the reactor scrams. The nominal operating conditions are shown in Table 2.

Table 2. Nominal operation conditions

Parameter	Value	Comments
Fission power	350 MW_f	Total nuclear energy deposited in fuel, structure, and coolant of core and reflector
Core inlet pressure	3.7 MPa	
Core coolant velocity	27.4 m/s	Between fuel plates
Core inlet temperature	49°C	
Accumulator volume	5 m^3	Each of three active accumulators
Accumulator gas volume	0.125 m^3	Each of three active accumulators
Break opening time	250 ms	
Pressure scram setpoint	80%	20% below nominal pressure

3.1.1 Steady State

Input parameters are listed in Tables 3–6. The normalized power density profile is shown in Table 3 based on the I3 fuel grading* at EOC with the preconceptual design uncertainty multipliers. Table 4 lists the relevant core input parameters while Tables 5 and 6 provide the accumulator and inertial flow diode as part of the loop input parameters.

Table 3. Normalized power density of I3 fuel grading at the end-of-cycle

Element zone	Average channel	Hot channel[a]	Hot stripe[b]
		Upper[c]	
5	1.243	1.517	1.991
4	1.252	1.517	1.886
3	1.261	1.566	1.886
2	1.222	1.614	1.965
1	0.991	1.362	1.900
		Lower[d]	
5	0.641	0.864	1.074
4	0.651	0.901	1.218
3	0.686	0.963	1.323
2	0.749	1.034	1.454
1	0.780	1.109	1.546

[a]With multiplier 1.14.
[b]With multiplier 1.31.
[c]Power split at the end-of-cycle (EOC) for the upper core = 0.702 (70.2%).
[d]Power split at EOC for the lower core = 0.294 (29.4%).

When this set of common input parameters was used, favorable agreement was found as shown in Tables 7 and 8. In Table 7, velocities, pressures, and bulk temperatures at key locations show insignificant differences, with the exception of wall temperatures. The discrepancy with wall temperatures can be attributed to different heat transfer coefficients. In the MOD2/VERSION3t, RELAP5 used the Dittus-Boelter correlation and ANSDM used the Petukhov for the single-phase forced convection. The heat transfer coefficient predicted by the Petukhov correlation is higher, which leads to the lower wall temperatures predicted by the ANSDM.

The RELAP5 loop model accounts for form losses resulting from isolation valves, check valves, pipe bends, and flow diodes in addition to wall friction losses over the loop. Because

*I3 is an internal designation representing a particular radial and axial distribution of fissile material within the active fuel region of each fuel plate.

Table 4. Core input parameters

Parameter	Value	Comments
Core mass flow (kg/s) Total mass flow (kg/s)	2053 2463	Core flow consists of the lower and upper average channels. Total mass flow consists of the core flow plus flows in bypass and the control rod channels.
Lower element flow area (m^2) Total core flow area (m^2)	0.02908 0.06922	Annuli cross-sectional areas less corroded fuel plates.
Hydraulic diameter (m)	0.002489	
Fuel surface roughness (μm)	2.0	RELAP5 uses a curve-fitting method to represent the Colebrook friction factor correlation for various flow regions, while ANSDM used Filonenko and Colebrook.

Table 5. Accumulator input parameters

Parameter	Value	Comments
Tank volume (m^3)	5	
Surge line length (m)	5	
Initial liquid volume (m^3) Initial gas volume (m^3)	4.875 0.125	The ratio of the initial liquid to gas volume was set at 40 to prevent the bubble from expanding into the primary coolant.
Pressure (MPa)		
Cover gas inside the accumulator At injection point	1.34 1.45	

Table 6. Inertial flow diode input parameters

Parameter	Value	Comments
Normal flow direction Kc (45° converging nozzle) Ke (10° diverging nozzle)	 0.3061 0.2266	Optimal K factors (with respect to the junction area of 203-mm diam) and nozzle length for the minimum loss of inventory in event of LOCAs[a] to be determined
Reversed flow direction Kc (10° converging nozzle Ke (45° diverging nozle	 0.0697 1.0	

[a]LOCAs = loss of coolant accidents.

Table 7. Core output parameters

Parameter	RELAP5	ANSDM[a]	Comments
Velocity (m/s)			Density variation over heated length ~3%
Average core exit	27.6	27.6	
Hot channel exit, l.c.[b]	26.6	26.15	
Hot channel exit, u.c.[c]	27.2	26.6	
Pressure (MPa)			Breakdown of the core Δp:
Core inlet plenum	3.78	3.76	friction loss = 1.750 MPa
Core inlet, l.c.	3.73	3.70	entrance change = 0.325 MPa
Core outlet, l.c.	1.83	1.82	exit change = –0.204 MPa
Core outlet plenum	1.83	1.81	
Δp over core	1.9	1.88	
Bulk coolant temperature (K)			
Core inlet plenum	323	322	
Core outlet plenum	357	356	
Hot channel outlet, l.c.	372	372	
Hot channel outlet, u.c.	401	401	
Wall temperature (K)			Both models used hot channel exit bulk temperatures as references for hot stripe wall temperature calculations
Hot stripe exit, l.c.	412	405	
Hot stripe exit, u.c.	462.3	452.5	
Heat transfer coefficient ($W/m^2/K$)			RELAP5 used the Dittus-Boelter correlation and ANSDM used the Petukhov for the single-phase forced convection; the heat transfer coefficient predicted by the Petukhov correlation is higher as expected; the higher heat transfer coefficients lead to lower wall temperatures.
Hot channel outlet, l.c.	1.465×10^5	1.8×10^5	
Hot channel outlet, u.c.	1.632×10^5	2.06×10^5	

[a]ANSDM = Advanced Neutron Source dynamic model.
[b]l.c. = lower fuel element.
[c]u.c. = upper fuel element.

ANSDM does not model each component in the heat exchanger loops explicitly, the input must simulate the equivalent losses using discrete concentrated resistance. The RELAP5 and ANSDM pressures at the pump suction and discharge agree quite well when proper concentrated resistance is used in ANSDM (see Table 8).

3.1.2 Transient

After the good agreement in steady-state comparison was established, it was decided to compare results from a small LOCA. A 51-mm-diam break at the interface between the top of the CPBT and the inlet of the hot leg riser was chosen. There is no 51-mm pipe connecting to the primary

Table 8. Main circulation pump output parameters

Parameter	Pressure (MPa) RELAP5	Pressure (MPa) ANSDM[a]
Pressure		
Suction	1.47	1.43
Discharge	4.13	4.09

[a]ANSDM = Advanced Neutron Source dynamic model.

coolant pressure boundary in this region, so the chosen break actually represents a rapidly opening crack in the CPBT or hot leg riser, which has a much larger diameter.

The overall transient response (see Figs. 4–12) agrees well in both shape and magnitude of key parameters with the exception of accumulator injection mass flow (see Fig. 12 and discussion below). The transient results are displayed on log-log or semi-log scales to allow detailed comparisons of thermal hydraulic behavior at all times between the break initiation and the end of the 30-s period of interest. The total power, which consists of neutron flux and decay heat, compares excellently as shown in Fig. 4. Both the neutron flux and the decay heat agree well before the scram and disagree insignificantly during post scram period, indicating that both models correctly implement their similar point kinetics models and reactivity profiles after scram.

The break flow is compared in Fig. 5. RELAP5 shows a slowly increasing but highly oscillatory break flow in the first 50 ms as opposed to the smooth and flat behavior predicted by ANSDM. After 50 ms, discrepancy in break flows starts to diminish until the break is fully opened at 250 ms. Beyond that, the maximum deviation remains <6%. The initial oscillatory behavior is a time-step-dependent numerical artifact that does not affect other predictions. It has been observed for other small LOCA calculations.[23] Investigations reveal that the time-averaged flow out of the break is independent of time steps used.

Heat fluxes at hot spots for the upper and lower cores, respectively, are compared in Figs. 8 and 9. In each plot, the lower pair of curves are local surface heat flux at the hot spot whereas the upper pairs are the limiting heat flux as predicted by the Costa correlation. Both models predict the correct trend in that the Costa limiting heat flux declines slowly during initial depressurization and reaches a minimum after scram. After scram, the allowable heat flux increases rapidly because of the corresponding rapid increase in coolant subcooling. For additional information, the CHF limiting heat flux at the hot spot calculated by the Gambill/Weatherhead correlation is included.

Makeup and letdown flows are compared in Fig. 11. Early in the transient, the makeup flow should be balanced by the letdown flow as correctly predicted by RELAP5 and ANSDM. Both models predict a constant makeup flow up to ~4 s into the transient and followed by a rapid increase caused by the start of the standby makeup pump. Also, both models predict a somewhat similar trend for the letdown flow from the nominal to zero (with the valve fully closed) flow as the system pressure continues to decline. Fluctuations (local pressurization and depressurization) in the letdown flow predicted by RELAP5 appear to respond to pressure fluctuations at the CPBT inlet and outlet when the break is fully opened (see Fig. 7).

Two significant differences in the injection flow from accumulator to primary coolant piping can be observed in Fig. 12. The ANSDM injection flow leads the RELAP5 injection by 50 ms or more during the initial depressurization because RELAP5 accounts for the finite acoustic propagation

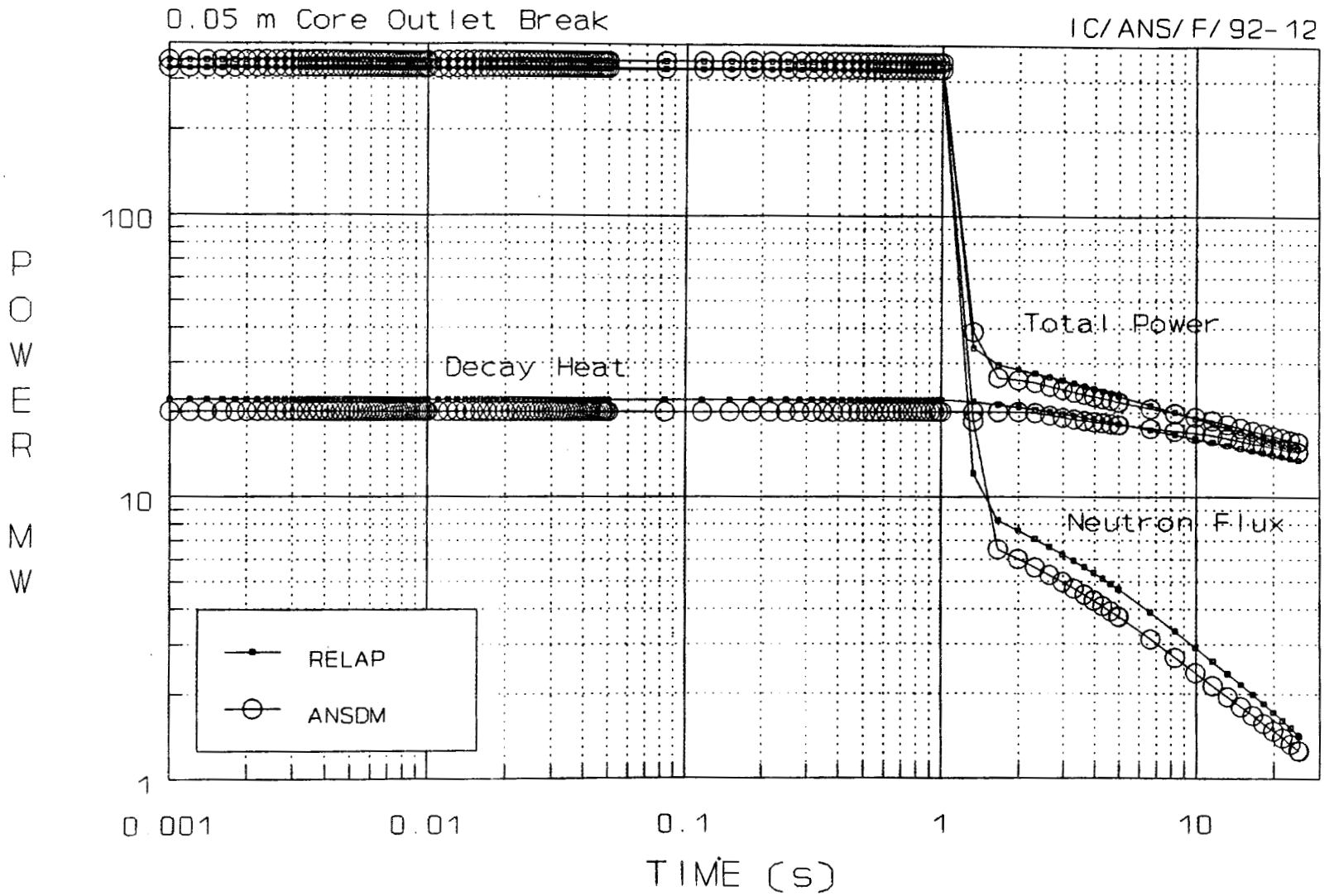

Fig. 4. Comparison in fission, decay, and total power during the 51-mm-diam core pressure boundary tube break with 250-ms opening time.

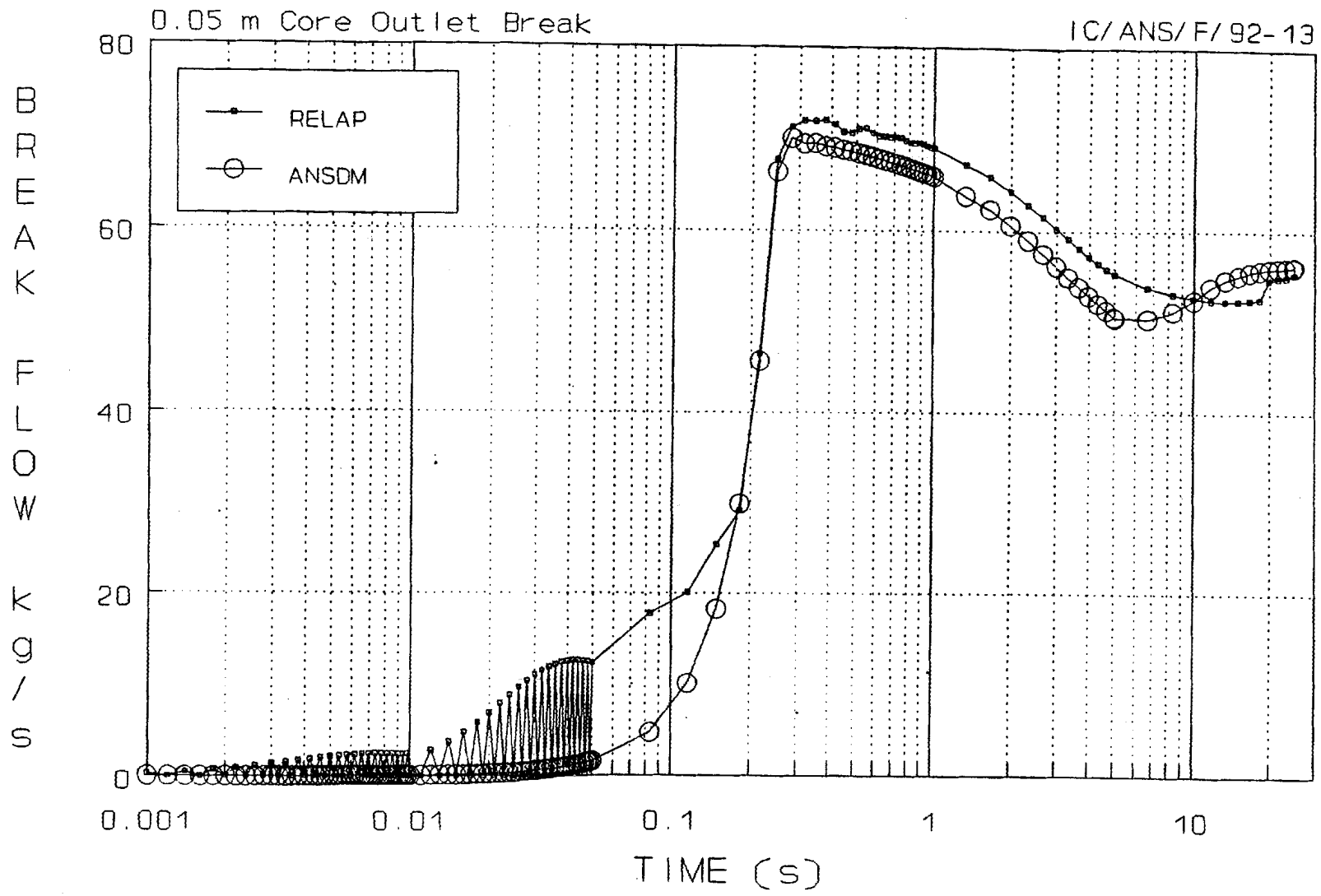

Fig. 5. Break flow comparison during the 51-mm-diam core pressure boundary tube outlet break with 250-ms opening time.

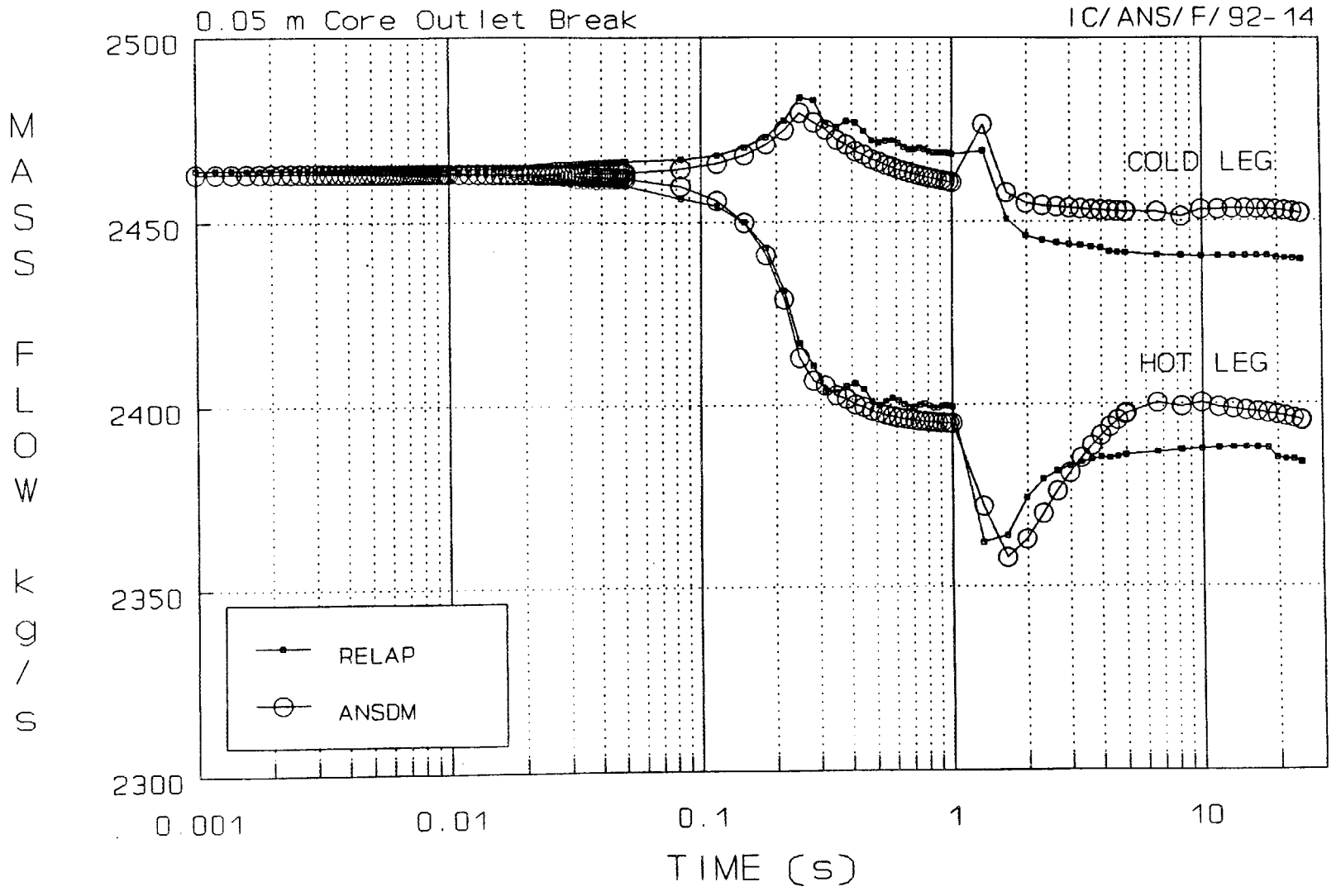

Fig. 6. Mass flow comparison at locations upstream and downstream of the break during the 51-mm-diam core pressure boundary tube outlet break with 250-ms opening time.

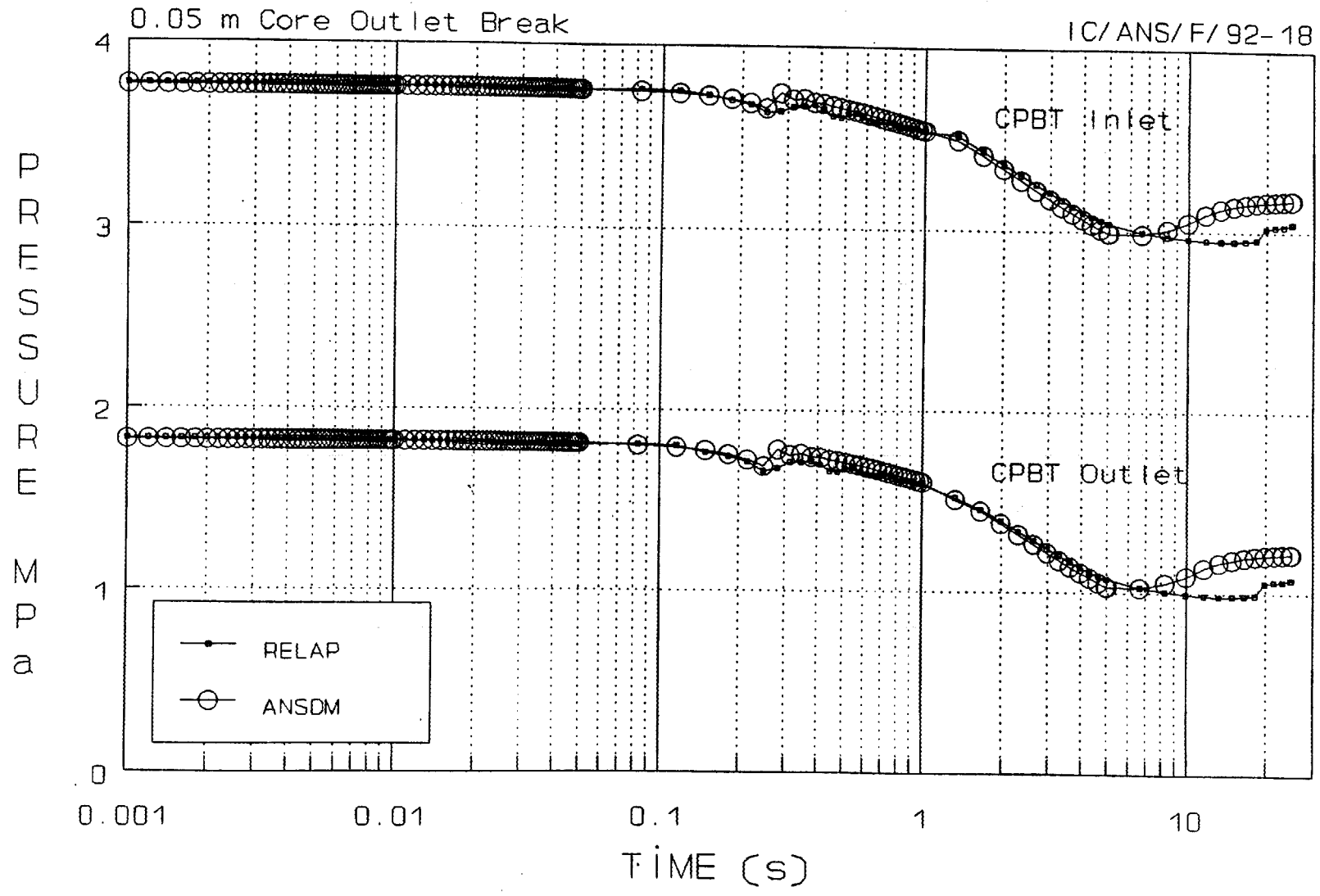

Fig. 7. Comparison in pressure responses at the core pressure boundary tube (CPBT) inlet and outlet during the 51-mm-diam CPBT outlet break with 250-ms opening time.

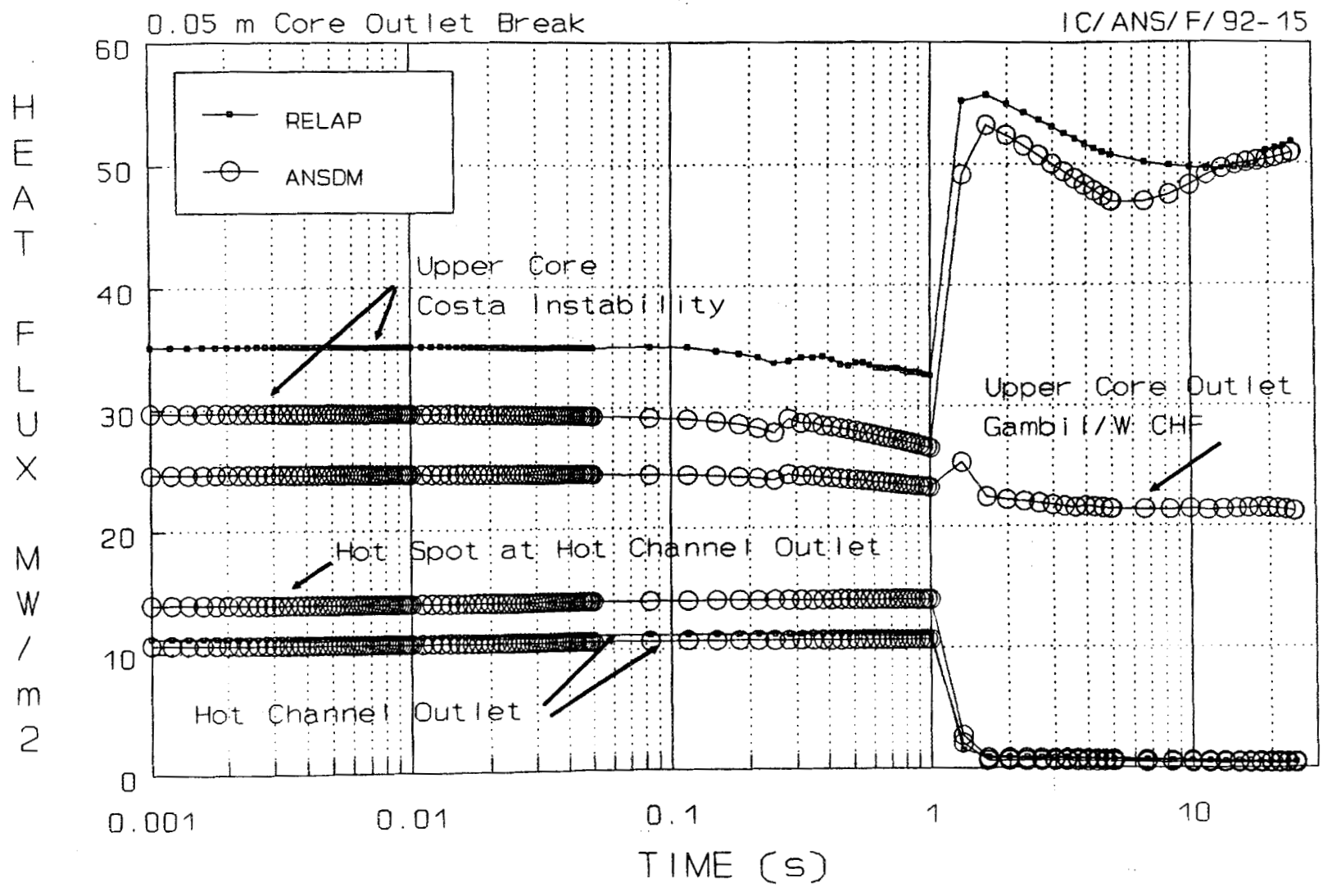

Fig. 8. Heat flux comparison at the hot spot of the upper core showing Costa, Gambill/Weatherhead, and local surface heat fluxes during the 51-mm-diam core pressure boundary tube outlet break with 250-ms opening time.

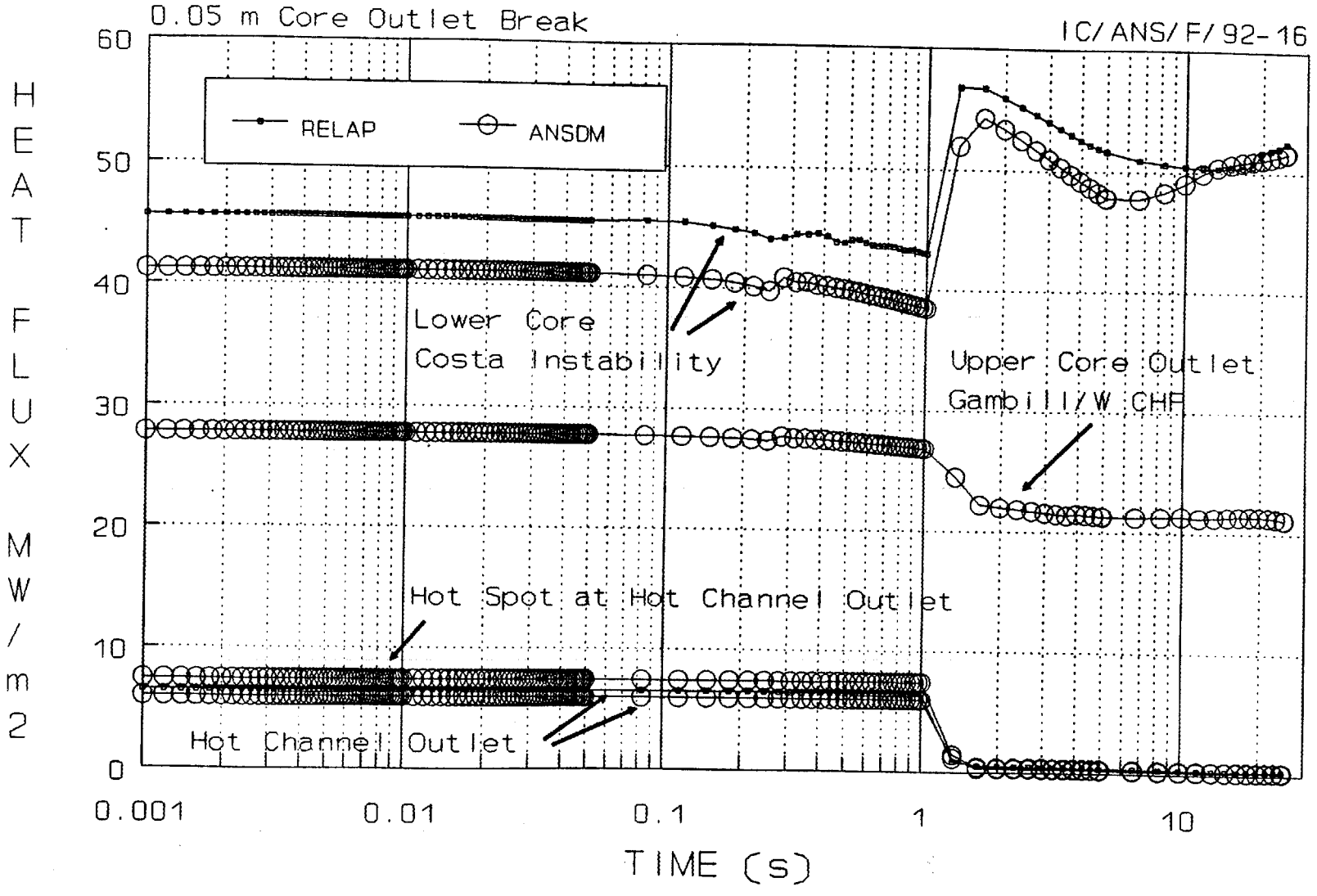

Fig. 9. Heat flux comparison at the hot spot of the lower core showing Costa, Gambill/Weatherhead, and local surface heat fluxes during the 51-mm-diam core pressure boundary tube outlet break with 250-ms opening time.

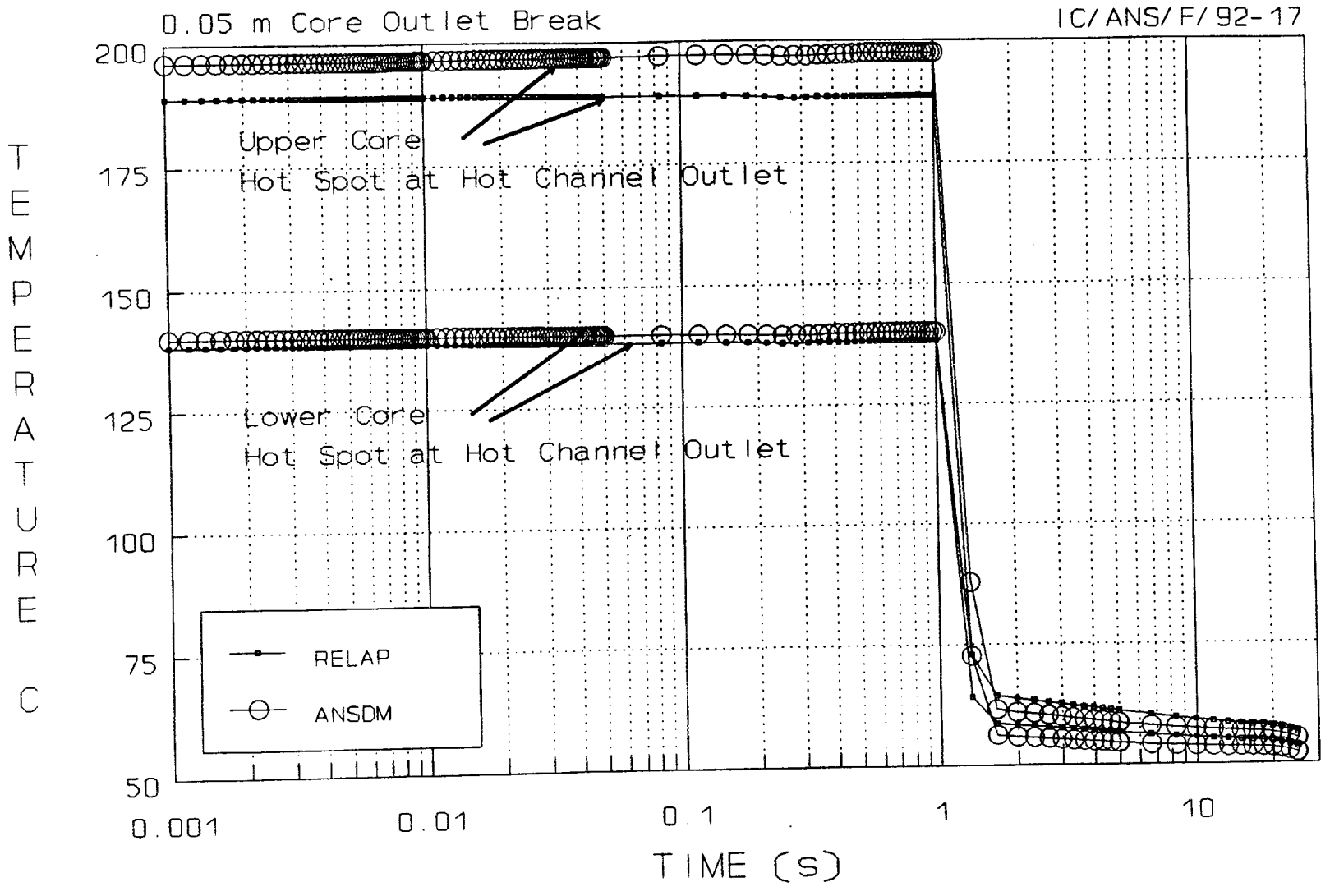

Fig. 10. Comparison in bulk coolant temperature at the hot channel outlet for the lower and upper cores during the 51-mm-diam core pressure boundary tube outlet break with 250-ms opening time.

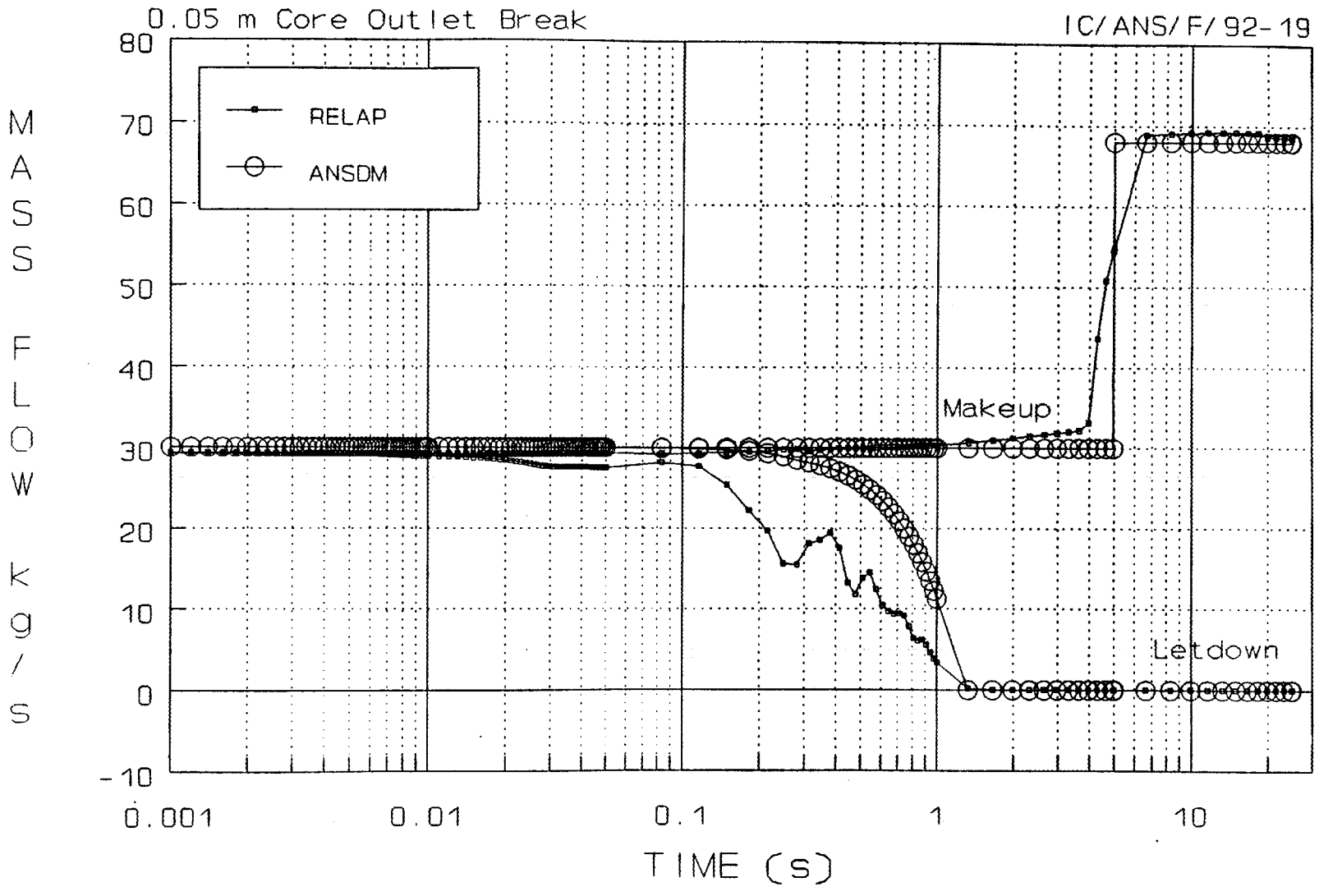

Fig. 11. Makeup and letdown flow comparison during the 51-mm-diam core pressure boundary tube outlet break with 250-ms opening time.

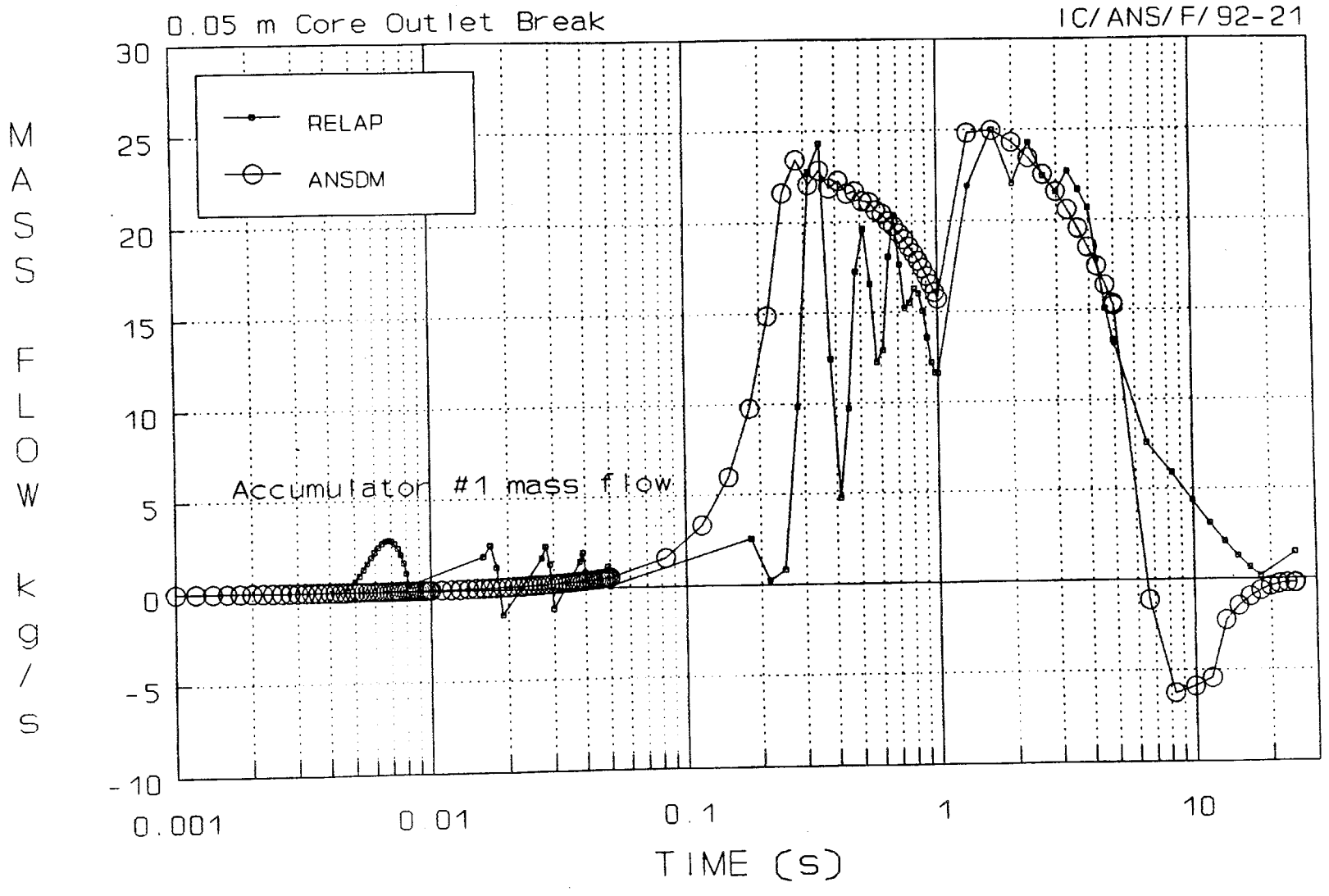

Fig. 12. Accumulator injection flow comparison during the 51-mm-diam core pressure boundary tube outlet break with 250-ms opening time.

velocity while it is assumed to occur instantaneously in ANSDM. After the initial depressurization, ANSDM predicts a period of negative injection (i.e., flow back into the accumulators) that is not observed on the RELAP5 trace. This period is not observable because the version of RELAP5 used for particular calculation has a default accumulator model that allows no return flow of primary coolant from piping back to the accumulators.

3.1.3 Discussion

The small break comparison was performed using RELAP5/MOD2/VERSION3t before the ANSR updates, including the three modifications described in Sect. 2.1.1, were available. As noted in Sect. 3.1.1, this caused a difference in wall temperatures of the fuel plates at steady-state conditions. The updated version RELAP5/MOD3/VERSION7AC became operational after the 51-mm break comparison was completed, and is the version used for the remaining comparisons as presented in Sects. 3.2–3.4.

The inability of RELAP5 to allow backflow of primary coolant from the coolant system to the accumulators is the result of an implicitly built-in check valve within the tank for the RELAP5 default accumulator model. This limitation was removed subsequent to the small break comparison. A new accumulator model using pipe components with appropriate heat structures for wall heat transfer has been developed and is used for the remaining comparisons of Sects. 3.2–3.4.

3.2 STATION BLACKOUT ACCIDENT

A hypothetical, beyond-design-basis accident that includes a station blackout, a coincident loss of the pony motors, and a small LOCA resulting from a stuck open letdown valve has been simulated to allow comparison of predicted core cooling performance under depressurized, natural circulation conditions.

The station blackout (i.e., a loss of off-site power with failure of emergency diesel generators to start) is assumed to initiate the following events simultaneously: (1) main circulation pump trips and begins coastdown to zero speed; (2) main and standby pressurizing pumps begin coasting down to a stop; and (3) letdown isolation is initiated by a low core inlet pressure signal, and secondary coolant flow is lost. The main circulation pumps are tripped concurrently with the low pressure reactor scram, and they coast down over a time period determined by the balance between pump torque and inertia.

The initial conditions for the station blackout comparison are based on a reduced power and flow operating condition studied during the post-conceptual design report (CDR) period as shown in Table 9.

3.2.1 Steady State

The steady-state comparison for the power of 208.4 MW is presented in Table 10. The overall comparison agrees satisfactorily. The good agreement in the core pressure drop (difference between the core inlet and outlet pressure) requires the use of the Colebrook correlation. RELAP5 uses the Colebrook correlation that is calculated by a curve-fitting as a function of flow regimes, while ANSDM uses the Filonenko correlation. The accuracy of the curve fitting was evaluated and improved by INEL; however, updates were not available in time for this study.

Table 9. Initial conditions for a station blackout comparison

Parameter	Value	Comments
Fission power	208.4 MW_t	104.2% with 200 MW_t nominal
Core inlet pressure	2.41 MPa	95% of nominal
Core coolant velocity	17.0 m/s	Between fuel plates
Core inlet temperature	45.62°C	0.6°C above nominal
Accumulator volume	5 m^3	Each of three active accumulators
Accumulator gas volume	0.1 m^3	Each of three active accumulators
Pressure scram setpoint	80%	20% below nominal core outlet pressure

3.2.2 Transient

The sequence of events for the station blackout is shown in Table 11. Total (fission plus decay heat) power generated by the two models is compared in Fig. 13. The good agreement in power is consistent with the good agreement in reactor scram time. After that, both models agree to within 1% of the nominal power to the end of calculations.

Figure 14 compares the coolant temperature at the lower core hot-channel outlet. RELAP5 calculates a significantly warmer hot channel outlet temperature than ANSDM during the decay heat phase of the transient, even though both models agree fairly well at steady-state conditions, and RELAP5 calculates an ~15% lower total decay heat level. Since the total core power and flow velocities agree, this difference arises from the way in which the two codes distribute the decay heat to various core regions (control rods, reflectors, and core). ANSDM deposits ~94% of the power in the fuel plate during full power operation, but only ~65% during decay heat conditions because many of the gamma rays leave the fuel element. The RELAP5 model deposits the same percentage of power (~94%) in the fuel plate during full power operation as it does during decay heat conditions. Although the ANSDM distributions are probably more accurate, the RELAP5 approach is conservative. For the purpose of this benchmark effort, the ANSDM distributions were modified to agree with these assumed by RELAP5. With these modifications, both models agree satisfactorily as shown in Fig. 15. The remaining comparisons below were computed using the temporarily modified ANSDM inputs.

Main circulation pump speed during coastdown is compared in Fig. 16. ANSDM initially exhibited a much longer coastdown time because zero friction is assumed during coastdown. RELAP5 assumes that friction torque is ~2% of the nominal torque. When ANSDM input was reprogrammed to use the RELAP5 friction torque, the two models agreed very well not only in the pump coastdown but also in the average core coolant velocity (Fig. 17) and total core coolant mass flow (Fig. 18). A small mismatch between 25 and 150 s induces a mismatch in outlet temperatures as shown in Fig. 15.

Comparison in depressurization rate (see Fig. 19) at the lower core exit shows that the results differ within 10–20%. This difference is explained by the differences in the letdown system modeling and the fact that a perfectly isothermal gas expansion inside the accumulator is assumed in ANSDM, while RELAP5 calculates nearly adiabatic behavior. In this comparison, the volume of each of the

Table 10. Steady-state comparison for 200-MW nominal core

Parameter	RELAP5	ANSDM[a]	PRSDYN
Fission power (MW)	208.4	208.4[b]	208.4[b]
Total mass flow (kg/s)	1336	1336[b]	1336[b]
Coolant velocity at fuel element inlet (ms/s)	17.0	16.9	16.7
Core inlet temperature (°C)	45.8	45.6	45.4
CPBT outlet temperature (°C)	81.2	81.8	81.3
Hot channel outlet temperature in lower element (°C)	130	128.6	127.5
Lower element outlet saturation temperature (°C)	203	201	202.7
Core inlet pressure (MPa)	2.41	2.40[b]	2.40[b]
Core outlet pressure (MPa)	1.65	1.66[c]	1.64[c]
Main coolant pump inlet pressure (MPa)	1.50	1.51	1.54
Main coolant pump outlet pressure (MPa)	2.45	2.43[d]	2.43[d]
Lower element hot channel heat flux at outlet (MW/m^2); includes 95% flow excursion uncertainty	3.29	3.15	3.2
Costa flow excursion limit at lower element hot channel outlet (MW/m^2)	22.97	23.14	23.5

[a]ANSDM = Advanced Neutron Source dynamic model.

[b]Input as parameter for benchmark.

[c]Requires use of Colebrook & White friction correlation. Using Filonenko, the pressure drop is 15% smaller.

[d]Pressure drops in cold leg adjusted upwards to account for unmodeled check valves, isolation valves, and pipe blends.

three accumulator tanks includes 4.9 m^3 of heavy water and 0.1 m^3 of nitrogen gas. If ANSDM is reprogrammed to assume an adiabatic gas expansion, the ANSDM and RELAP5 pressures agree satisfactorily, as illustrated in Fig. 20.

Since ANSDM was, as discussed above, temporarily modified so that it would distribute decay heat in the same manner as RELAP5, the long term ($t > 100$ s) natural circulation velocity and hot leg temperature match relatively well (see Figs. 15 and 17). This match is independent of the pump coastdown characteristics. Such good agreement indicates that both codes provide fairly consistent results on the low velocity pressure drops and temperature distributions.

Table 11. Sequence of events for station blackout benchmark

Time	RELAP5	ANSDM[a]
0	Initialize reactor power to 208.4 MW (200 nominal at 104.2%), and 16.7 m/s coolant velocity	Initialize reactor power to 208.4 MW (200 nominal at 104.2%) and 16.7 m/s coolant velocity
0	Trip makeup pump	Trip makeup pump; flow decays exponentially as exp (–t/0.5)
0	Isolate secondary; flow reduced linearly to zero in 10 s	Trip secondary coolant pumps; flow reduces exponentially as exp (–t/2)
		Artificially reduce secondary coolant loop elevation to 0.1 m to minimize natural circulation and model the isolation approximately
0	Fail the three letdown values "as is"; inhibit block valve from closing on low pressure	Fail the three letdown valves "as is"; inhibit block valve from closing on low pressure
6.74	RELAP5 detects low pressure scram conditions	
6.74	Main coolant pumps tripped; coastdown to zero speed in ~25 s	
6.76		ANSDM detects low pressure scram conditions
6.76		Main coolant pumps tripped; coastdown to zero speed in ~25 s
7.02		Inner control rods fully inserted from critical position at BOC[b]
7.09		Outer rods fully inserted

[a]ANSDM = Advanced Neutron Source dynamic model.
[b]BOC = beginning-of-cycle.

3.2.3 Discussion

The FE and CHF thermal limit ratios at the hot spot for the lower core are shown only for RELAP5 calculations in Fig. 21. Because the Costa FE limiting heat flux is always significantly higher than the actual heat flux at the lower core hot spot, it may be concluded that the core survives this station blackout transient without violating any safety margins. During this transient, there are two points of minimum margin—the first minimum occurs right after the reactor scrams (~6.7 s into the transient), and the second minimum occurs at the transition (~40 s into the transient) from forced convection to natural circulation.

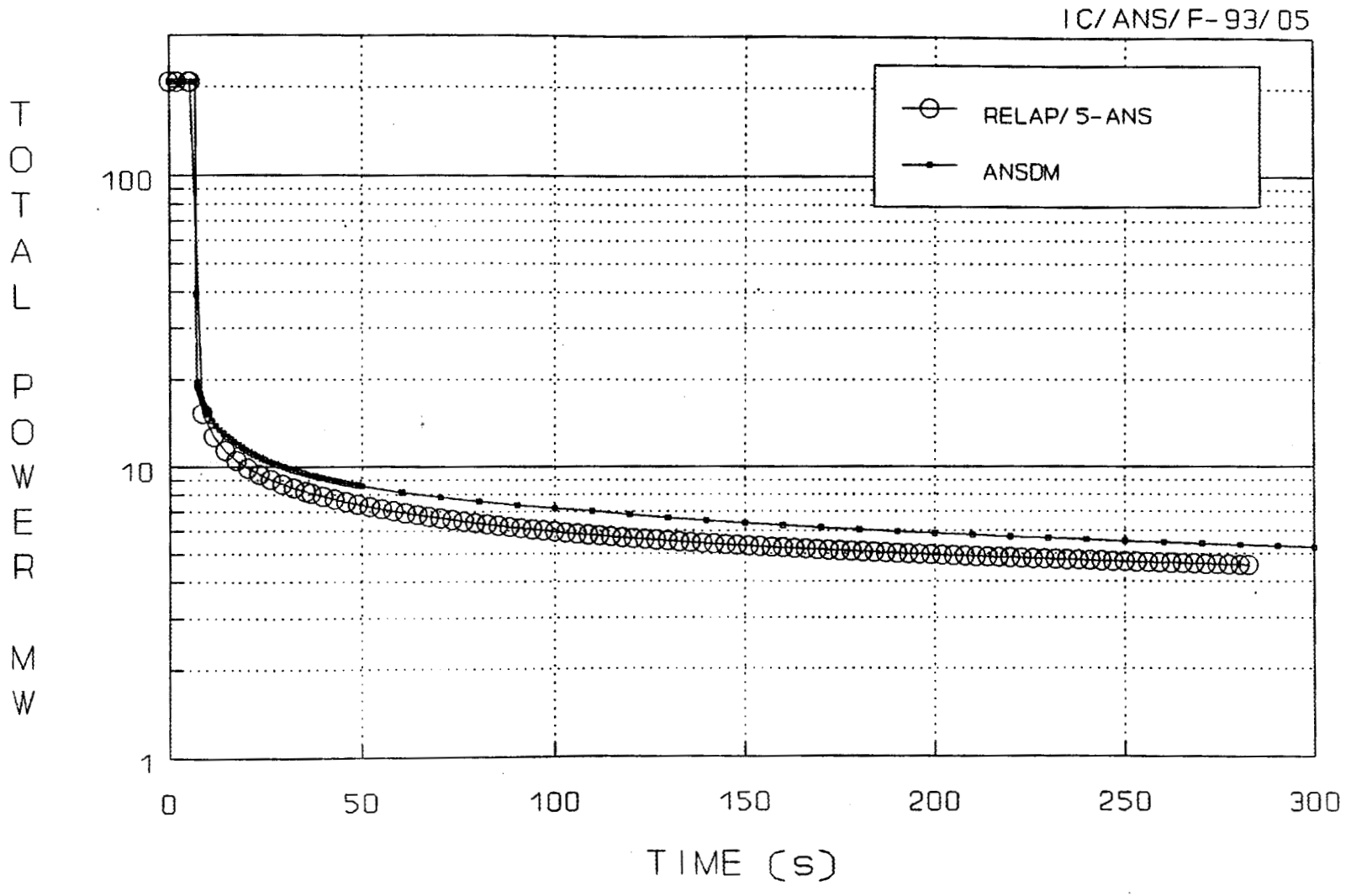

Fig. 13. Total (fission plus decay heat) power generated in the two models during the station blackout accident.

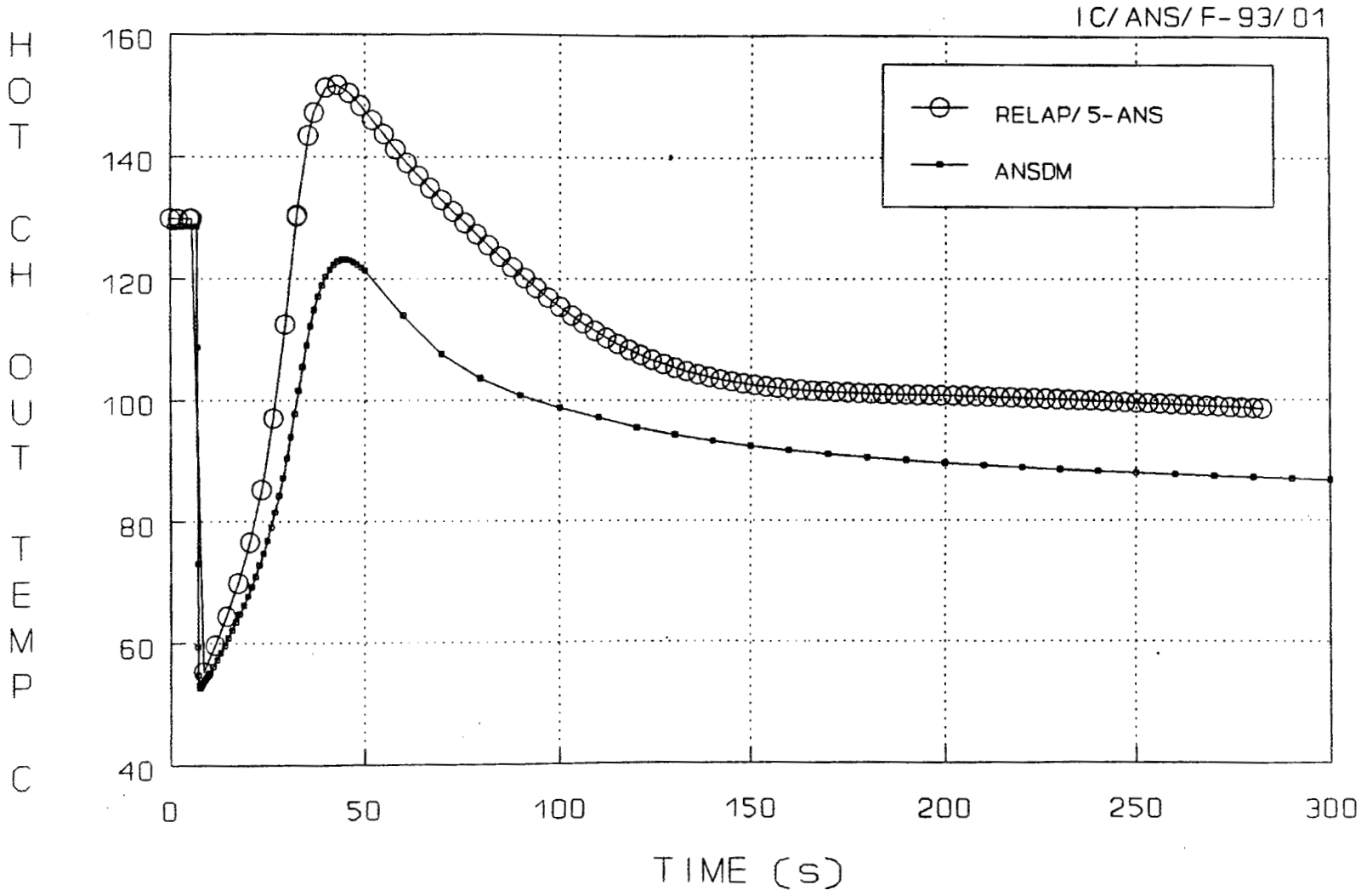

Fig. 14. Comparison in coolant temperature at the lower-core hot-channel outlet during the station blackout accident. (The Advanced Neutron Source dynamic model deposits only 65% of the decay heat on the fuel plate, whereas the Advanced Neutron Source reactor RELAP5 model deposits 94%.)

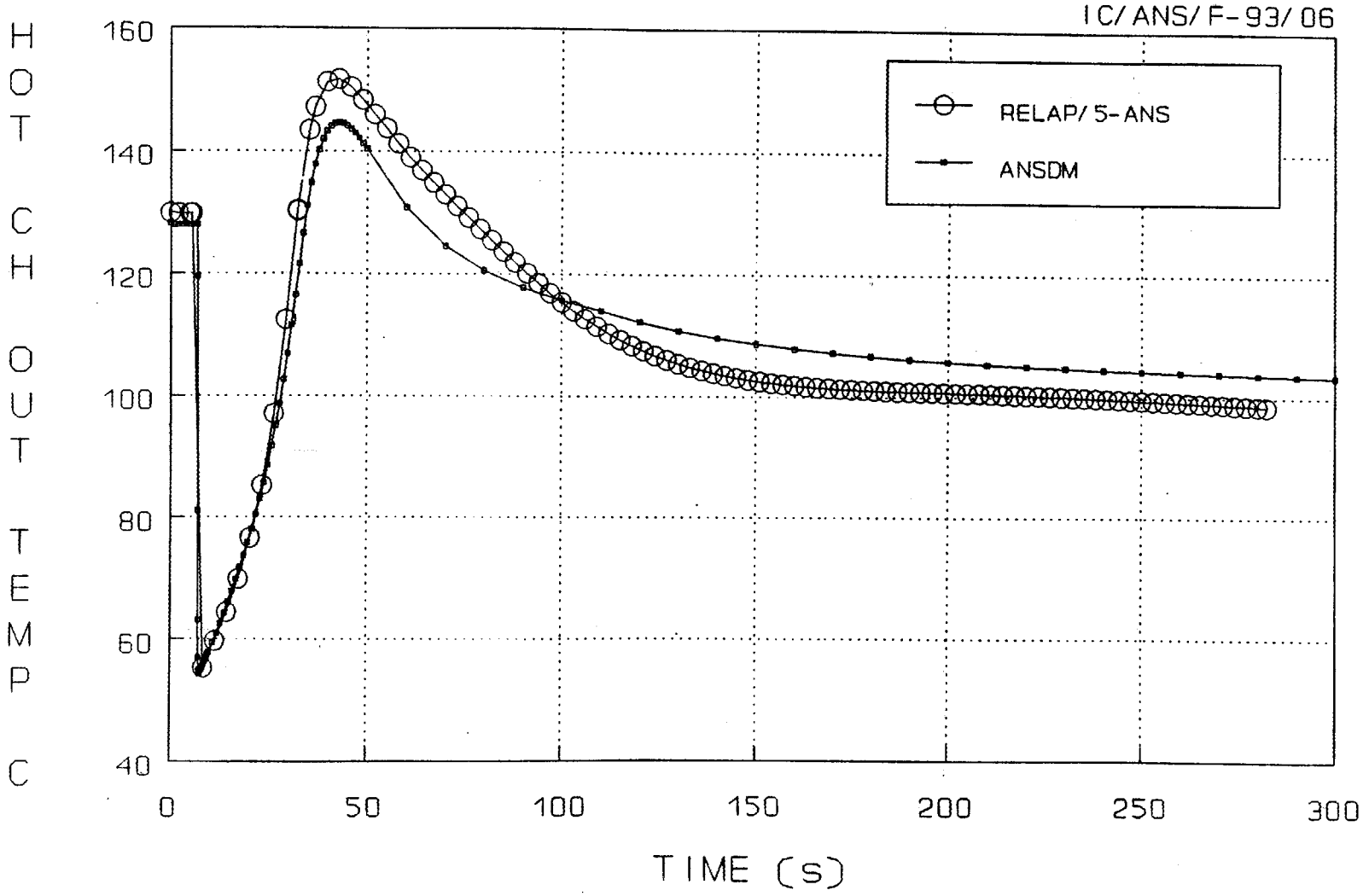

Fig. 15. Coolant temperature at the lower-core hot-channel outlet during the station blackout accident. If the Advanced Neutron Source dynamic model assumes regional distribution of decay heat power similar to RELAP5's, both models agree satisfactorily.

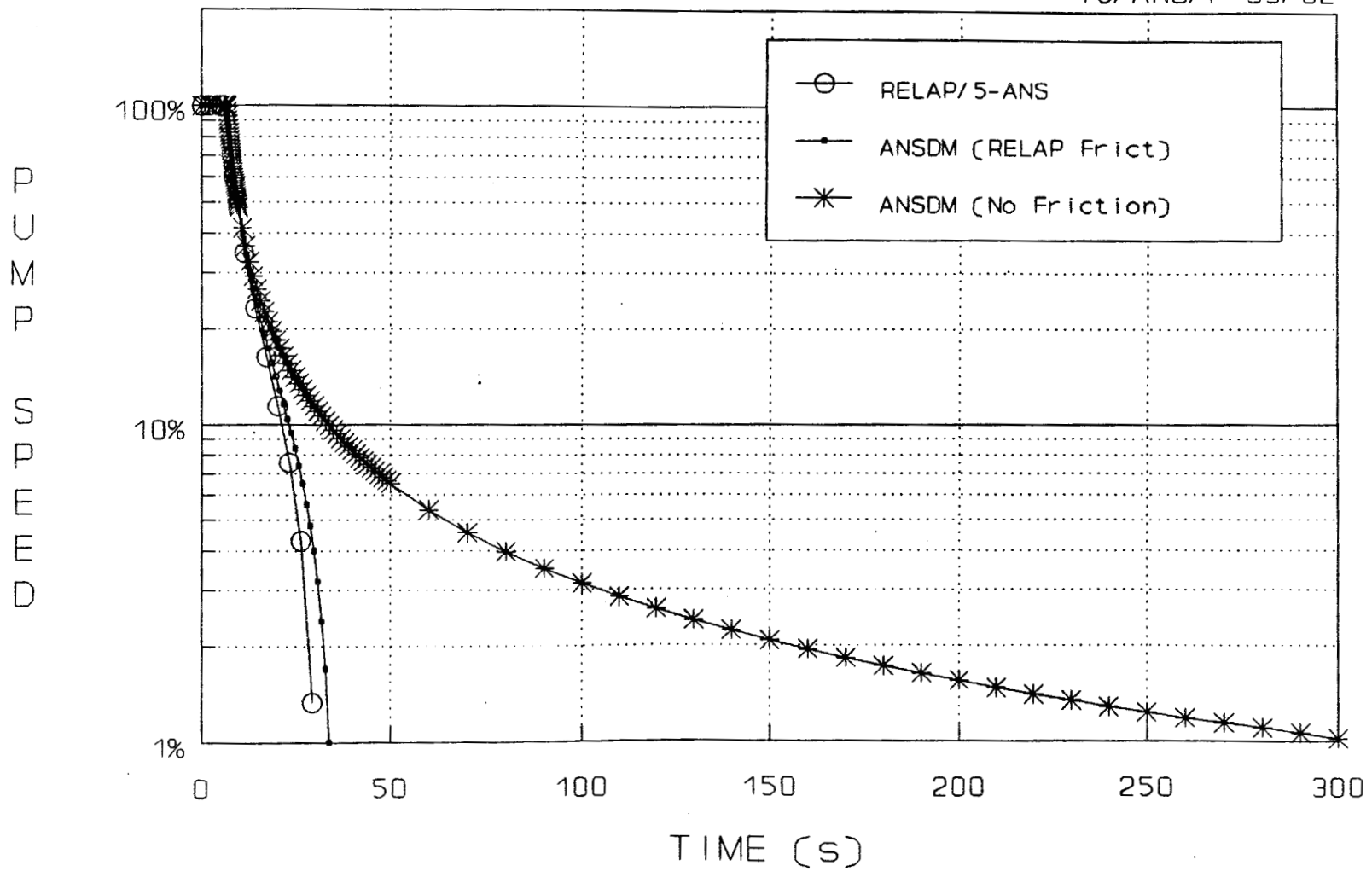

Fig. 16. Main circulation pump castdown speed during the station blackout accident. [Depending on assumed friction, pump coastdown characteristics below pony speed (10–15%) differ significantly.]

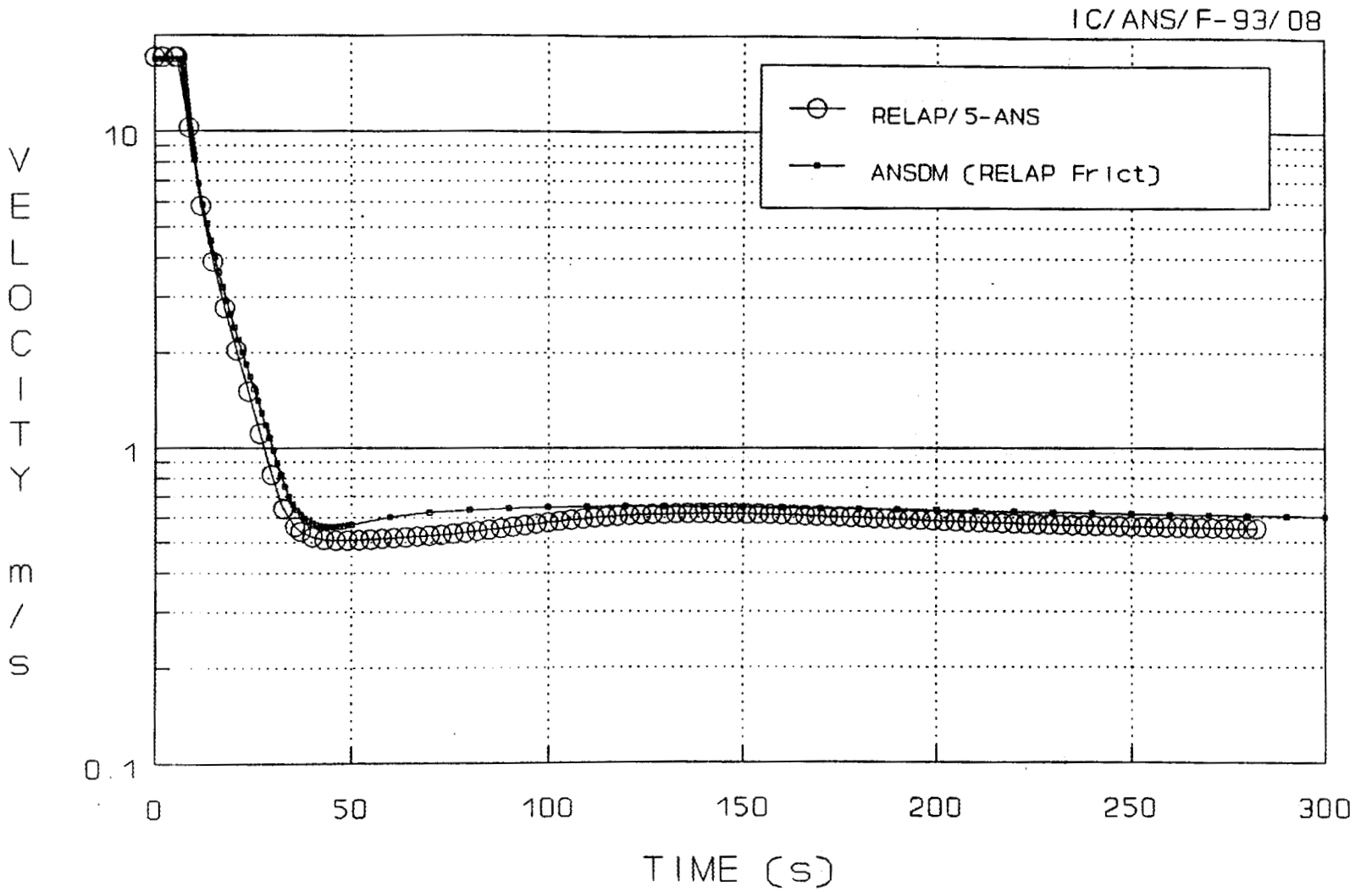

Fig. 17. Core coolant velocity during the station blackout accident. (There is good overall agreement when the Advanced Neutron Source dynamic model used RELAP pump friction, but a small mismatch between 25 and 150 s induces a mismatch in outlet temperatures.)

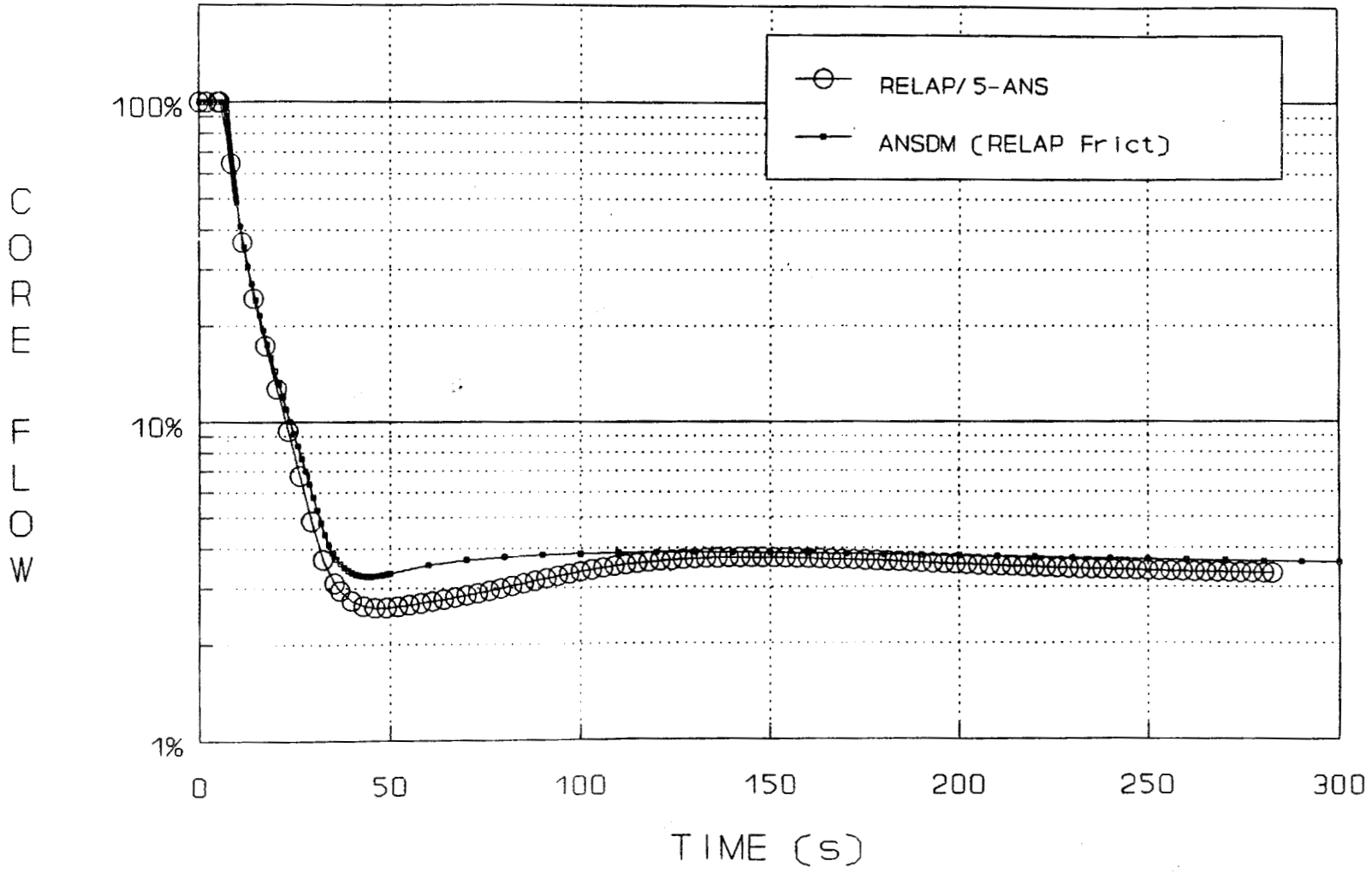

Fig. 18. Core coolant mass flow during the station blackout accident. (There was good overall agreement when the Advanced Neutron Source dynamic model used RELAP pump friction, but a small mismatch between 25 and 150 s induces a mismatch in outlet temperatures.)

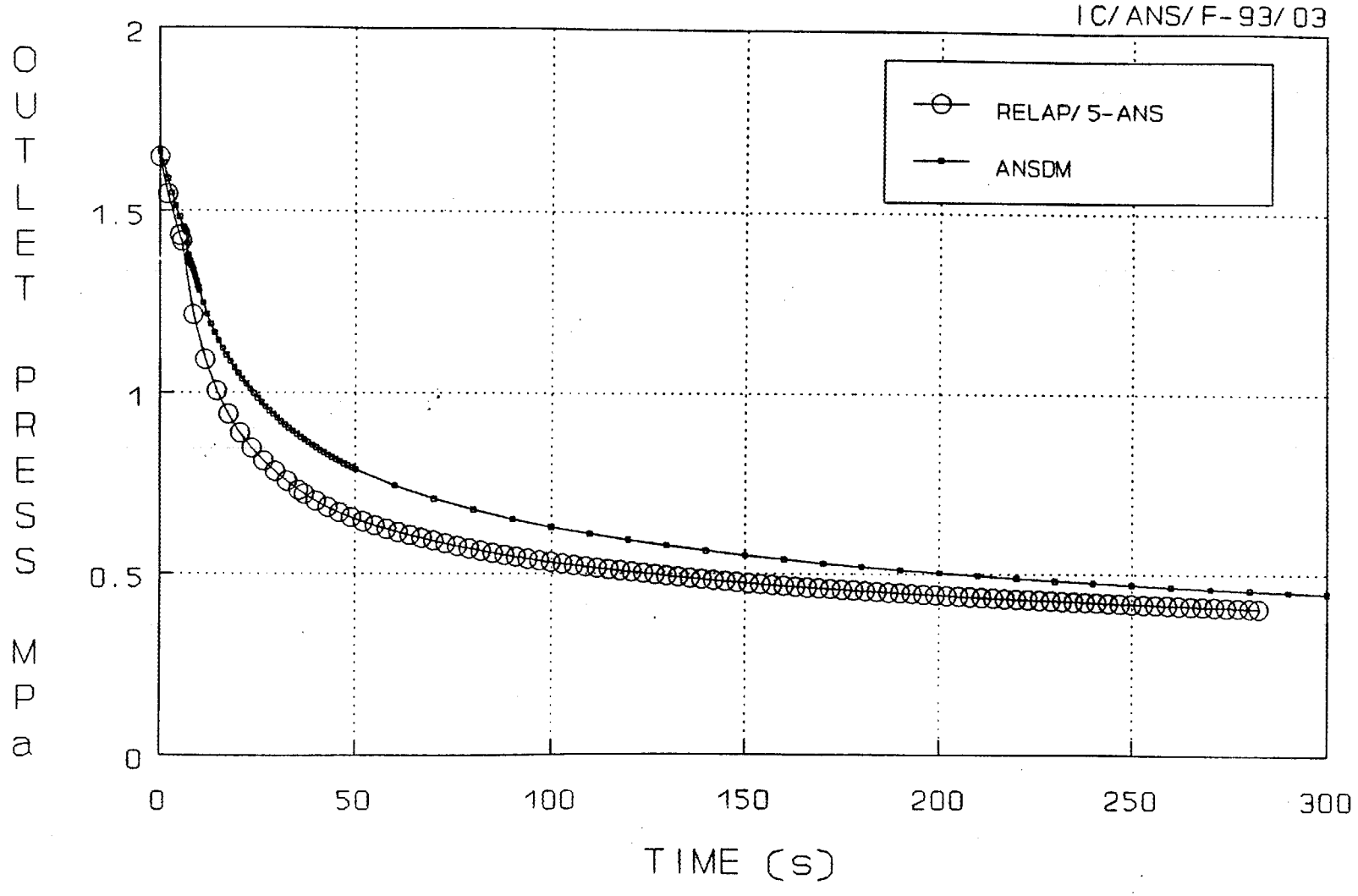

Fig. 19. Comparison in core outlet pressure during the station blackout accident. (The Advanced Neutron Source dynamic model assumes a perfect isothermal accumulator; the RELAP5 accumulator is not perfectly isothermal.)

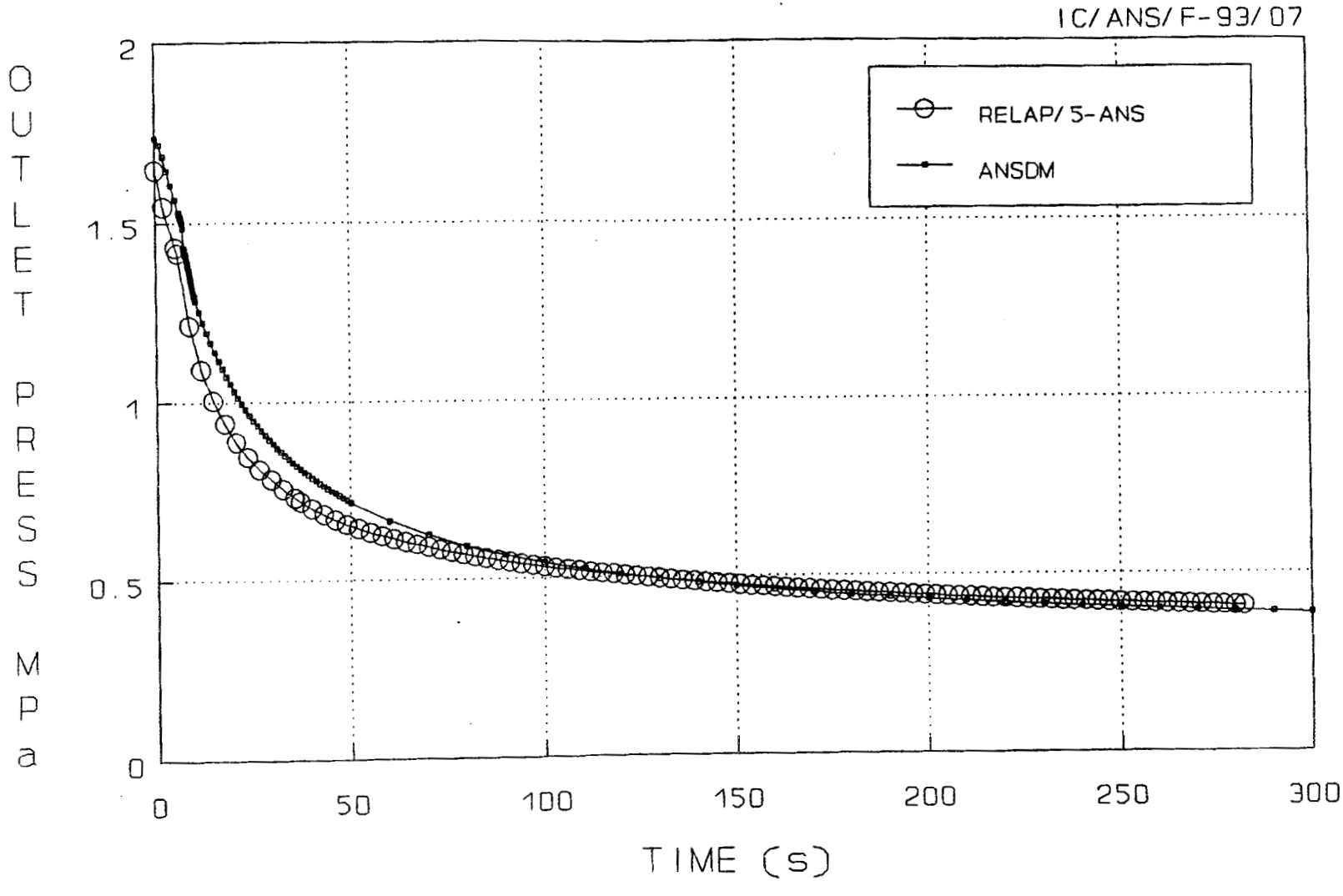

Fig. 20. Comparison in core outlet pressure during the station blackout accident. [If the Advanced Neutron Source dynamic model models an adiabatic accumulator (with 0.1 m^3 gas volume), the pressures agree satisfactorily in both models.]

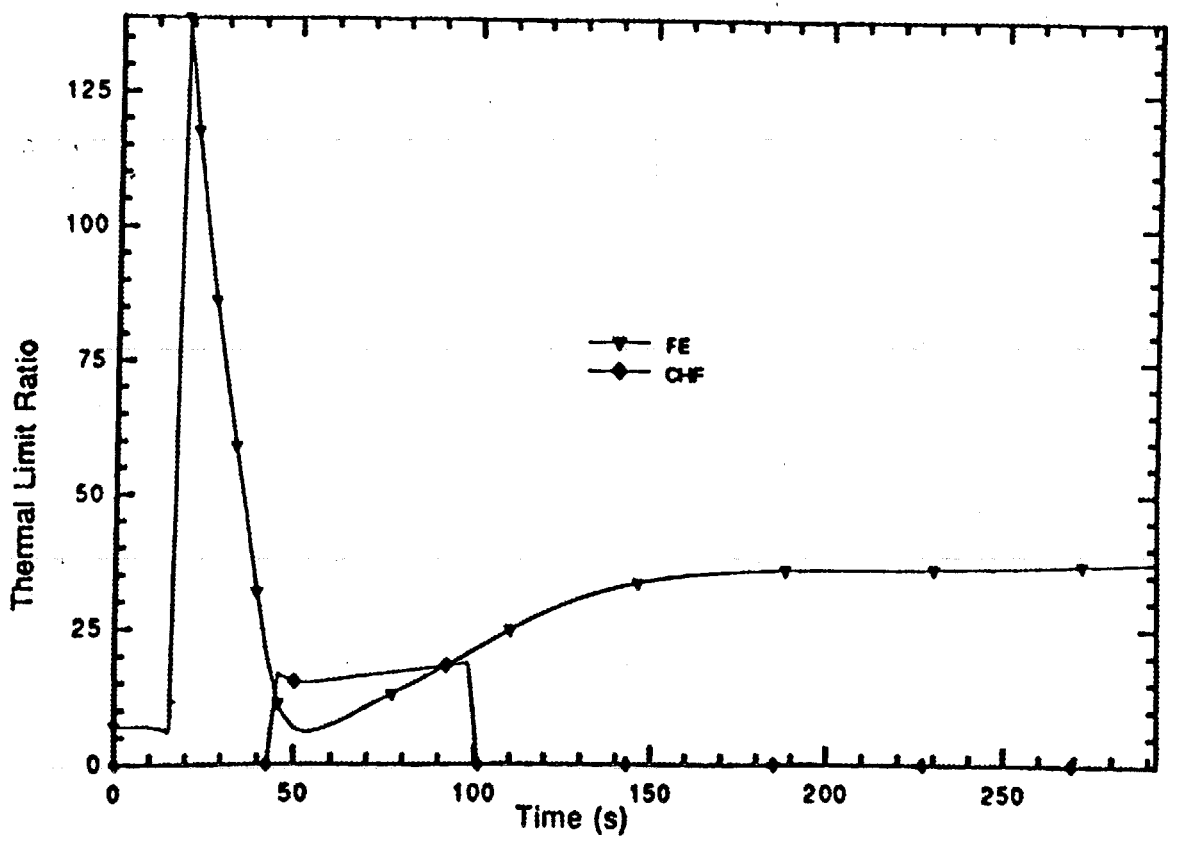

Fig. 21. RELAP5-calculated thermal limit ratios during the station blackout accident. (Note that the critical heat flux values are not printed out by RELAP5 if the wall temperature stays below the local coolant saturation temperature.)

Core survivability during natural circulation critically depends on decay heat power and pump coastdown characteristics. All ANSR models agree to within 1% as to the nominal power following shutdown, but differences arise in the regional distribution (i.e., the fraction of decay heat that is deposited in the core, reflector, and control rod bypass regions) of post-shutdown heat load. The heat load distribution is significantly different depending on whether the power originates from fission (where most power remains in the fuel plate) or from decay heat (where ~50% of the gamma-ray energy leaves the fuel plate). For this reason, different regional distribution values for fission power than for decay heat levels are used in ANSDM. In this way, ~94% of the power at nominal (100%) conditions remains in the fuel plate, but only ~65% of the power remains in the plate at decay heat levels.

The ANSR RELAP5 model uses the same regional distribution values for nominal power than for decay heat levels, so that ~94% of RELAP5's power remains in the fuel plate during decay heat. The ~65% decay heat power used in ANSDM was extrapolated from numbers used in the ILL reactor (see Table 12). More accurate ANSR-specific MCNP results calculated by INEL following the CSAR activities indicate that the decay heat distribution is closer to 72% in the core, 13% in the reflector, and 15% in the CPBT bypass. For this benchmark effort, the input to ANSDM was modified to simulate the constant regional power distribution used in RELAP5, which is conservative.

Table 12. Post-scram decay heat regional distribution extrapolated from the Institut Laue-Langevin

Type of power	Reflector (%)	Bypass C.R.[a] (%)	Core (%)
Fission	4.40	2.14	93.46
Decay heat	8.64	26.36	65

[a]C.R. = control rod channel.

The pump coastdown characteristics are very relevant to natural circulation results. However, no ANSR-specific pump data are currently available. Given the lack of data, all natural circulation results performed to date should be viewed cautiously, particularly between 20 and 100 s into the transient. The closest approach to the safety limit occurs during this period where transition from forced convection to natural circulation takes place.

Accumulator performance affects the depressurization rate significantly. An accumulator with isothermal gas expansion responds faster than an adiabatic accumulator for a given pressure change. A rapid response results in a higher injection. Consequently, the pressure can be maintained higher at the hot spot where the thermal criteria is the most limited. In the comparison, both ANSDM and PRSDYN use analytical expressions for an ideal gas expansion, whereas the ANSR RELAP5 model uses a fixed nodalization grid to account for the gas-liquid interface heat transfer and wall heat transfer. However, the RELAP5 model can not account for the thermal and hydrodynamic effects of the honeycomb insert of the isothermalizer design. The baseline ANSR conceptual design includes the isothermalizer packing material inside the accumulators.

3.3 LARGE LOSS OF COOLANT ACCIDENT

This is a post-CSAR comparison among three models (RELAP5, ANSDM, and PRSDYN) for a slow-opening (1.1 s) large DEG break at the core inlet. The break is located downstream of the inertial flow diode but upstream of the primary supply vessel adapter weldment (PSVAW). For ANSR, this is the worst possible location for a large break. Although ANS staff members do not believe that large breaks are credible, a large, beyond-design-basis DEG break was postulated for this analysis to demonstrate that cooling can be maintained during and after a large break that does open fully and with some rapidity. As illustrated in Fig. 22, the PSVAW is the component where the four cold legs combine and flow is routed into the core region.

For conceptual safety analysis, the policy for all events has been to modify the initial conditions from nominal (in the conservative direction) by the amount necessary to account for measurement error and routine control variations. The conservative direction to perturb the initial conditions is generally in the direction of decreasing CHF—higher power and coolant temperature and lower coolant pressure and flow.

The parameters shown in Table 13, modified for typical safety analysis conservatisms to account for routine process control variations and heat balance error, are important to this analysis.

Table 13. Parameters for a large loss of coolant accident

Parameter	Value	Comments
Fission power	344 MW_t	104.2% of 330 MW_t nominal (includes all heat deposited in fuel, structures, coolant, and reflectors)
Core inlet pressure	3.22 MPa	Nominal
Core coolant velocity	25.0 m/s	Between the fuel plates
Core inlet temperature	45.6°C	0.6°C above nominal
Accumulator volume	7.52 m^3	Each of three active accumulators
Accumulator gas volume	0.52 m^3	Each of three active accumulators
Pressure scram setpoint	80%	20% below nominal core outlet pressure

3.3.1 Steady-State

The steady-state results agree well, as shown in Table 14. The same comment on pressure drop across the core as stated in Sect. 3.2.1 applies here. In addition, ANSDM underestimates the pressure drops in the loop (outside the core) by not accounting directly for check valves, isolation valves, and pipe bends.

3.3.2 Transient

During the first iteration to attempt to benchmark this transient, all three models agreed on flows and pressures but disagreed on heat flux and time to scram. As shown in Fig. 23, the three models agree extremely well on both total core flow and total break flow. It is seen that an almost

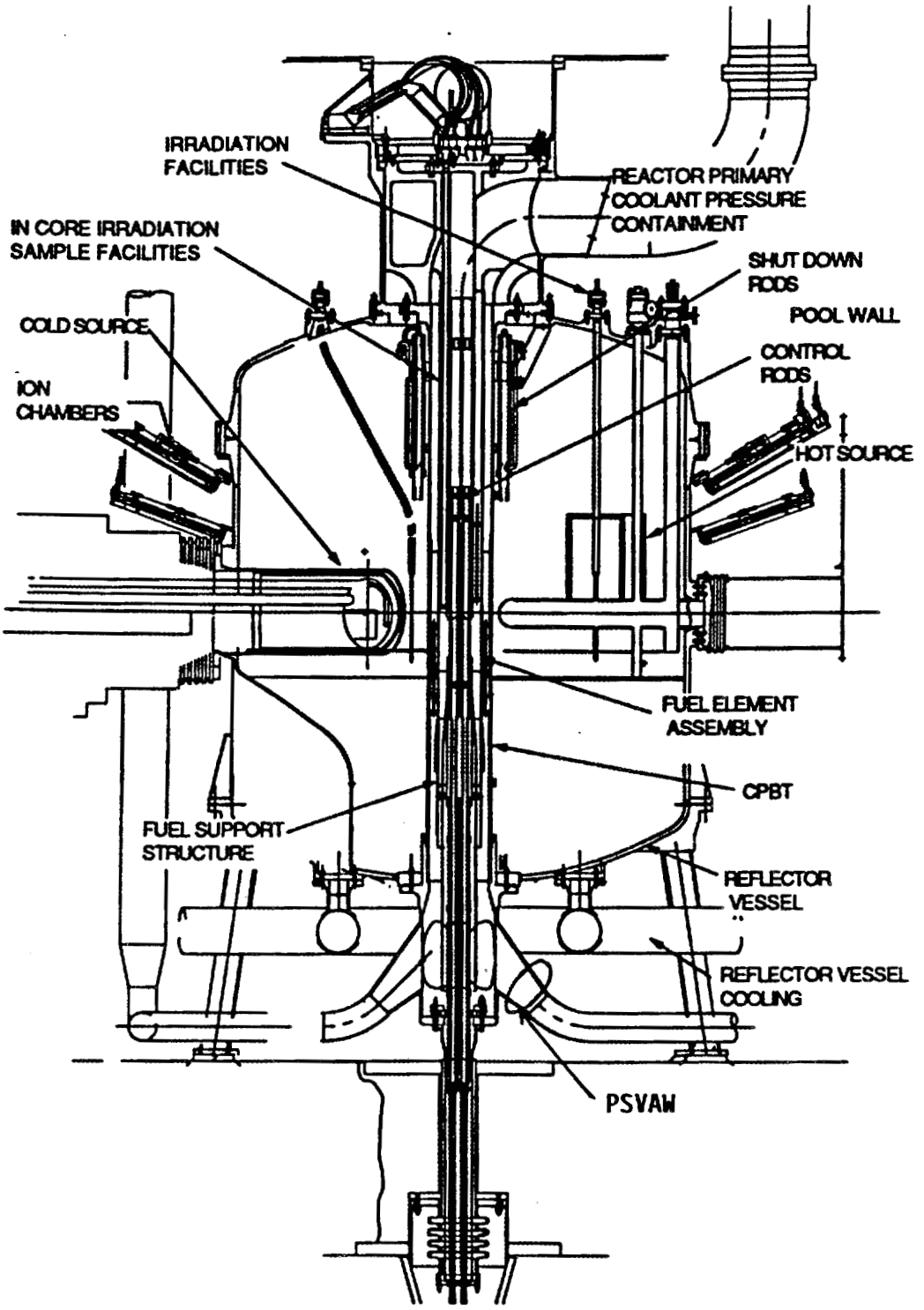

Fig. 22. Advanced Neutron Source reactor core region showing the primary supply vessel adapter weldment.

Table 14. Steady-state comparison for 330-MW nominal core

Parameter	RELAP5	ANSDM[a]	PRSDYN
Fission power (MW)	344.0	343.9[b]	344.0[b]
Total mass flow (kg/s)	1944	1994[b]	1994[b]
Coolant velocity at fuel element inlet (m/s)	25.0	25.2	25.2
Core inlet temperature (°C)	45.6	45.2	45.0
CPBT[c] outlet temperature (°C)	84.5	85.2	85.0
Hot channel outlet temperature in lower element (°C)	139.0	137.2	135.6
Lower element outlet saturation temperature (°C)	202.0	196.1	201.0
Core inlet pressure (MPa)	3.22	3.18[b]	3.22[b]
Core outlet pressure (MPa)	1.62	1.60[d]	1.62[d]
Main coolant pump inlet pressure (MPa)	1.41	1.40	1.53
Main coolant pump outlet pressure (MPa)	3.43	3.40[e]	3.43[e]
Lower element hot channel heat flux at outlet (MW/m^2); includes 95% FE[f] uncertainty	5.44	5.19	
Costa FE limit at lower-element hot-channel outlet (MW/m^2)	23.63	23.14	

[a]ANSDM = Advanced Neutron Source dynamic model.
[b]Input as parameter for benchmark.
[c]CPBT = core pressure boundry tube.
[d]Requires use of Colebrook & White friction correlation. If the Filonenko correlation is used, the pressure drop is 15% smaller.
[e]Pressure drops in cold leg adjusted upwards to account for unmodeled check valves, isolation valves, and pipe bends.
[f]FE = flow excursion.

perfect match persists throughout the first half of a second into the transient, with the maximum discrepancy being limited to ~10% at 1 s. Excellent agreements are also found in pressures at the lower fuel element inlet and outlet (see Fig. 24). All three models correctly predicted a similar depressurization rate in response to break flow. They also predicted a similar declining pressure drop across the core resulting from the diminishing core flow. When the system pressure approaches the pool pressure, the pressure drop across the core converges to the same constant as predicted by all models.

The Costa limiting and local surface heat fluxes at the hot spot in the lower core hot channel exit are compared in Fig. 25. Two disagreements are found in the time to scram and initial Costa limit.

ANSDM detects the scram (including sensor delay) in 385 ms and the scram takes effect (rods start inserting significantly) in 450 ms. RELAP5 does not significantly insert the rods until 650 ms.

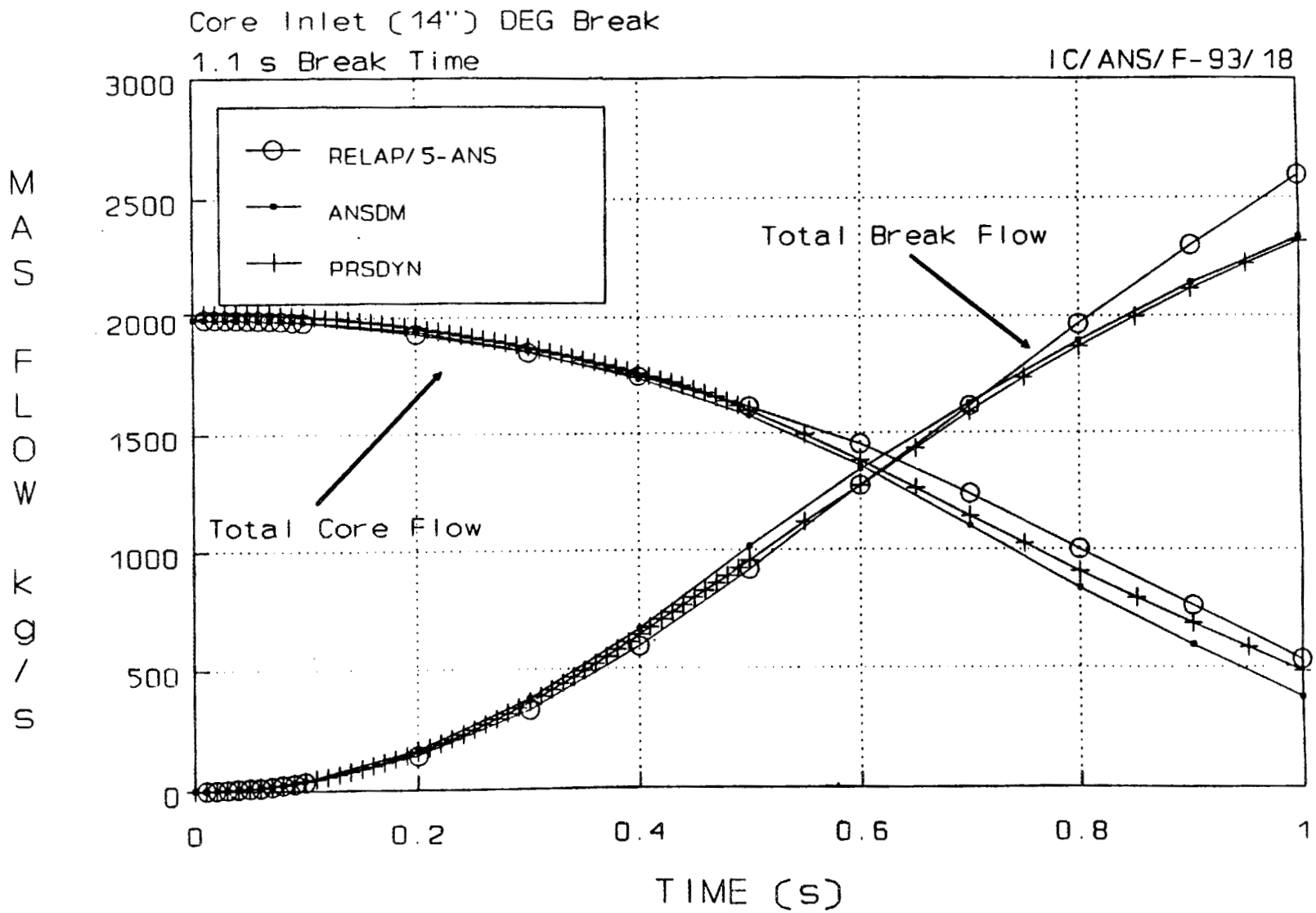

Fig. 23. Comparison in total core and break flows during the double-ended guillotine break at primary supply vessel adapter weldment with 1100-ms opening time.

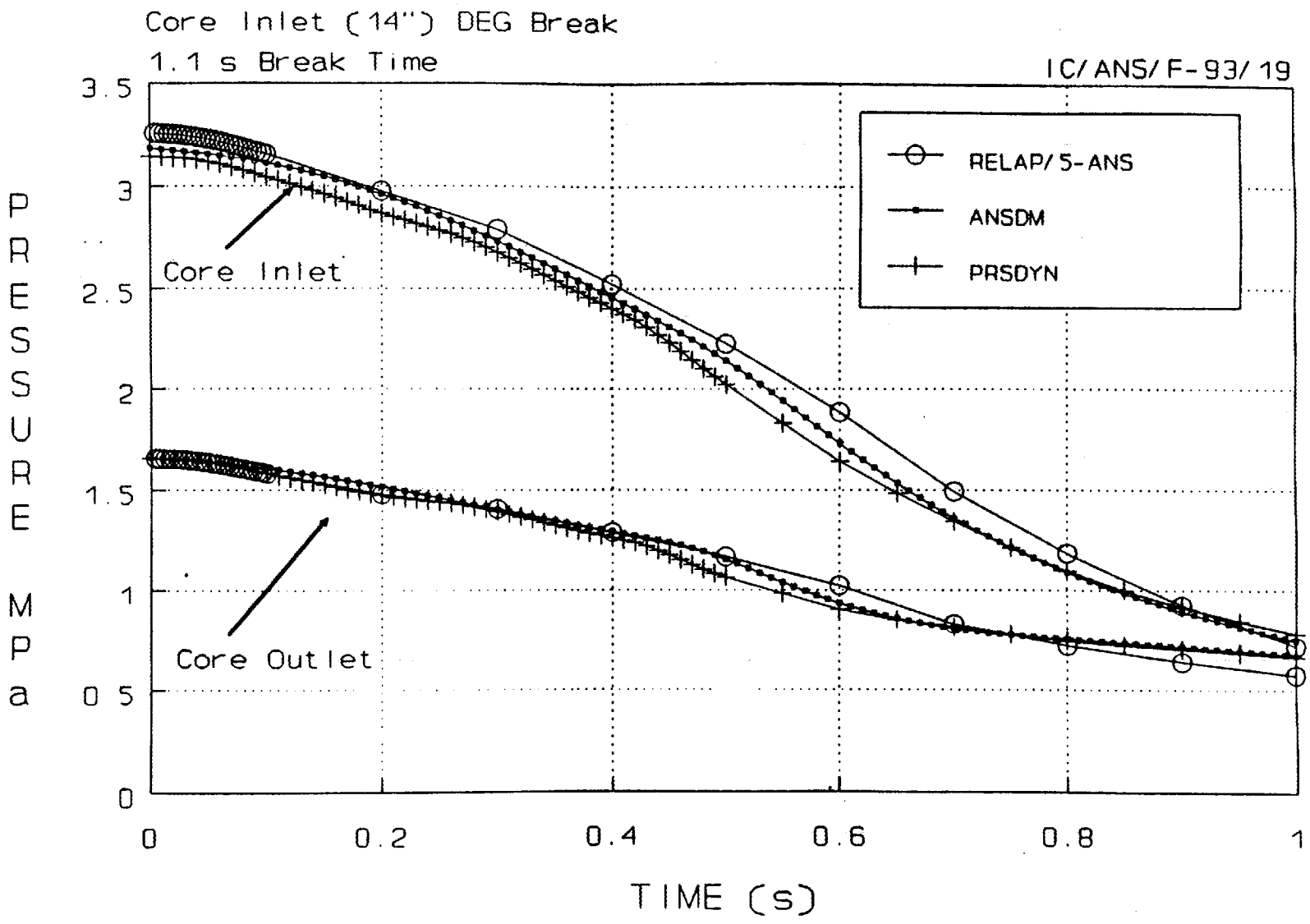

Fig. 24. Comparison in pressures at the lower core inlet and outlet during the double-ended guillotine break with 1100-ms opening time.

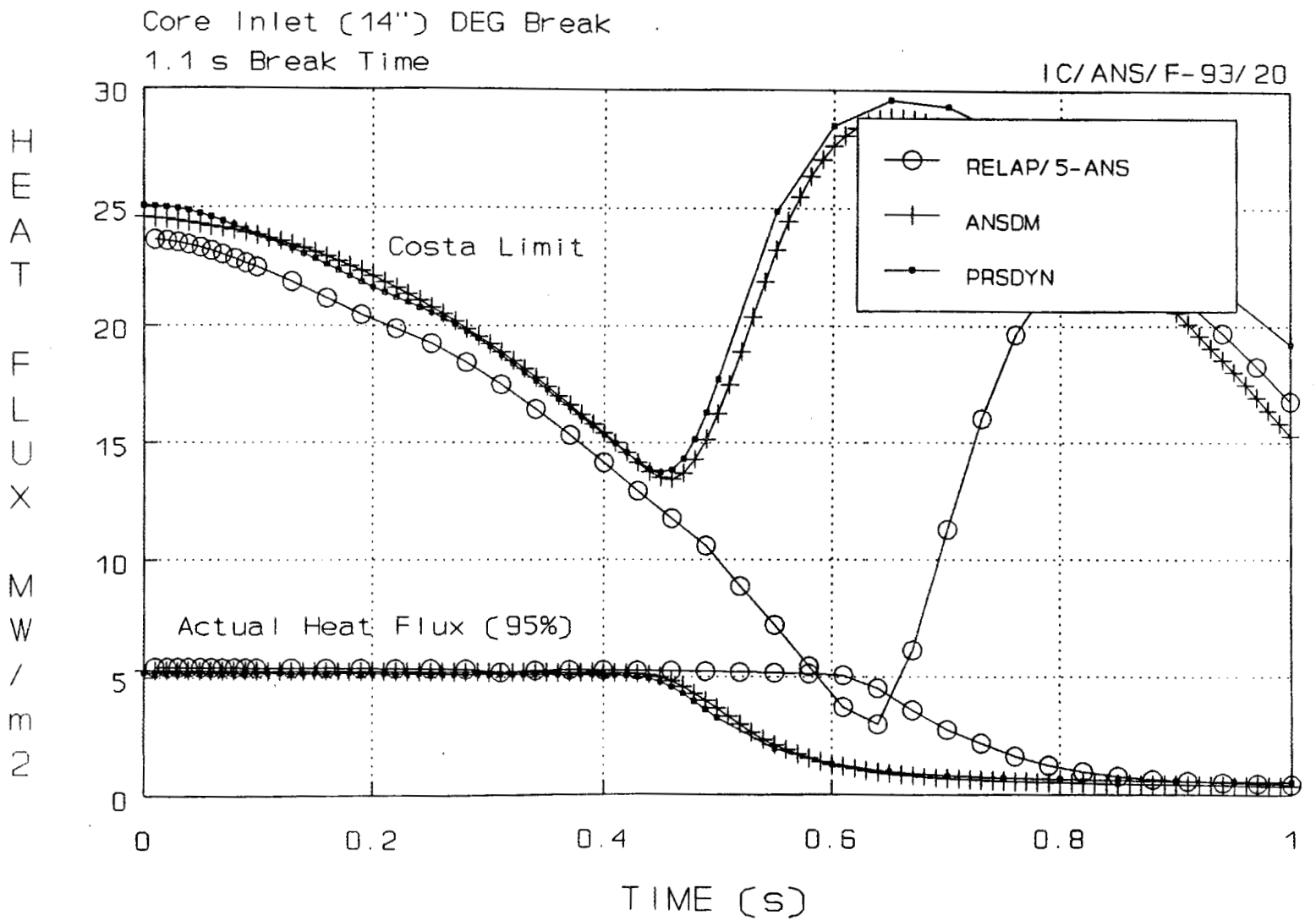

Fig. 25. Costa limit and local surface heat fluxes at lower core exit during the double-ended guillotine break with 1100-ms opening time. The difference in pressure scram setpoint causes RELAP5 results to differ from the other models.)

The difference in the Costa limiting heat flux is ~1 MW/m^2 and may be the result of small differences in initial pressure at the hot spot location.

The difference in the scram time is the result of a difference in the assumed pressure scram setpoints. RELAP5 used the setpoint based on 80% of the initial pressure, while ANSDM used 80% of the nominal pressure. The initial conditions are biased in this transient to account for uncertainties in the operating condition. This bias results in the initial pressure being 95% of nominal; therefore, RELAP5 was scramming on a pressure of ~75% of nominal (i.e., 80 of 95%), which accounts for the additional time delay. To complete the benchmark process, the ANSDM setpoint was modified to agree with the RELAP5-assumed setpoint, and good agreement was obtained as indicated in Fig. 26.

3.3.3 Discussion

To allow a proper comparison of scram time (elapsed time between exceedance of the pressure setpoint and initiation of control rod motion), all models should have the same (1) sensor location, (2) pressure scram setpoint, (3) initial pressure at sensor location, and (4) delay time in pressure switch and control rod unlatching. When these factors are standardized, there remains a small difference in scram time that cannot be eliminated. This difference results from the finite time, limited by the speed of sound in heavy water, that it takes for pressure changes to be transmitted through the system. Therefore, a finite time is required for a depressurization wave to propagate from the break location to the sensor location. The shortest distance between these two points in the ANSR conceptual design is ~40 m, and it requires ~30 ms for the depressurization wave to propagate from the PSVAW inlet to the limited volume air cell. RELAP5 and PRSDYN account for this finite propagation time, but ANSDM assumes that the acoustic wave that transits the initiation of the depressurization propagates at infinite speed. Consequently, RELAP5 and PRSDYN predict an additional delay in the scram time as opposed to the values obtained from ANSDM.

These factors are examined further to resolve initial discrepancies in scram time. On the sensor time delay, RELAP5 models the pressure sensor as a pure delay while ANSDM and PRSDYN model as a first-order-lag. However, all three models predict a resultant 30 ms of instrument delay.

These findings indicate that sensor location and scram pressure setpoints are the most probable causes of scram time differences. ANSDM and PRSDYN have pressure detectors at the outlet of hot leg riser, and RELAP5 has the detector at the hot leg distribution header, downstream of the hot leg riser outlet. As shown in Fig. 27, pressure at the hot leg distribution header crosses the setpoint ~100 ms later than the riser outlet pressure.

During this benchmark, the calculations were found to demonstrate the importance of the selection of the scram low pressure setpoint. Figure 28 shows the Costa limiting heat flux as a function of setpoint pressure (expressed as a percentage of the nominal pressure at the detector location). Increasing the setpoint has an obvious beneficial effect for these slow-opening breaks.

It should be noted that there is a core flow reversal problem late in the transient. All three models predict the flow reversal and its approximate timing. The total core flow decreases initially as the break flows increase and continues to decline after the pump trip, becoming negative (flowing downward) at ~1.26 s into the transient as predicted by RELAP5 (see Fig. 29). Other flow rates at both ends of the break and from the accumulators are also shown. In this case, the slower depressurization rate and the lack of pressure oscillations give sufficient time for the accumulators to respond to the break. The break flows upstream and downstream of the break are very similar, with both flows directed into the pool up to the time that the break is totally open. Then, because the

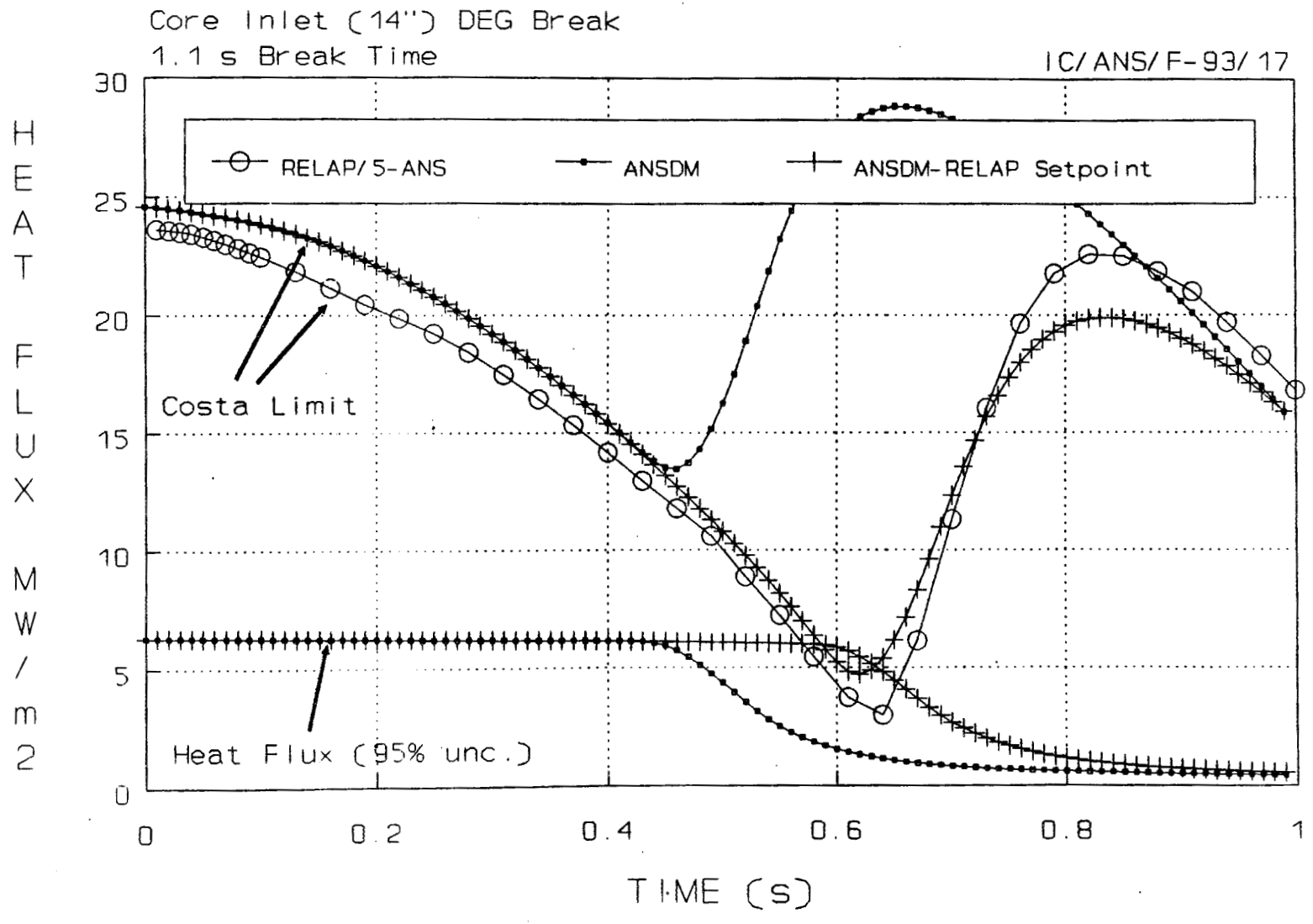

Fig. 26. Good agreement in heat fluxes at the lower core exit during the double-ended guillotine break at primary supply vessel adapter weldment when three models used the same setpoint.

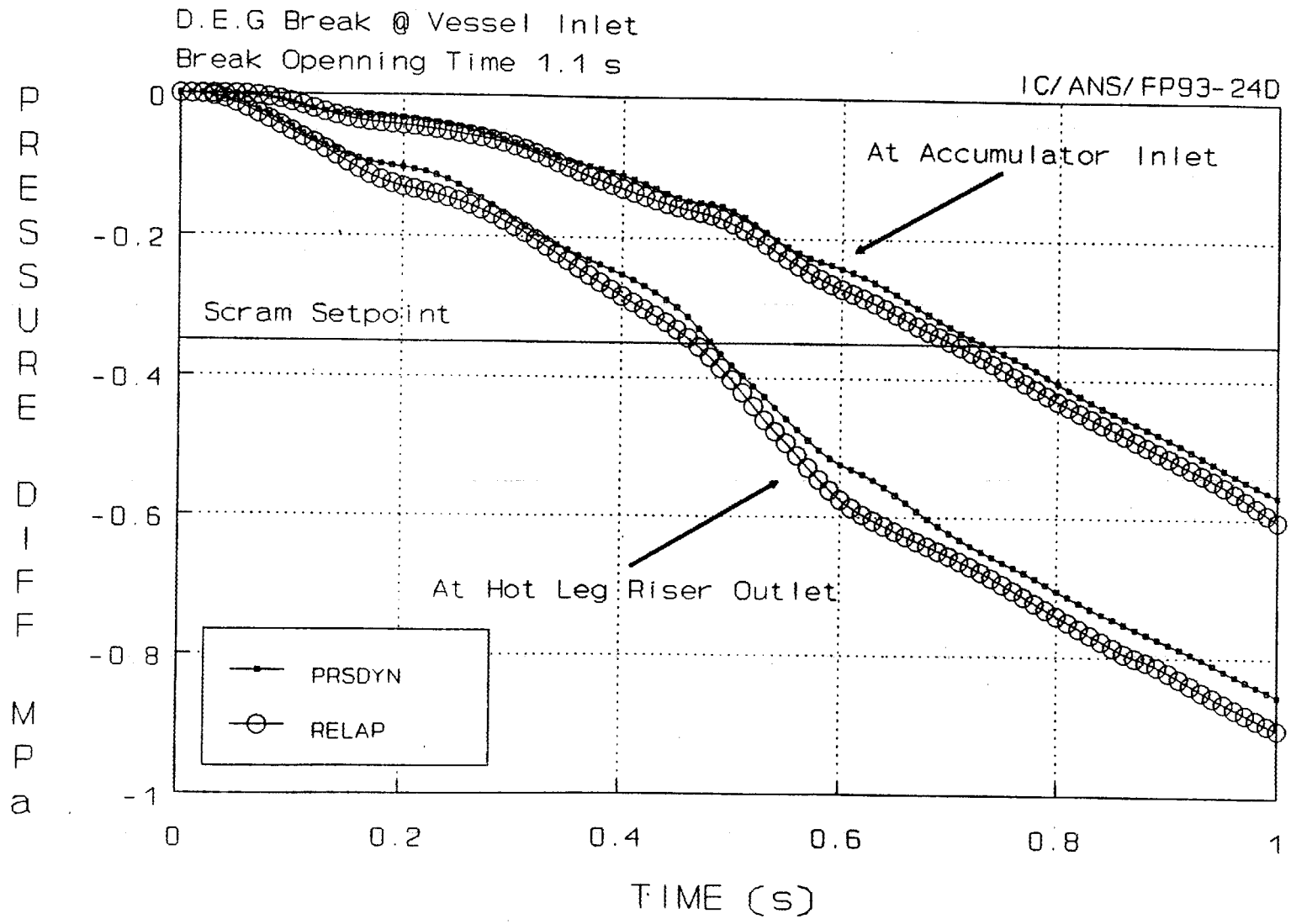

Fig. 27. Pressure difference (change from steady state) at the hot leg riser outlet and accumulator inlet during the double-ended guillotine break with 1.1 s opening time. (The accumulator inlet is further from the core outlet than the hot leg riser outlet.)

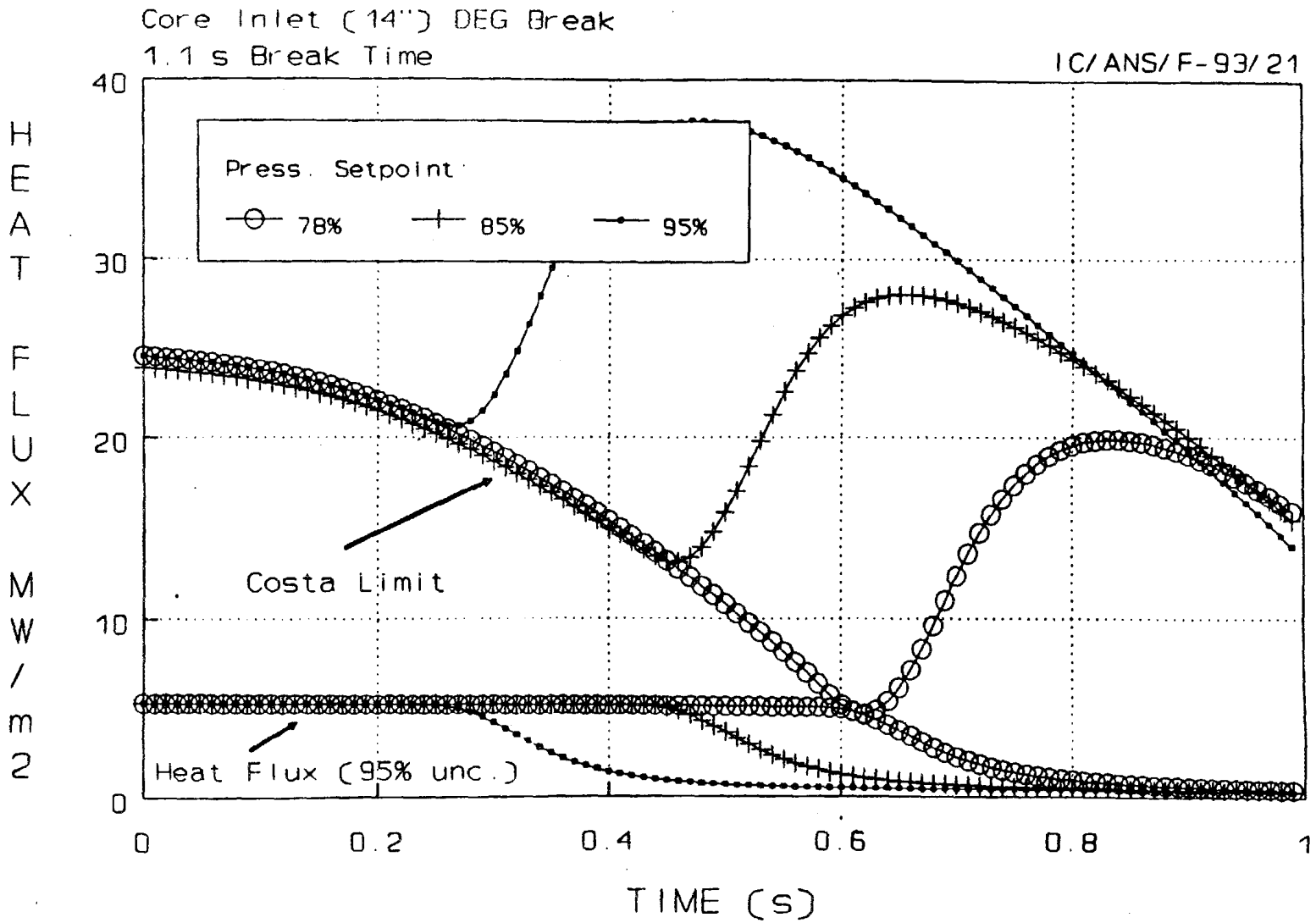

Fig. 28. Advanced Neutron Source dynamic model-calculated heat fluxes showing the importance of pressure setpoints in terms of the nominal value during the double-ended guillotine break with 1100-ms opening time.

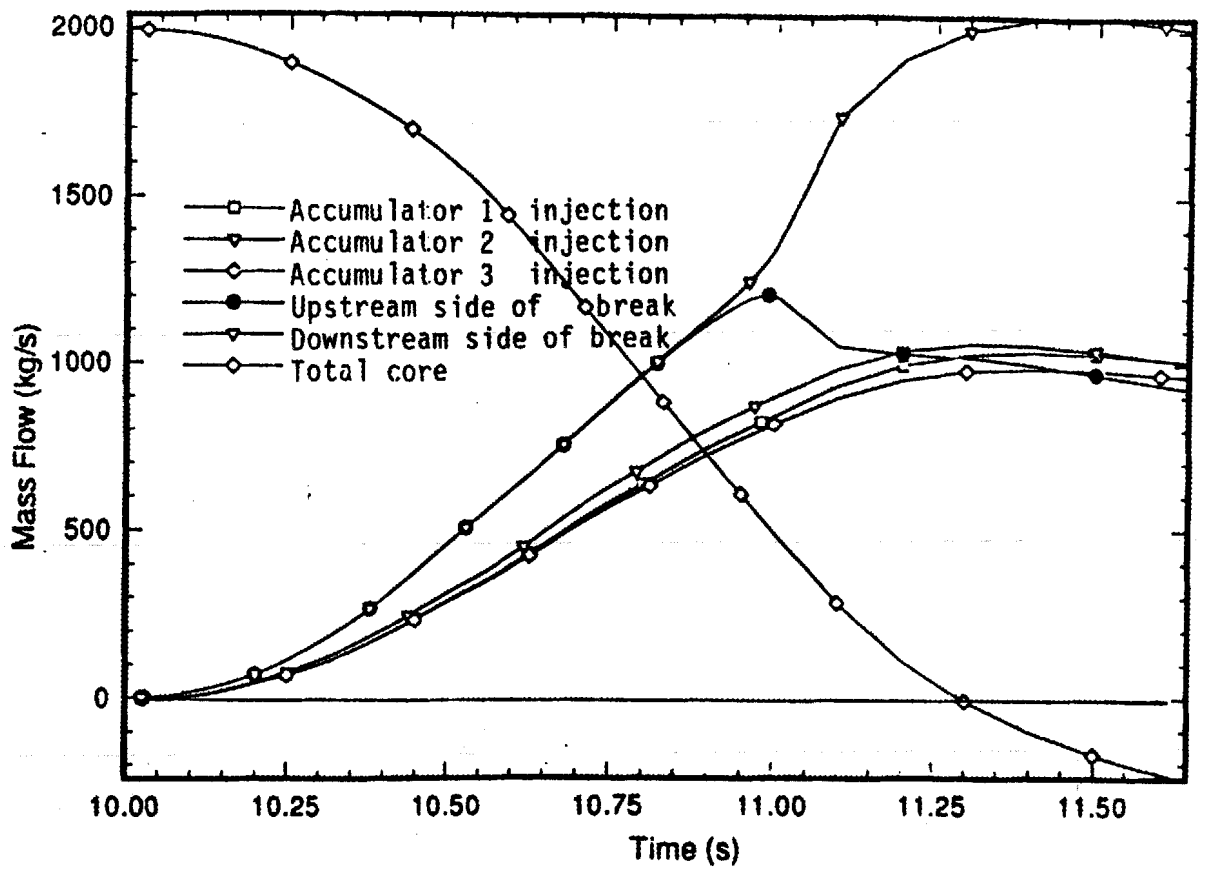

Fig. 29. RELAP5-calculated flows showing the total core flow, break flows upstream and downstream of the break, and individual accumulator flows during the double-ended guillotine break with 1100-ms opening time. (The core flow reversal occurs at ~1.3 s into the transient.)

downstream opening is connected to the PSVAW, which is supplied with coolant by the two intact loops, the flow out of this end of the break continues increasing as depressurization proceeds.

Core flow reversal would be a safety problem for ANSR because of its very high power density. Several options to prevent core flow reversal are proposed. These options include (1) lowering the pump trip setpoint as low as possible while avoiding or minimizing pump cavitation, (2) increasing the pump moment of inertia as much as possible to maintain a higher core flow while avoiding or minimizing pump cavitation, and (3) replacing the standard one-stage gas space accumulator configuration with a two-stage configuration.

3.4 REACTIVITY INSERTION ACCIDENT

This reactivity event is chosen for comparison because the CSAR showed that the limiting event for the reactivity insertion transients is bounded by a \$0.80 reactivity step. It has conservatively been assumed that multiple beam tubes fail and both the aluminum and vacuum volumes are instantaneously replaced by D_2O, resulting in a positive reactivity step of \$0.80, even though no mechanism for this has been identified. This event is considered extremely unlikely, and, thus, the 95% nonexceedance criterion is applied.

The event is initiated by a positive reactivity addition of \$0.80 inserted as a step at the beginning of the transient. The initial control rod position represents the BOC, xenon-free, which corresponds to ~150-mm above the core midplane. The control rod worths are those used in the CSAR (Tables 4.3-14 and 4.3-16). Scram-latch delays are 30 ms for the inner rods and 120 ms for the outer rods. The neutron flux sensor is conservatively modeled with a "first-order-lag" delay, τ_{sensor}, of 25 ms.

$$\dot{\phi}_{sensor} = \frac{\phi - \phi_{sensor}}{\tau_{sensor}} \quad . \tag{44}$$

The reactor scrams on "high-rate of-flux" if $R > 0.2\ s^{-1}$, where the rate of change of flux, R, is defined as follows:

$$\frac{dR}{dt} = \frac{\dot{\phi}_{sensor} - R}{\tau_{rate}} \quad . \tag{45}$$

The rate of change of flux is approximately equal to the derivative of the detector flux, but it is "low-pass" filtered with a time constant, τ_{rate} = 250 ms, so that small neutron flux fluctuation with small amplitude (<5%) will not scram the reactor. In these calculations, the generation time of Λ = 1.3 ms and an effective delayed neutron fraction of β = 0.0078 were used. (Note: These point kinetics parameters are most recent values and differ from the ones used in the CSAR reactivity-event calculations.) Also, the transient is initiated from CSAR nominal conditions—104.2% power, 94.6% pressure, and a core inlet temperature of 45.6°C (which is 0.6°C above nominal).

3.4.1 Steady State

The initial operating conditions are the same as those assumed for the core inlet DEG break with 1100-ms opening time. Thus, the steady-state comparison remains the same as presented in Table 14.

3.4.2 Transient

Preliminary results showed that the fission power compared well, but not the heat power at the fuel surface (average heat flux times fuel surface area). The good comparison in fission power profile (see Fig. 30) is a result of using a similar point kinetics model for calculating the core power, the same reactivity vs time table after scram, the same rate-of-power-change scram setpoint, the same neutron generation time, and effective delayed neutron fraction. The discrepancies in heat power result from a difference in active fuel thermal inertia (product of density and specific heat). The difference in thermal inertia values was traced to the fact that RELAP5 accounted for the density and heat capacity of both the uranium silicide and the aluminum filler, while ANSDM used heat capacity values for pure aluminum. After ANSDM reprogramming to use the more accurate thermal inertia in input, the two models compared excellently in the heat power profile as shown in Fig. 31. These thermal inertia values were used in the remaining comparisons.

The two models compare satisfactorily in the FE thermal limit ratio (see Fig. 32). A similar trend in CHF limit ratio is also indicated. Note that RELAP5 does not print CHF values when the wall temperature is calculated to be less than the saturation temperature; therefore, there is no CHF data to be compared after ~0.2 s into the transient.

More detailed comparisons in the key parameters that affect the FE thermal limit ratio are presented in Figs. 33–35. The local surface heat flux at the exit of the lower core hot channel is compared in Fig. 33. Both models predict the correct trend—rising heat flux during the power excursion, declining after the reactor is scrammed, and finally approaching the decay heat power level.

Likewise, comparisons in the saturation temperature and local velocity (see Fig. 34) are satisfactory, with the maximum differences in saturation temperature and velocity staying below ~2.5°C and 0.8 m/s, respectively. Pressure and coolant temperature at the exit of the lower core hot channel are compared in Fig. 35. The deviations between the two models are within 5°C and 0.05 MPa for the temperature and the pressure, respectively, at the time of the closest approach of the FE limit ratio.

3.4.3 Discussion

Some interesting observations between pressure and temperature at the lower core outlet shown in Fig. 35 call for special attention. As the power excursion occurs upon a positive reactivity step insertion, temperature rises, followed by the pressure rise, as expected. After the reactor is scrammed, the temperature declines and is followed by the pressure decrease as evidenced by the respective peaks predicted by ANSDM (both pressure and temperature peak at 120 ms). On the other hand, RELAP5 predicts a higher frequency for this pressure oscillation. Moreover, RELAP5 predicts a rapid initial pressurization rate that peaks earlier than that of the temperature peak (pressure peaks at 90 ms and temperature at 130 ms).

Pressure increases around the coolant loop are not uniform during the power burst phase. RELAP5 predicts that an acoustic pressure transient is transmitted around the coolant system. The pressurization process in the system (illustrated in Fig. 36) is not threatening to any part of the pressure boundary because the maximum amplitude of pressure change is only ~0.035 MPa. In this figure, time zero refers to the onset of the power excursion and distance is measured from the core exit such that both ends of the x-axis refer to the core exit. Pressure change with respect to the initial steady state distribution is plotted at discrete times during the transient. At time zero, it is quiescent because there is no pressure disturbance. Soon after, the local pressure disturbance caused by the onset of power excursion inside the core begins propagating outward upstream and downstream of the core. At time 24 ms, the disturbance grows to about 5 kPa at the core exit because of a slow temperature

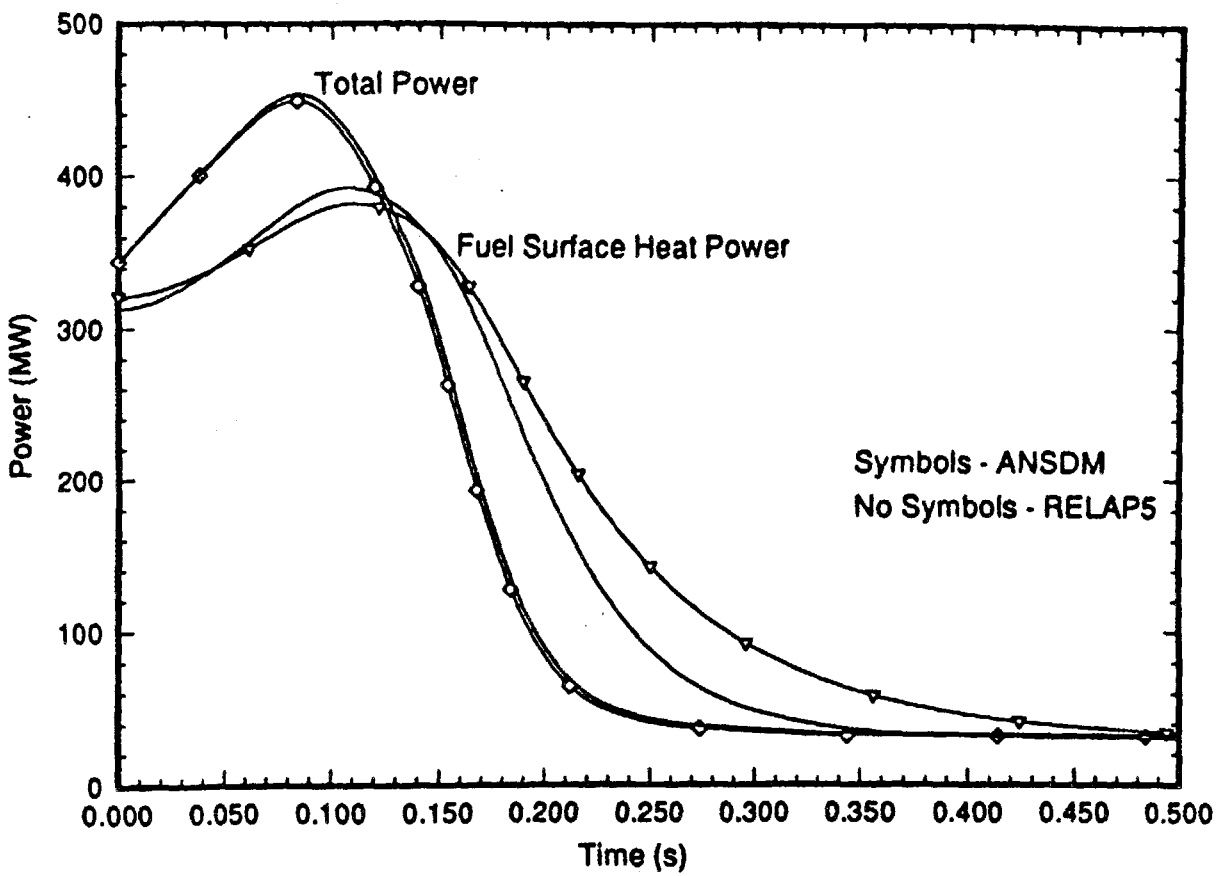

Fig. 30. Advanced Neutron Source dynamic model (ANSDM) vs RELAP5 comparison in total and fuel surface heat powers for the $0.80 reactivity step accident before correction of ANSDM fuel heat capacity.

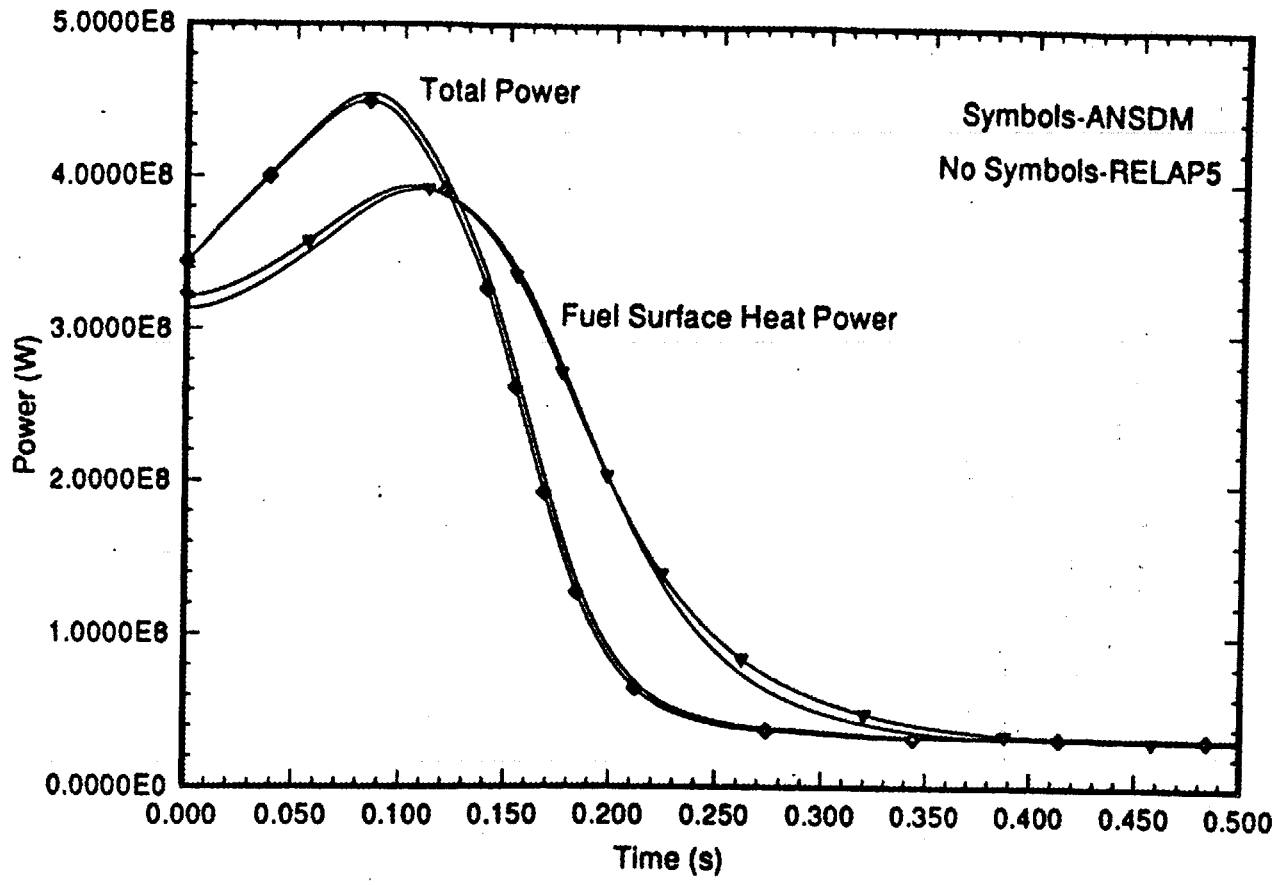

Fig. 31. Advanced Neutron Source dynamic model (ANSDM) vs RELAP5 comparison in total and fuel surface heat powers for the $0.80 reactivity step accident after correction of ANSDM fuel heat capacity.

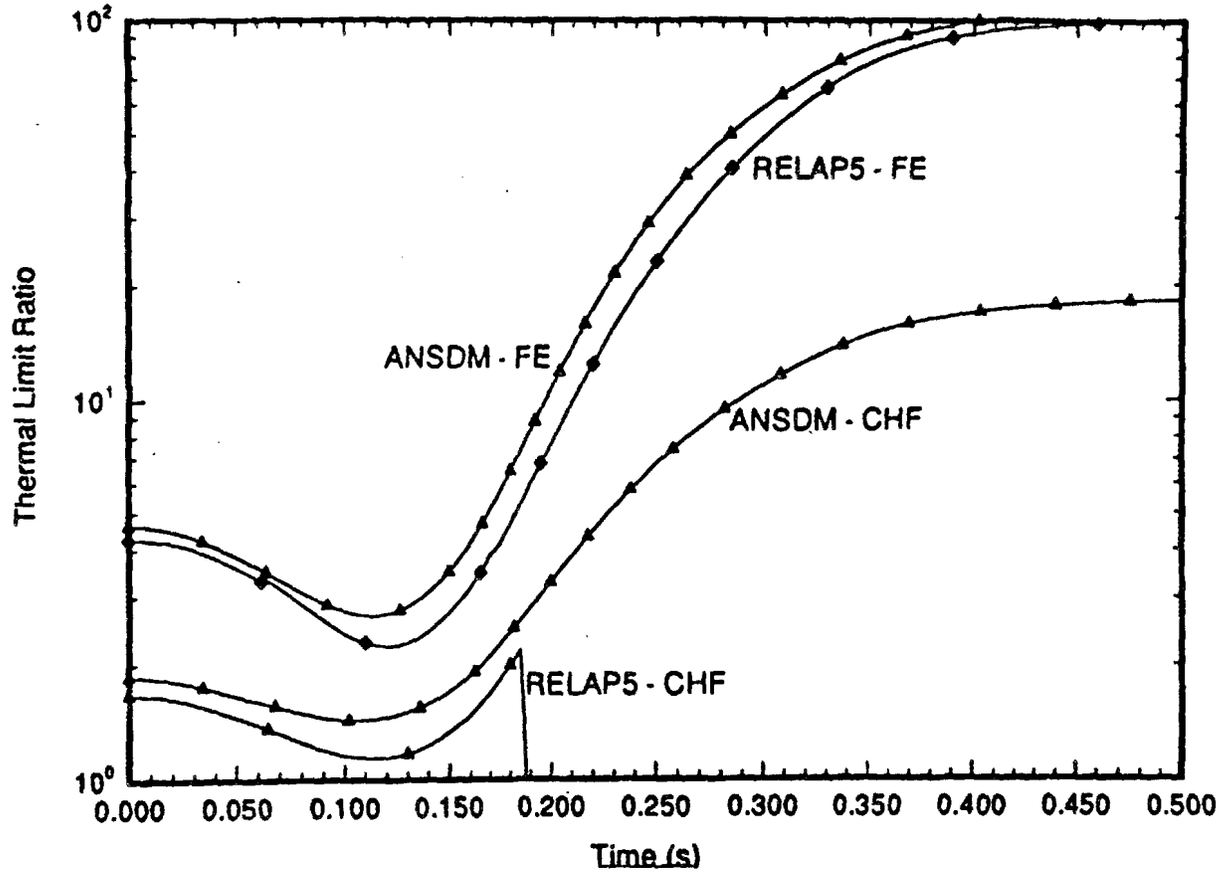

Fig. 32. Advanced Neutron Source dynamic model vs RELAP5 comparison in thermal limit ratios for the $0.80 reactivity step accident. (Note: The critical heat flux values are not printed out by RELAP5 if the wall temperature stays below the local coolant saturation temperature.)

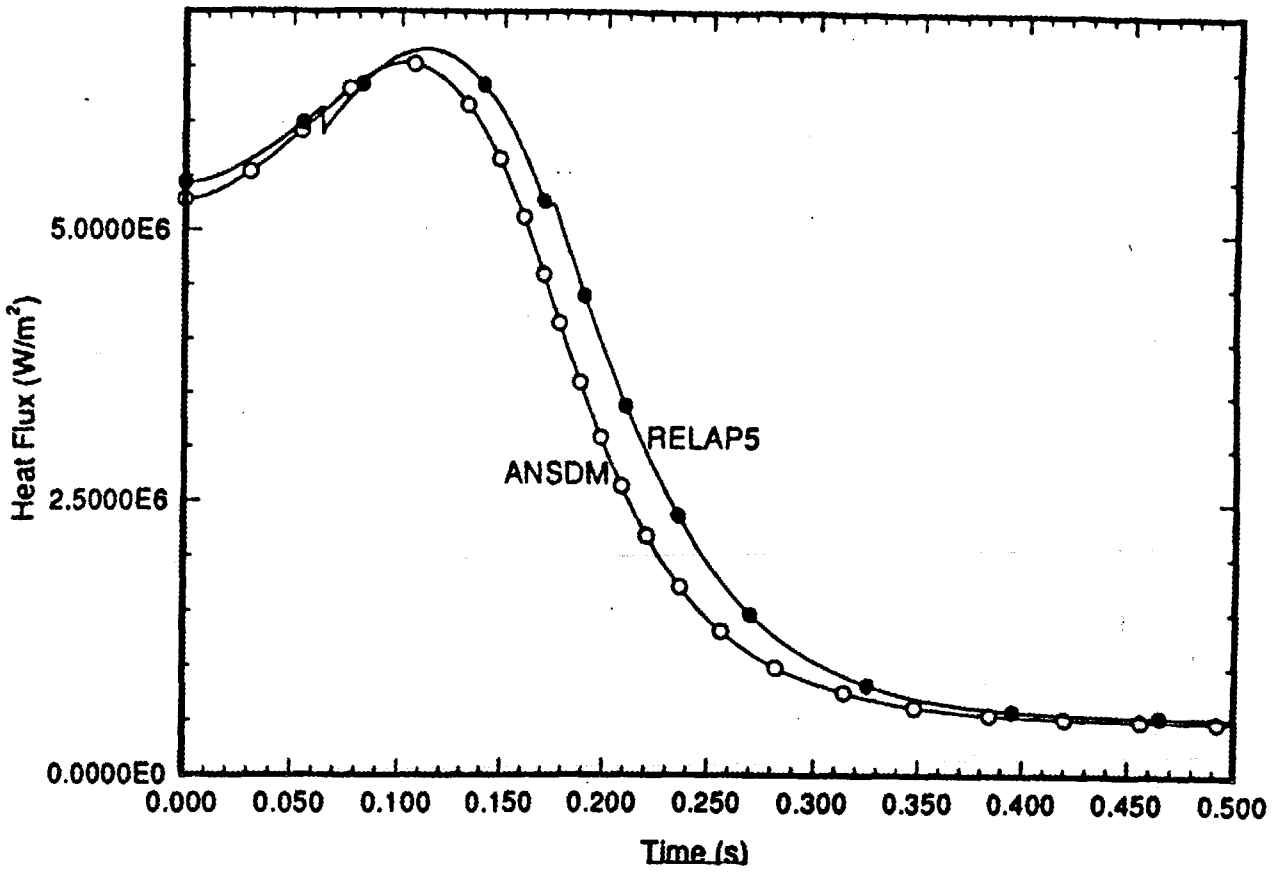

Fig. 33. Advanced Neutron Source dynamic model vs RELAP5 comparison in local surface heat flux at the lower core exit for the $0.80 reactivity step accident.

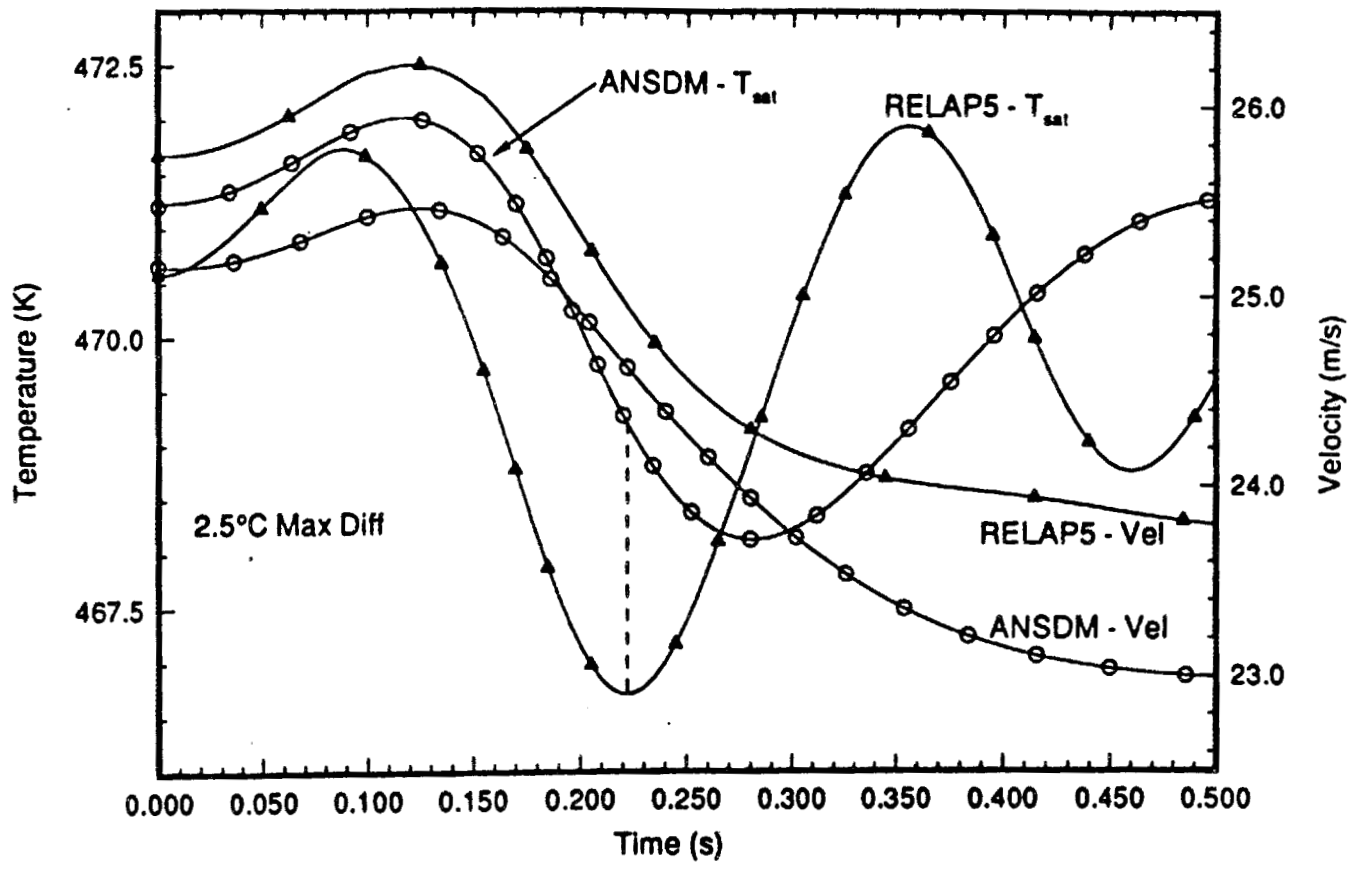

Fig. 34. Advanced Neutron Source dynamic model vs RELAP5 comparison in the local coolant velocity and saturation temperature at the lower core exit for the $0.80 reactivity step accident.

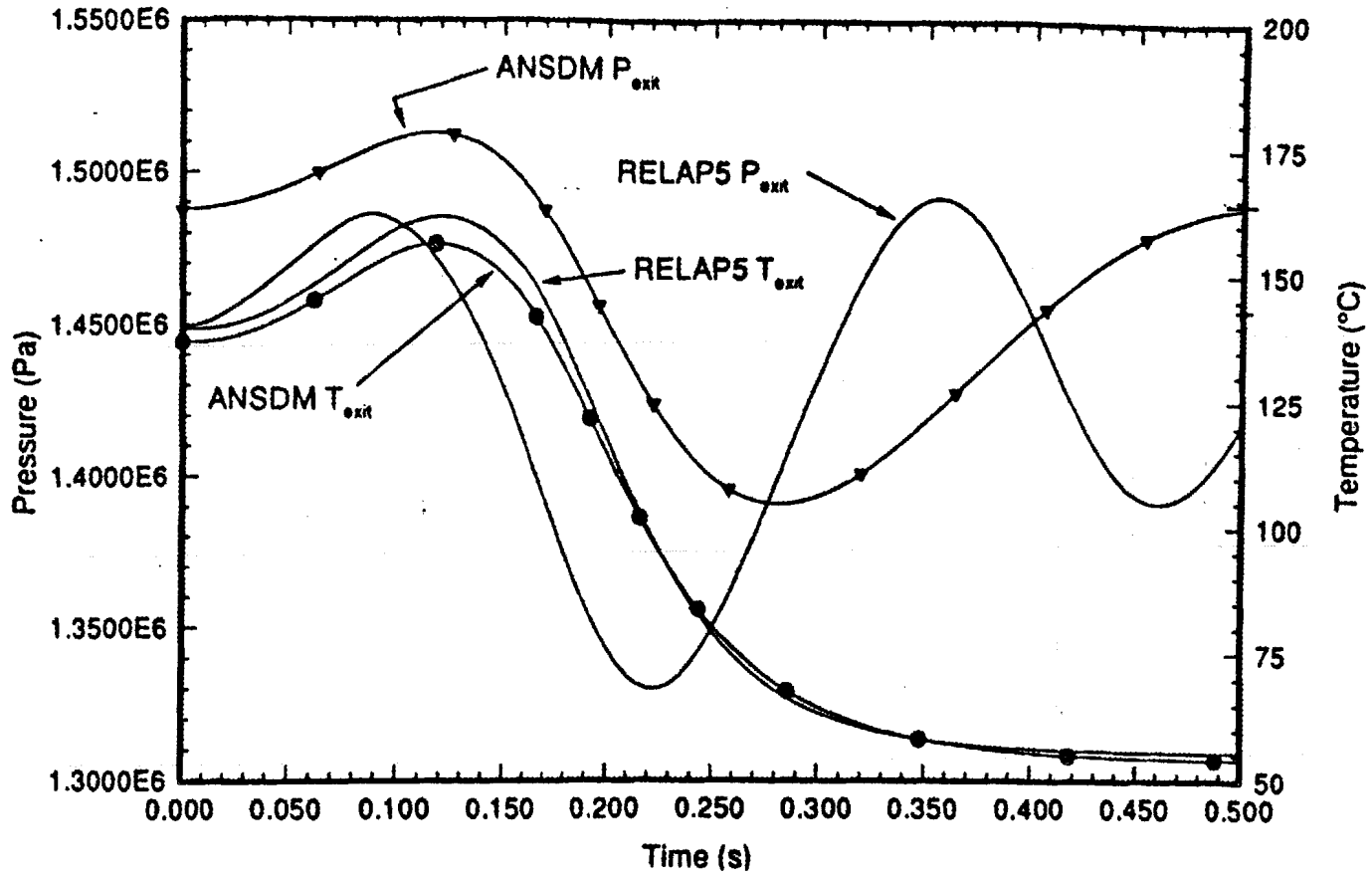

Fig. 35. Advanced Neutron Source dynamic model vs RELAP5 comparison in the local pressure and coolant temperature for the $0.80 reactivity step accident.

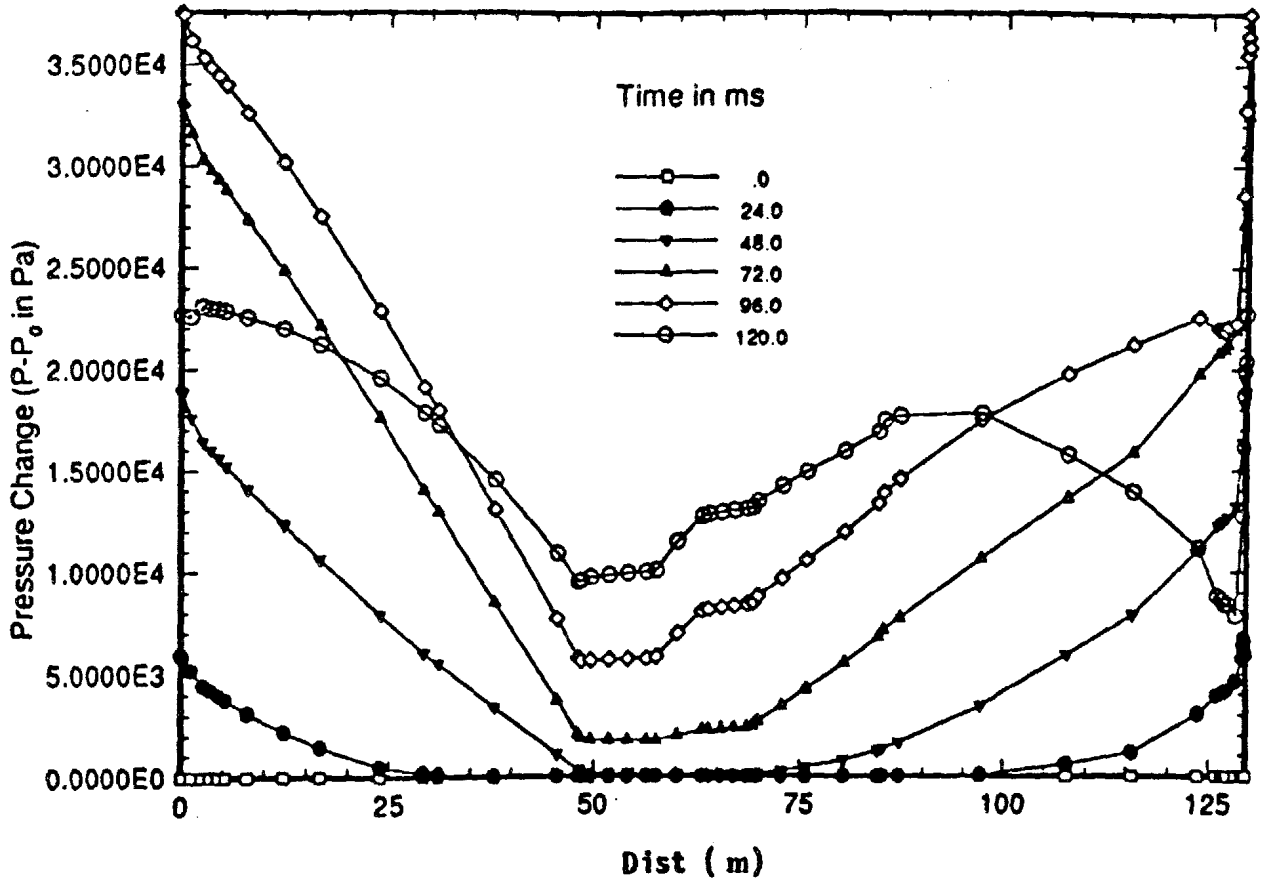

Fig. 36. RELAP5-calculated pressure changes with reference to the steady-state showing the acoustic propagation during the power burst along the loop for the $0.80 reactivity step accident.

rise while the leading edge of the wave propagates a distance ~35 m from the core exit upstream and downstream (acoustic velocity of 1450 m/s × time of 24 ms = 35 m) as evidenced by a nearly symmetric pattern. The zone beyond 35 m is unaffected. As time progresses to 72 ms, the pressure disturbance grows to 33 kPa at the core exit and reaches the center portion of the loop as indicated by relatively small pressure changes. Thereafter, the waves lose their symmetry as a result of combined effects of differences in flow resistance of cold and hot legs and interferences from reflected waves. At 96 ms, the pressure amplitude at the core exit peaks; however, at other locations in the system, the pressure continues to rise. The average pressure change from the initial steady state at any given time can be derived by integrating the corresponding area under each curve. Note that the depressurization process during the cooldown phase is not shown here.

RELAP5 predicts a rapid rise and earlier fall in pressure because the initial pressurization caused by the reactivity step change is highly localized and the core outlet pressure depends not only on the local temperature effects but also on the mass fluxes through the control volume, and the position of the acoustic wave. However, ANSDM assumes that the acoustic wave propagates at an infinite speed so that the pressure disturbance, once created inside the core, reaches everywhere in the system spontaneously. As a consequence, pressure (global rather than local) and temperature respond together. If the ANSDM predicted pressure disturbance should be plotted in the same graph (Fig. 36), every curve would appear as a horizontal line.

4. CONCLUSIONS AND RECOMMENDATIONS

The overall conclusion from this exercise is that RELAP5, ANSDM, and PRSDYN will give very similar results if the input parameters are the same. With respect to the transient events calculated in this report, there are no important differences in code capabilities, with the single exception that ANSDM does not capture the sonic limitation on pressure wave propagation through the coolant system. This difference is significant only in very rapidly opening pipe break events. Major conclusions and recommendations are summarized in the following sections.

4.1 CONCLUSIONS

The overall comparisons establish the fact that a set of common input parameters (e.g., operating conditions, system configuration, correlations, etc.) is a prerequisite for a satisfactory steady-state comparison. However, modeling differences in pump coastdown characteristics, gas expansion behavior inside accumulators, and pressurizing/letdown systems are not apparent during normal operating conditions. For a successful comparison in transient results, the set of input parameters further requires identical (1) initial conditions resulting from the steady-state operating conditions, (2) pump coastdown characteristics including shaft friction torque, (3) gas expansion characteristics inside accumulators, (4) pressurizing/letdown system modeling, and (5) safety protection systems (such as sensor locations, sensor delay time, setpoint, and reactivity profiles), and (6) other characteristics (such as heat capacity) that may influence the transient.

For the small LOCA comparison (51 mm-diam break with 250-ms opening time at the CPBT outlet), it is shown that RELAP5 and ANSDM predictions agree reasonably well in spite of minor modeling differences, such as nodalization scheme and friction correlations. Nevertheless, the importance of using common pump coastdown characteristics, letdown valve controlling logic, gas expansion behavior inside accumulators, and break opening formation characteristics is immediately recognized.

For the station blackout accident comparison, it has been shown that satisfactory agreement in results can be obtained if the same pump coastdown characteristics, decay heat power, and gas expansion behavior within accumulators are assumed for RELAP5 and ANSDM. Also, it has been demonstrated that two FE margin minima exist. The first minimum occurs as the result of initial depressurization after the reactor is scrammed, and the second one occurs at the transition from the forced convection to natural circulation much later in the transient.

For the large LOCA comparison (DEG break with 1100-ms opening time at PSVAW), it was demonstrated that two FE margin minima exist. The first minimum occurs as the result of initial depressurization after the reactor is scrammed. Whether the core can survive depends strongly on the pressure sensor location and sensor setpoint as well as the initial conditions. The second minimum occurs when the accumulator injection flow overwhelms the diminishing upward core flow after the pump is tripped.

For the reactivity insertion accident comparison (reactivity step of $0.80), it is shown that matching the fission power requires an identical reactivity profile along with an identical scram mechanism. More importantly, it is shown that RELAP5 can reproduce the acoustic transient during the heatup and cooldown cycle upon the reactivity step change. Although the acoustic phenomena affects the safety margin insignificantly in the reactivity results, it significantly affects results for instantaneous large break LOCAs because of the delay it introduces between event initiation and the initiation of the reactor scram by the hot leg pressure switches.

4.2 RECOMMENDATIONS

Since the majority of differences noted throughout this study resulted from different model input parameters, the single most important recommendation for future safety analysis is that the ANS Project should work on ways to ensure that the correct design data is conveniently available and used by analysts.

Other improvement to the ANSR thermal hydraulic models (RELAP5, ANSDM, and PRSDYN) based on comparison findings is summarized in Table 15. The following general recommendations can be applied to all models for further improvements.

Table 15. Improvement to the Advanced Neutron Source reactor thermal-hydraulic models based on comparison findings

Parameter	ANSDM[a] and PRSDYN	RELAP5
Point kinetics	Need to develop a one-dimensional (axial) model for better representation during control rod insertion and a three-dimensional model for beam-tube flooding events	Needs to develop a one-dimensional (axial) model for better representation during control rod insertion and a three-dimensional model for beam tube flooding events
Decay heat partition		Needs to develop capacity for post-scram decay heat regional distribution
Fuel thermal inertia	Need to include appropriate thermal inertia for both uranium silicide and aluminum filler (pure aluminum currently assumed)	
Pressure drop over the core		Improved Colebrook friction correlation by calibrating to THTL[b] data
Accumulator model	Need to develop capability for representing flow into tank and honeycomb inert heat structure	Needs to develop capability for representing flow into tank and honeycomb insert heat structure
Pump model	Need to develop capability for representing (1) pump moment of inertia, (2) pump friction torque (zero torque currently assumed), and (3) pump cavitation	Developed and implemented a HFIR[c]-like pump cavitation model

[a]ANSDM = Advanced Neutron Source dynamic model.
[b]THTL = thermal-hydraulic test loop.
[c]HFIR = High Flux Isotope Reactor.

The reactivity profile has an important bearing in determining the power. It is recommended that a unified reactivity vs time table be used when updated information in total rod length and total rod worth becomes available.

During natural circulation, decay heat is critical in determining the survivability of the core. It is recommended that the partition of the decay heat into various regions in core and noncore components must be revised and updated using the more accurate ANSR-specific MCNP results calculated by INEL after completion of the CSAR.

Degradation of pump performance can be important upon onset of cavitation. Once pump cavitation occurs, the reduced core flow could affect the safety margin. Thus, it is recommended that all models include a pump cavitation model based on the real ANSR pump performance curves and net positive suction head (NPSH) required data to assess cavitation effects on the safety margin and quantify the duration of cavitation.

If the following specific recommendations are incorporated, RELAP5 analyses can be significantly improved.

The discrepancy in pressure drop across the core appears to be caused by an ill-fitted friction correlation used in RELAP5 for ANSR flow conditions. Therefore, it is recommended that INEL examine and verify the curve fitting of the Colebrook correlation over various flow regions against the analytical expression, as well as data, if possible. The final code implementation should be documented and released for future safety analyses. Actually, the final implementation, documentation, and release have already occurred, and the updated version RELAP5/MOD3/VERSION8k0 is operational at ORNL.

Accumulator performance affects the depressurization rate significantly. To improve the accumulator model to accommodate the thermal and hydraulic effects of the isothermalizer, it is recommended that a lumped-parameter model using RELAP5 control variables or other methods be developed. This model will represent the basic accumulator phenomena and reduce the accumulator behavior to a pressure or flow rate boundary condition on the primary coolant system piping.

REFERENCES

1. J. Costa, *Measurement of the Momentum Pressure Drop and Study of the Appearance of Vapor and Change in the Void Fraction in Subcooled Boiling at Low Pressure*, presented at the Meeting of European Group Double-Phase, Winfrith, France, 1967, translated from French as ORNL/TR-90/21, Martin Marietta Energy Systems, Inc., Oak Ridge Natl. Lab., 1990.

2. *Conceptual Safety Analysis Report*, Chap. 15, ORNL/ANS/INT-33/V4, Martin Marietta Energy Systems, Inc., Oak Ridge Natl. Lab., June 1992.

3. V. H. Ransom, et al., *RELAP5/MOD2 Code Manual*, Volumes I–IV, NUREG/CR-4312, EGG-2396, August 1985.

4. D. G. Morris and M. W. Wendel, *High Flux Isotope Reactor System RELAP5 Input Model*, ORNL/TM-11647, Martin Marietta Energy Systems, Inc., Oak Ridge Natl. Lab., January 1993.

5. G. C. Slovik, U. S. Rohatgi, and J. Jo, *RELAP5/MOD2.5 Analysis of the HFBR for a Loss of Power and Coolant Accident*, Brookhaven National Laboratory, Upton, New York, BNL-52243, May 1990.

6. S. T. Polkinghorne, T. K. Larson, and B. J. Buescher, "RELAP5 Simulation of Advanced Test Reactor Scaled LOCA Experiments 7, 8, 12, and 14," *Nucl. Technol.* 93, 240–251 (February 1991).

7. J. S. Bollinger and C. B. David, "Benchmarking of the RELAP5/MOD2.5 r-0 Model of an SRS Reactor to the 1989 L-Reactor Tests (U)," *Joint RELAP5 and TRAC-BWR International User Seminar*, Chicago, September 1990.

8. C. S. Miller and R. W. Shumway, *RELAP5/MOD3 Code Quality Assurance Plan for ORNL ANS Narrow Channel Flow and Heat Transfer Correlations*, EGG-NE-10326, EG&G, Inc., Idaho Falls, Idaho, November 1992.

9. P. W. Dittus and L. M. K. Boelter, "Heat Transfer in Automobile Radiators of the Tubular Type," University of California Pub. Eng., No. 13, pp. 443–461, reprinted in *Intl. Comm. Heat and Mass Transfer* 12, 3–22 (1985).

10. B. S. Petukhov, Heat Transfer and Friction in Turbulent Pipe Flow with Variable Physical Properties, *Advances in Heat Transfer* 6, 528 (1970).

11. W. R. Gambill, "Generalized Prediction of Burnout Heat Flux for Flowing, Subcooled, Wetting Liquids," *Chem. Eng. Prog. Symp. Series* 59, (41), 71–87, (1963).

12. R. J. Weatherhead, *Nucleate Boiling Characteristics and the Critical Heat Flux Occurrence in Subcooled Axial-Flow Water Systems*, ANL-6675, Argonne National Laboratory, Chicago, March 1963.

13. D. C. Groeneveld, S. G. Cheng, and T. Doan, "1986 AECL-U0 Critical Heat Flux Lookup Table," *Heat Transfer Eng.* 7 (1-2) 46-62 (1986).

14. P. Griffith et al., "Counter Flow Critical Heat Flux," *AICHE*, Paper No. 25, presented at 15th National Heat Transfer Conference, San Francisco, August 1975.

15. J. F. Briesmeiter, ed., *MCNP-A General Monte Carlo Code for Neutron and Photon Transport*, LA-7396-M, Rev. 2, Los Alamos National Laboratory, Los Alamos, 1986.

16. D. R. Vondy, T. B. Fowler, and G. W. Cunningham, *The BOLD-VENTURE Computational System for Nuclear Reactor Core Analysis, Version III*, ORNL-5711, Union Carbide Corporation, Oak Ridge Natl. Lab., 1981.

17. A. J. Stepanoff, *Centrifugal and Axial Flow Pumps*, 2nd ed., John Wiley & Sons, New York, 1957.

18. D. B. Collins et al., "Pump Operation with Cavitation and Two-Phase Flow," *Proceedings 4th Western Canadian Heat Transfer Conference*, Winnipeg, Manitoba, May 1972.

19. American National Standards Institute/American Nuclear Society (ANSI/ANS), *American National Standard for Decay Heat Power in Light Water Reactors*, ANSI/ANS5.1-1979 (1979).

20. *ACSL-Advanced Continuous Simulation Language*, Reference Manual, Edition 10, Mitchel and Gauthier Associates, Concord, Massachusetts, 1991.

21. C. O. Bennett and J. E. Myers, *Momentum Heat and Mass Transfer*, 3rd edition, McGraw Hill, New York, 1982.

22. F. Kreith, *Principles of Heat Transfer*, 3rd edition, Intext Educational Publisher, New York, 1967.

23. M. W. Wendel, *RELAP5 LOCA Analysis Parametric Studies*, C-HFIR-91-020, April 1992.

INTERNAL DISTRIBUTION

1. C. W. Alexander
2. D. J. Alexander
3. R. R. Allen
4. E. E. Alston
5. J. L. Anderson
6. B. R. Appleton
7. J. G. Arterburn
8. R. E. Battle
9. R. S. Booth
10. W. W. Bowman
11. R. A. Brown
12. G. J. Bunick

13-17. J. H. Campbell

18. P. F. Cento
19. N. C. J. Chen
20. K. W. Childs
21. K. K. Chipley
22. J. E. Cleaves
23. J. T. Cleveland
24. G. L. Copeland
25. W. G. Craddick
26. J. R. Dixon
27. F. F. Dryer
28. K. Farrell
29. D. K. Felde
30. R. E. Fenstermaker
31. G. F. Flanagan
32. J. D. Freels
33. M. L. Gildner
34. H. A. Glovier
35. D. C. Haberkost
36. R. M. Harrington
37. J. B. Hayter
38. D. M. Hetrick
39. S. E. Holliman
40. M. M. Houser
41. R. O. Hussung
42. M. Ibn-Khayat
43. D. T. Ingersoll

44-47. R. L. Johnson

48. J. E. Jones, Jr.
49. R. A. Lillie
50. M. A. Linn
51. P. S. Litherland
52. A. T. Lucas
53. J. A. March-Leuba
54. B. S. Maxon
55. G. T. Mays
56. S. V. McGrath
57. T. J. McManamy
58. G. R. McNutt
59. J. T. Mihalczo
60. R. M. Moon
61. D. G. Morris
62. D. L. Moses
63. R. E. Pawel
64. H. R. Payne
65. F. J. Peretz
66. C. C. Queen
67. S. Raman
68. C. T. Ramsey
69. J. S. Rayside
70. W. R. Reed
71. J. P. Renier
72. J. B. Roberto
73. R. E. Rothrock
74. T. L. Ryan
75. J. P. Schubert
76. D. L. Selby
77. H. B. Shapira
78. M. Siman-Tov
79. C. D. Sulfredge
80. R. P. Taleyarkhan
81. D. W. Theisen
82. P. B. Thompson
83. K. R. Thoms
84. S. R. Tompkins
85. B. D. Warnick
86. M. W. Wendel
87. C. D. West
88. J. L. Westbrook
89. D. M. Williams
90. P. T. Williams
91. B. A. Worley

92. G. T. Yahr
93. G. L. Yoder
94. ORNL Patent Office
95. Central Research Library
Document Reference Section
96. Laboratory Records Department
97. Laboratory Records, RC
98. Y-12 Technical Library

EXTERNAL DISTRIBUTION

99. R. Awan, U.S. Department of Energy, NE-473, Washington, DC 20585.
100. L. Cheng, Brookhaven National Laboratory, Upton, NY 11973.
101. K. K. Conway, Laboratory Facilities Branch, U.S. Department of Energy, Oak Ridge Operations Office, CE-523, P.O. Box 2001, Oak Ridge, TN 37831-2001.
102. C. D. Fletcher, Idaho National Engineering Laboratory, P.O. Box 1625, Idaho Falls, ID 83415-3885.
103. R. R. Fullwood, Brookhaven National Laboratory, Upton, NY 11973.
104. W. R. Gambill, Routh 5, Box 220, Clinton, TN 37716.
105. A. F. Henry, Professor, Department of Nuclear Engineering, Massachusetts Institute of Technology, 77 Massachusetts Avenue, Cambridge, MA 02139.
106. R. A. Hunter, Director, Office of Facilities, Fuel Cycle, and Test Programs, Nuclear Energy Division, U.S. Department of Energy, NE-47, Washington, DC 20585.
107. T. L. Kerlin, University of Tennessee, College of Engineering, 315 Pasqua Engineering Building, Knoxville, TN 37996-2300.
108. J. A. Lake, Manager, Nuclear Engineering and Reactor Design, Idaho National Engineering Laboratory, P.O. Box 1625, Idaho Falls, ID 83415.
109. J. E. Mays, Research and Test Reactor Fuel Elements, Babcock and Wilcox Co., P.O. Box 785, Lynchburg, VA 24505.
110. J. P. Mulkey, U.S. Department of Energy, NE-473, Washington, DC 20585.
111. W. T. Oosterhuis, Materials Sciences Division, Office of Basic Energy Sciences, Office of Energy Research, U.S. Department of Energy, ER-132, Washington, DC 20585.
112. J. M. Ryskamp, Idaho National Engineering Laboratory, P.O. Box 1625, Idaho Falls, ID 83415-3885.
113. J. L. Snelgrove, Coordinator, Engineering Applications, RERTR Program, Argonne National Laboratory, 9700 South Cass Avenue, Argonne, IL 60439.
114. I. Thomas, Acting Associate Director, Materials Science Divison, Office Of Energy Research, U.S. Department of Energy, ER-13, Washington, D.C. 20585.
115-117. U.S. Department of Energy, ANS Project Office, Oak Ridge Operations Office, FEDC, MS-8218, P.O. Box 2009, Oak Ridge, TN 37831-8218.
118. H. G. Wood, III, Associate Professor, Department of Mechanical and Aerospace Engineering, Thornton Hall, University of Virginia, Charlottesville, VA 22901.
119. Office of Scientific and Technical Information, P.O. Box 62, Oak Ridge, TN 37831.